CHALMERS
UNIVERSITY OF TECHNOLOGY

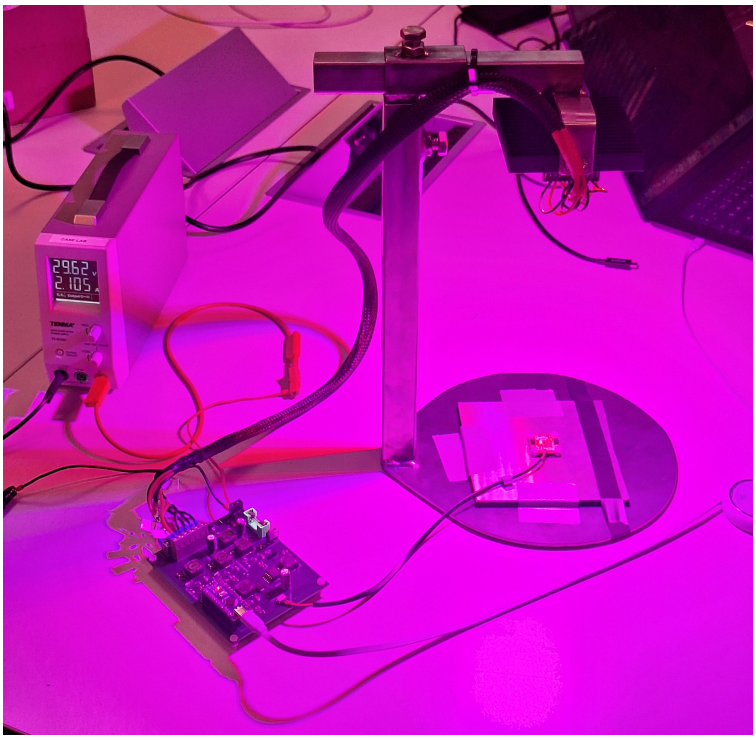

# Dynamic LED Control System for Agriculture

## Controlling Multiple LED Drivers with Pulse Width Modulation Based on Plant Light Requirements

Bachelors thesis report in Electrical Engineering

ALEXANDER AMBERG, ANTON GYBRANT, ATLE PETERSON, THEO THORSELL, ELLIOT VIGELIUSSON

DEPARTMENT OF ELECTRICAL ENGINEERING
CHALMERS UNIVERSITY OF TECHNOLOGY
Gothenburg, Sweden 2026
www.chalmers.se

Bachelors Thesis Report 2026

# Dynamic LED Control System for Agriculture

Controlling Multiple LED Drivers with Pulse Width Modulation
Based on Plant Light Requirements

ALEXANDER AMBERG, ANTON GYBRANT, ATLE PETERSON, THEO THORSELL, ELLIOT VIGELIUSSON


CHALMERS
UNIVERSITY OF TECHNOLOGY

Department of Electrical Engineering
Chalmers University of Technology
Gothenburg, Sweden 2026

Dynamic LED Control System for Agriculture

Controlling Multiple LED Drivers with Pulse Width Modulation Based on Plant Light Requirements

ALEXANDER AMBERG, ANTON GYBRANT, ATLE PETERSON,
THEO THORSELL, ELLIOT VIGELIUSSON



Supervisor: Vaishnavi Ravi, Department of electrical engineering
Examiner: Jimmy Ehnberg, Department of electrical engineering

Bachelors Thesis Report 2026
Department of Electrical Engineering
Chalmers University of Technology
SE-412 96 Gothenburg
Sweden
Telephone +46 31 772 1000

Cover: Lighting setup of the project, with both PCBs and light sensor connected.

Typeset in LaTeX
Gothenburg, Sweden 2026

Dynamic LED Control System for Agriculture

Controlling Multiple LED Drivers with Pulse Width Modulation Based on Plant Light Requirements

ALEXANDER AMBERG, ANTON GYBRANT, ATLE PETERSON,
THEO THORSELL, ELLIOT VIGELIUSSON
Department of Electrical Engineering
Chalmers University of Technology

# Abstract

This thesis focuses on the design and construction of a LED based lighting system for agricultural applications. The purpose is to develop a system that employs PWM dimming to adjust the spectral composition and intensity of the emitted light by changing the duty cycle with a microprocessor. This enables the spectral output of the lighting system to be controlled to meet the requirements of different plants. The goal is to achieve higher efficiency than current HPS-based lighting systems used in agriculture. The project encompasses the design and testing of a PCB used to drive and control a LED PCB. The prototype was constructed to allow both manual control of individual channels and automatic regulation via a PI controller that utilizes real-time input from an external light sensor.

The results show that the efficacy of the system is nearly doubled that of a HPS based lighting system. The lighting system was able to produce a PPFD of 235 μmol/($m^2$s) with an intended light mix at the ratio 20:60:20 between blue, red and far-red light. At this PPFD, the blue and far-red light intensities could be increased by more than 100%, allowing substantial flexibility in spectral composition. With this light mix, the system had a calculated efficacy of 3.43 PPF/W, with up to 61% of the input power being translated into photosynthetically active light. Disregarding light mix, the maximum achievable PPFD of the system is 378 μmol/($m^2$s). Incorrect dimensioning of some LED driver components and suspected electromagnetic interference causes lower than intended ON current from the LED drivers. This results in the spectral output being less adjustable than intended.

While the system can compensate for ambient light, the spectral sensor used is only capable of measuring relative light intensity and lacks the ability to measure absolute photon flux density. The control system is highly sensitive to positional changes of the spectral sensor. A calibration method was implemented to dynamically set the target based on the current sensor position. Electrical protection measures were successfully implemented into the design.

Keywords: Horticultural Lighting, LED Lighting, Spectral Sensing, Photosynthetic Photon Flux Density (PPFD), Lighting Control, Pulse Width Modulation (PWM), PI Regulator, DC–DC Converters, Peak Current Mode (PCM) Control.

# Acknowledgements

We want to thank our supervisor Vaishnavi Ravi for her vital guidance and support. Her invaluable feedback and expertise were instrumental in achieving the goals of this thesis.

We also want to thank Stefan Lundberg for helping with using the reflow solder oven.

Finally, we would like to thank Jimmy Ehnberg for the increased budget.

# Acronyms

**ADC** Analog-to-Digital Converter.
**ATP** Adenosine Triphosphate.

**B** Blue Light.
**BJT** Bipolar Junction Transistor.
**BMS** Battery Management System.

**CAD** Computer-Aided Design.
**CCM** Continuous Conduction Mode.
**CEA** Controlled Environment Agriculture.
**Chl *a*** Chlorophyll *a*.
**Chl *b*** Chlorophyll *b*.
**cry** Cryptochromes.

**DC** Direct Current.
**DCM** Discontinuous Conduction Mode.

**EMI** Electromagnetic Interference.
**EOD** End-of-Day.
**ESD** Electrostatic Discharge.

**FR** Far-Red Light.

**G** Green Light.

**HPS** High-Pressure Sodium.

**IC** Integrated Circuit.
**IDE** Integrated Development Environment.

**LDO** Low-Dropout.
**LED** Light-Emitting Diode.
**LHC** Light-Harvesting Complex.

**MOSFET** Metal-Oxide-Semiconductor Field-Effect Transistor.

**NADP** Nicotinamide Adenine Dinucleotide Phosphate.
**NADPH** Reduced Nicotinamide Adenine Dinucleotide Phosphate.
**NMOS** N-Channel MOSFET.

**PAR** Photosynthetically Active Radiation.

**PAS** Photosynthetic Action Spectrum.
**PCB** Printed Circuit Board.
**PCM** Peak Current Mode control.
**Pfr** Phytochrome far-red.
**phot** Phototropins.
**phy** Phytochromes.
**PI** Proportional–Integral.
**PID** Proportional–Integral-Derivative.
**PMOS** P-Channel MOSFET.
**PPF** Photosynthetic Photon Flux.
**PPFD** Photosynthetic Photon Flux Density.
**Pr** Phytochrome red.
**PSI** Photosystem I.
**PSII** Photosystem II.
**PWM** Pulse Width Modulation.

**R** Red Light.
**RMS** Root Mean Square.

**SMD** Surface Mount Device.

**TVS** Transient-Voltage-Suppression.

# Nomenclature

Below is the nomenclature of the parameters and variables that have been used throughout this thesis.

## Parameters and Variables

| | |
|---|---|
| $A$ | Area ($m^2$) |
| $A_c$ | Light cone area ($m^2$) |
| $c$ | Speed of light (m/s) |
| $C_B$ | Bulk capacitance, electrolytic capacitance (µF) |
| $C_{CE}$ | Ceramic capacitance (µF) |
| $C_{CE\_Total}$ | Total ceramic capacitance (µF) |
| $C_{in}$ | Input capacitance (µF) |
| $C_{out}$ | Output capacitance (µF) |
| $t$ | Thickness (m or mm) |
| $D$ | Duty cycle (%) |
| $D_{nom}$ | Nominal duty cycle (%) |
| $D_{MAX}$ | Max duty cycle (%) |
| $e(t)$ | Error function |
| $E$ | Energy (J) |
| $f_c$ | Cutoff frequency (Hz) |
| $f_{SW}$ | Switching frequency of the LED driver (Hz) |
| $h$ | Planck's constant (Js), height (m) |
| $I$ | Intensity ($W/m^2$) |
| $I_d$ | Average drain current over one time period (mA or A) |
| $i_d$ | Time variant diode current (mA or A) |
| $I_{f(peak)}$ | Peak forward current |
| $I_{f(typ)}$ | Typical forward current |

| | |
|---|---|
| $I_{\text{LED}}$ | LED current (mA or A) |
| $I_{\text{LED(ripple)}}$ | LED ripple current (mA or A) |
| $I_{L\text{(peak)}}$ | Peak inductor ripple current (mA) |
| $I_{L\text{(ripple)}}$ | Inductor ripple current (mA or A) |
| $I_{\text{STEP}}$ | Step current (mA or A) |
| $I_{\text{tot}}$ | Total current, total maximum current (mA or A) |
| $I_{\text{zk}}$ | Zener diode current (mA or A) |
| $K_{\text{nom}}$ | Nominal light mix |
| $K_{\text{i}}$ | Integral coefficient |
| $K_{\text{p}}$ | Proportional coefficient |
| $K_{\text{PPF}}$ | Relative PPF factor |
| $K_{\text{PPFD}}$ | Relative contribution of a specific LED channel |
| $L$ | Inductance (µH) |
| $n_{\text{LEDs}}$ | Number of LEDs |
| $N_{\text{A}}$ | Avogadro's constant (photons/µmol) |
| $P$ | Power (mW or W) |
| $P_{\text{tot}}$ | Total power loss, total maximum power loss (W) |
| PPF | Photosynthetic photon flux (µmol/s) |
| $\text{PPF}_{\text{LED}}$ | Typical photosynthetic photon flux of one LED (µmol/$m^2$-s) |
| $\text{PPF}_{\text{sum}}$ | The sum of photosynthetic photon flux of several LEDs (µmol/$m^2$-s) |
| PPFD | Photosynthetic photon flux density (µmol/$m^2$-s) |
| $\text{PPFD}_{\text{LED}}$ | Photosyntehic photon flux density of one LED (µmol/$m^2$-s) |
| $\text{PPFD}_{\text{max}}$ | Maximum photosynthetic photon flux density of several LEDs (µmol/$m^2$-s) |
| $\text{PPFD}_{\text{nom}}$ | Nominal PPFD value (250 µmol/$m^2$-s) |
| $\text{PPFD}_{\text{tot}}$ | Total PPFD emitted by all LEDs (µmol/$m^2$-s) |
| $r$ | Radius (m) |
| $R$ | Resistance (Ω) |
| $R^2$ | Coefficient of determination |
| $R_{\text{ds}}$ | Drain-source resistance (Ω) |
| $R_{\text{gate}}$ | Gate resistance (Ω) |
| $R_{\text{LED}}$ | Dynamic LED resistance (Ω) |
| $R_{\text{sense}}$ | Sense resistance (Ω) |
| $R_{\text{th,heatsink}}$ | Thermal resistance of heatsink (°C/W) |

| | |
|---|---|
| $R_{\text{th,LED}}$ | Thermal resistance of the LED (°C/W) |
| $R_{\text{th,PCB}}$ | Thermal resistance of the PCB (°C/W) |
| $t_{\text{int}}$ | Integration time (s) |
| $T_{\text{d}}$ | Derivative time constant (s) |
| $T_{\text{ambient}}$ | Ambient temperature of the room (°C) |
| $T_{\text{junction}}$ | Maximum rated temperature at the LED p-n junction (°C) |
| Tol. | Tolerance |
| $T_{\text{R\_PS}}$ | Power supply response time (µs) |
| $u(t)$ | Input function |
| $V_{\text{CBO}}$ | Collector-Base Voltage, Emitter open (V) |
| $V_{\text{drop}}$ | Voltage drop (mV) |
| $V_{\text{f}}$ | Forward-bias voltage (V) |
| $V_{\text{f(peak)}}$ | Peak forward voltage (V) |
| $V_{\text{f(typ)}}$ | Typical forward voltage (V) |
| $V_{\text{FB}}$ | Feedback voltage (V) |
| $V_{\text{gs}}$ | Gate-source voltage (V) |
| $V_{\text{in}}$ | Supply voltage (V) |
| $V_{\text{IN\_Tran}}$ | Allowed input transient undershoot or overshoot (V) |
| $V_{\text{out}}$ | Output voltage (V) |
| $V_{\text{ref}}$ | Reference voltage (V) |
| $V_{V\text{in(max)}}$ | Maximum input voltage (V) |
| $V_{\text{z}}$ | Zener diode voltage (V) |
| $x(t)$ | Target function |
| $y(t)$ | Output function |
| $Z_{C_{\text{out}}}$ | Output capacitor impedance (Ω) |
| $Z_{\text{out}}$ | Output impedance (Ω) |
| $\Delta I_{\text{f}}$ | Difference in forward-bias current (mA or A) |
| $\Delta V_{\text{f}}$ | Difference in forward-bias voltage (V) |
| $\lambda$ | Wavelength (nm) |
| $\Phi$ | Radiant flux (W) |
| $\varphi$ | Angle (°) |

# Contents

# List of Figures

# List of Tables

# 1
# Introduction

All plants harvest energy from light sources to grow. The development of artificial lighting enables farming in environments where it is otherwise not possible. Research shows that optimizing the light spectrum and intensity from artificial lighting can improve plant growth [1]. This project encompasses the design and prototyping of a device that can adjust the intensity and spectral range of light for farming applications. The goal is to achieve high efficiency and to allow optimizing for plant growth across different species and growth stages. The product uses Pulse Width Modulation (PWM) to dim LEDs that emit four different wavelengths to control the spectral output.

## 1.1 Background

Agriculture has been crucial for the human existence for over 10,000 years [2], and horticulture is a natural extension of that. Up until over a century ago, sunlight was the exclusive energy source for photosynthesis, after which various artificial light sources began to be used to supplement or replace natural lighting [3]. The types of supplemental lighting commonly used were incandescent, fluorescent, metal halide, and High-Pressure Sodium (HPS) lamps. These lamps produce a wide spectral distribution with some parts of the created light falling outside the wavelengths used for plant growth, meaning a part of the power is wasted [4]. In greenhouses, the currently most common lamp is of the HPS variation [1]. The light output of HPS lamps is primarily infrared, which means a large part of the power consumption is turned into heat instead of being useful for photosynthesis. One study [5], shows that 36% of the input energy for HPS lamps is turned into light within the Photosynthetically Active Radiation (PAR) spectrum, with an efficacy (PPF/W) of 1.8 µmol/J. In indoor farming, artificial lighting is a large part of the costs, accounting for 20–30% of total production costs making it a key area to improve overall efficiency.

The development of LEDs, with their low power consumption and ability to emit a narrow spectrum of light, has led to an increased viability of artificial lighting for farming [4]. The LEDs ability to produce a narrow spectrum of light can be used to produce light to match thespecifc Photosynthetic Action Spectrum (PAS) of a specific plant. The PAS is the curve which describes the ability of a plant to use different wavelengths of light for photosynthesis. Wavelengths in the range from 360 nm to 760 nm have been shown to contribute to photosynthesis [1], but to a varied

degree of effectiveness. By combining LEDs of different wavelengths, the resulting color spectrum can be tailored to conform to the specific PAS curve of each plant. There are devices with assemblies of LEDs to fit the specific light requirements of different plants. These devices are driven by constant current, and no control of the light spectrum is possible after installation. Devices with multiple independently driven LED channels have started to become popular with different manufacturers, making artificial lighting systems that can adjust the output dynamically [6], [7]. Research has shown that by splitting the LEDs into different channels, and dimming the output of the channels independently, finer control of the produced light spectrum is possible [4]. By controlling the spectral output in real time, depending on the plant species or plant growth stage, a general purpose lighting system can be used while making the light emitted have maximum potency.

## 1.2 Purpose

The objective of this thesis is to design and build an artificial lighting system for use in horticultural applications. The device is supposed to be able to produce light with an adjustable spectral output to fit the requirements of different plants. The spectral composition and the light intensity can be optimized for specific plants to meet requirements based on growth stages and physical characteristics. Consequently, this results in an increase in photosynthetic efficiency, and an improvement of plant development. By targeting only the PAS, the total efficiency of the lighting system can be increased.

## 1.3 Goals and Specifications

The desired end result of this thesis is a device with multiple LED channels consisting of LEDs that emit different wavelengths. The intensity of each channel being individually controllable allows for an adjustable color spectrum. The specific design goals are listed as the following:

- Individually driven LED channels.
- Adjustable total intensity.
- Adjustable spectral distribution.
- Feedback system to achieve constant incident light in terms of intensity and spectral distribution.
- More efficient than existing HPS-based systems.
- Adjust LED output based on supplemental ambient light to reduce power input and increase efficiency.
- Implementation of electrical protection measures.

## 1.4 Limitations and Demarcations

The design and testing of the device is focused on the spectral power output and efficiency. This project does not evaluate how plants respond to spectral power output. The measurement of the spectral output is limited due to the absence of a spectroradiometer. Measurements are performed with a spectral sensor that only measures relative spectral intensity.

The aim of this project is not to design more complex components such as Direct Current (DC) converters and sensors from scratch, but instead to obtain Integrated Circuits (ICs) from commercial producers. These are incorporated into the design according to manufacturer guidelines.

The device is powered by a DC power supply to provide input voltage. In actual deployments, the device may be powered by a battery or a separate DC power supply, but no Battery Management System (BMS) is incorporated into the device. The device is relatively low powered with a total power budget of 60 W and a max input voltage of 30 V DC. Real applications may require a higher power consumption, but due to safety constrains and ease of manufacturing the power budget is set conservatively for this device.

In farming, the goal is to achieve high yields while minimizing the costs of production [1]. This project only studies the power use effectiveness of a LED-based artificial lighting solution. It does not encompass the feasibility of deploying the device, nor the market competitiveness of the device based. The only comparison is made in regards to light output efficiency and efficacy.

# 2
# Theory

This chapter outlines the theoretical background to provide a fundamental understanding of the concepts used for designing and implementing the device. Fundamental principles about the different electronics used is also presented to understand the theory used to dimension the system.

## 2.1 Indoor Plant Cultivation

The ability to cultivate plants, regardless of season and weather, is crucial to keep up with increasing demand for crops and other plants [8]. The solution to growing demand has mostly been the deployment of greenhouses, which with the help of supplemental lighting, enable longer growing seasons. Advanced farming solutions, such as Controlled Environment Agriculture (CEA) in which every aspect is optimized to the fullest extent, has become popular [9]. CEA can offer an increased crop yield, reduced production costs, and more predictable output. If implemented correctly, CEA can be used for crop production year around. Current areas of improvement are the efficiency of the artificial lighting, and the optimization of spectral composition produced by the artificial lighting [9], [10].

LEDs with their small size, high efficiency, long lifetime, and ability to produce specific wavelengths, have made them suitable for horticultural uses [9], [11]. Most of the testing on LEDs for plant growth has been conducted using LEDs with wavelengths in the Red Light (R) region (600–700 nm) paired with LEDs with wavelengths in the Blue Light (B) region (400–500 nm). Light composed of wavelengths in these two regions yield higher photosynthetic rates compared to plants grown with only R [11]. Modern CEAs are often deployed with adjustable 24-hour LED illumination. The artificial lighting system is programmed to emit a specific light spectrum that is optimal for photosynthesis at all times. The output changes depending on factors such as plant species, plant growth stage and time of day. The important metrics in optimizing the produced light are the spectral power distribution, total light intensity, as well as photoperiod [8]. To improve the overall efficiency of CEA, the light energy use efficiency has to be improved [10]. This can be achieved by optimizing the light for photosynthetic efficiency by understanding what effect different wavelengths have on photosynthesis [12]. Thus, it is essential to outline the biological mechanisms of plants that respond to light, and what impact different wavelengths have on processes that drive plant growth.

### 2.1.1 Plant Biology

Photosynthesis is the synthesis of carbohydrates and generation of oxygen using carbon dioxide and water. The carbohydrates act as energy storage and are used to power cellular processes [13]. The most active photosynthetic tissue in plants are the mesophyll of green leaves, which have a high concentration of chloroplasts, a specialized light absorbing pigment. The two primary light absorbing pigments are Chlorophyll *a* (Chl *a*) and Chlorophyll *b* (Chl *b*) [13]. These have absorption maxima around 430 nm and 662 nm, and around 453 nm and 642 nm respectively, as depicted in Figure 2.1.

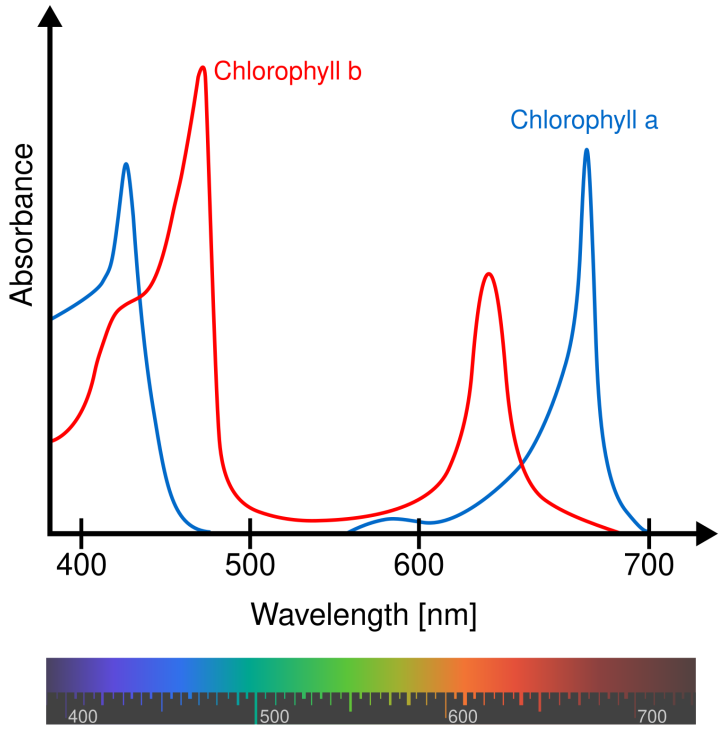


**Figure 2.1.** Absorption spectrum for Chl *a* and Chl *b* [14].

The light reactions, also called the thylakoid reactions take place in the internal membrane of the chloroplasts. These contain all the Chl *a* and Chl *b* and is the site of all light dependent reactions in photosynthesis [13]. The core principle is the process of excitation by light in Chl *a*, Chl *b*, and other pigments, in which an electron is promoted to a higher energy state. First, a low energy electron is excited and then transferred to the next photosystem, where it is excited again to create a Reduced Nicotinamide Adenine Dinucleotide Phosphate (NADPH) molecule. This process is commonly referred to as the Z-scheme.

#### 2.1.1.1 Thylakoid Reactions

The thylakoid membrane within the chloroplasts is made up of pigment-protein complexes where the light absorption spectrum of Chl *a*, Chl *b*, and other pigments are adjusted. The pigment-proteins constitute the antenna complex (also called Light-Harvesting Complex (LHC)) and the reaction centers in the membrane [13]. The LHC funnels the energy by reducing it in multiple steps, until it can be used in the reaction center. The reaction center is where the oxidation and reduction reactions take place that leads to the long term energy storage. The reaction center is similar across different plant species, while the LHC differs significantly, reflecting evolutionary adaptation [13].

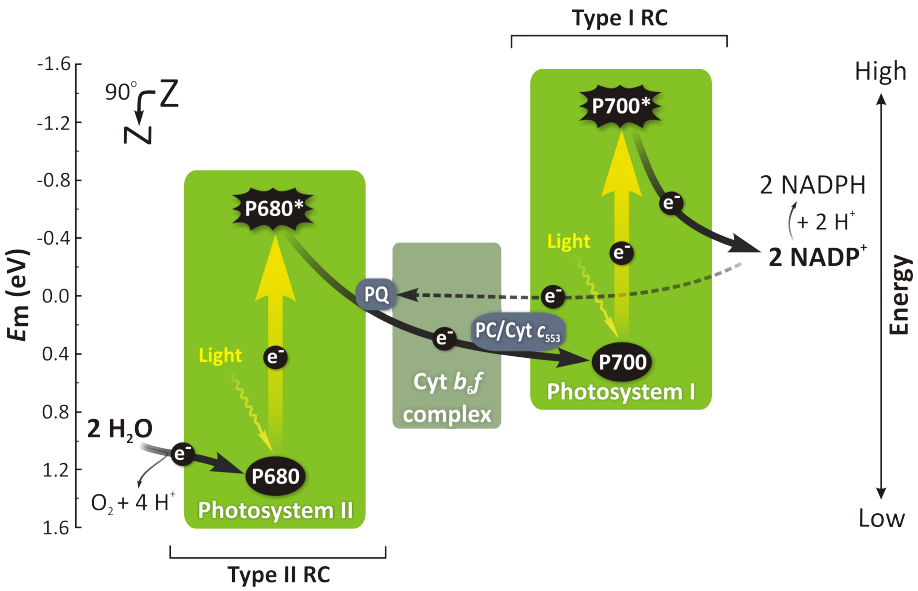


**Figure 2.2.** The electrons journey in energy and redox potential, visualized by the Z-scheme. The figure shows the two photosystems, as well as the electron transfer chain that connects the two [15].

Photosystem I (PSI) and Photosystem II (PSII), shown in Figure 2.2, contain the two photochemical complexes that carry out the energy storage reactions in the reaction center. PSI mainly absorbs Far-Red Light (FR) (wavelengths greater then 680 nm), whereas PSII preferentially absorbs R of 680 nm and is poorly driven by FR [13], [16]. The PSI reaction center contains P700 (absorbs maximally 700 nm) and the PSII reaction center contains P680 (absorbs maximally 680 nm).

The funneled energy from LHC excites P680 in PSII which starts the electron transfer chain. P680 is then re-reduced by oxidizing water which enables PSII to restart its cycle, as seen in Figure 2.2. The electron transfer chain transfers the electron from PSII to PSI through the Cytochrome $b_6f$ complex [13]. In PSI, P700 is excited, and the electron is ultimately used to reduce $NADP^+$ to NADPH, which is the goal of the Z-scheme. The electron delivered through the electron-transfer chain is then used to re-reduce P700, thus enabling PSI to restart its process. The way the elec-

tron moves through the Z-scheme is visualised in Figure 2.2.

Adenosine Triphosphate (ATP) production is driven by the proton concentration gradient over the thylakoid membrane. This electric potential forces the proton to pass through the enzyme complex ATP synthase, losing energy on the way which is used in the creation of ATP [13]. This proton gradient is achieved through the reactions inside both PSI and PSII during the Z-scheme, and processes during the electron-transfer chain.

A direct consequence of PSI and PSII operating in series are the red drop and enhancement effect found by Emerson [13]. The enhancement effect shows that if R and FR are supplied together, the rate of photosynthesis will be higher than the sum of the individual rates [12], [13]. This is explained by the over-excitation of PSII compared to PSI when exposed light composed of shorter wavelengths (400–670 nm) [12], [16]. This effect can be balanced by adding supplemental FR that preferentially excites PSI. When FR is added, there are indications that point to an increase in efficiency of photochemistry through an increase in the effectiveness of PSII [12]. The supplementing of FR needs to be regulated, as continuous exposure to FR decreases chlorophyll content [17]. This may decrease leaf photosynthetic capacity, thus lowering the effectiveness of PSII. Overall the information regarding the exact effects on different plants in response to FR is limited [17].

#### 2.1.1.2 Signals From Light

Light also serves as a signal to the plants and is responsible for the regulation of various developmental processes. This includes seed fermentation, fruit development, and directional cues for growth [13]. Photoreceptors are similar to pigments where they absorb a given wavelength. However, unlike the pigments, they then use the absorbed energy to send signals that initiate photoresponses rather than using the energy for energy storage reactions.

Phytochromes (phy) are one such receptor that mainly absorb R and FR (600–750 nm), but also some B (350–500 nm). The phy are responsible for photomorphogenesis (light-controlled development), such as stem growth or leaf expansion as well as seed germination [13]. For plants grown in dark environments, phy exists in an inactive state as a R absorbing form called Phytochrome red (Pr). Exposing Pr to R turns it into its active, FR absorbing form, Phytochrome far-red (Pfr). The R:FR ratio is what makes shade avoidance possible and determine if the plant has access to direct sunlight. A high Pr:Pfr ratio inhibits shade avoidance, meaning it will inhibit stem elongation, leading to a more compact growth while a low ratio will promote stem elongation [13], [17], [18]. The consequence of promoting stem elongation is that other processes need to be down-prioritized, such as the thickness and chlorophyll content of the leaves. In [18], it is also mentioned that a plant that is in shade avoidance for a long time will cause reduced branching, altered leaf development, and accelerated flowering. Some studies also attribute leaf expansion as a response to a low Pr:Pfr ratio [17]. This is done to increase the light interception

area of the plants when exposed to a low R:FR ratio.

Cryptochromes (cry), much like phy, play a large role in photomorphogenesis but respond only to B [13]. Cry are activated by exposure to B, when activated they act to suppress shade avoidance [18], meaning more B suppresses shade avoidance behavior. Green Light (G) can partially inhibit cry signaling, which means that lowering the B:G ratio by introducing more G will further in-activate cry [18]. Studies also show that absence (or low levels) of B increase stem elongation and leaf expansion, while high B inhibits stem elongation and gives more compact plants [19].

The Pr:Pfr ratio is also a critical regulator in photoperiodism, and consequently also the flowering of the plant. During the night, Pfr will slowly decay into Pr because of the absence of R [13]. Depending on the ratio at dawn, the plant can determine whether it was a long or a short night. This information can then be used by the plant to know when to flower. Introducing supplemental FR or R during the night or evening will then consequently lead to higher or lower ratios at dawn, which will influence the photoperiod of the plant. End-of-Day (EOD) FR is often used, which is a way to stimulate a longer night by influencing the Pr:Pfr ratio [17]. The cry also has an influences on the photoperiod and the circadian cycle where it interacts with phy to regulate flowering, growth timing, and metabolism cycles [13]. Both cry and phy are also major regulators of gene expression in plants, controlling processes such as chlorophyll synthesis, stress responses, and the expression of genes encoding light-harvesting proteins. Activating these photoreceptors is thus neccesary for multiple imporant aspects of plant development.

Phototropins (phot) responds to B and is the photoreceptor responsible for phototropism, which is the growth movement of plants towards or away from a directional light source [13], [18]. It also has important functions in optimizing light capture, protecting against high intensity light as well as opening the stomatal to allow intake of $CO_2$. Overall, responses by the different photoreceptors can be summarized as follows: phot optimize light capture and gas exchange in response to B as a near instant response system whereas cry and phy regulate plant development in response to B and R respectively over longer timescales [13].

### 2.1.2 Light Requirements

The wavelengths that make up the incident light on a plant canopy is imperative to the photosynthetic efficiency [1]. Likewise, the intensity of the light must be adequate for a plant to receive the energy it needs to sustain itself and grow. The exact light intensity and wavelength distribution that are most useful for plant growth depends on several factors. The plant species and its growth stage affect the light mix and minimum Photosynthetic Photon Flux Density (PPFD) required for growth.

Typically, R and B are absorbed at a greater rate than G, and are essential for the energy storage and plant growth. The exact light mixture, B:R:FR used in different

studies vary greatly. A PPFD at 200 μmol/(m$^2$s) with a light mixture that roughly corresponds to a 10:90:0 ratio, together with 50 μmol/(m$^2$s) of FR, was used by one study [17]. This proved that dry mass production of lettuce increased with 39% (FR day) and 25% (FR EOD) compared to when FR was not used. Studies also shows an increase in plant leaf area given FR supplementation [17], [20]. This follows from the fact that a low R:FR ratio will stimulate leaf expansion given a sufficient PPFD. It will on the other hand inhibit leaf expansion if PPFD is too low for plant growth [20]. This can be beneficial in earlier stages of growth when the total leaf area is too small to capture all of the incident light. FR supplementation can therefore stimulate leaf expansion and establish a larger effective leaf area earlier, and thus a larger light interception area [17]. Another study shows that growth and nutritional content relative to power consumption was optimal for lettuce and basil at a PPFD of 250 μmol/(m$^2$s), with a light mix of 25:75:0 [21]. According to one study [22], a ratio of 20:80:0 at 200–1000 μmol/(m$^2$s) is deemed an efficient mixture. Another study [12] uses a R and B mixture, which yields roughly 25:75:0 ratio at 50–750 μmol/(m$^2$s). Furthermore, a 110 μmol/(m$^2$s) FR was supplemented on top of the normal light mixture. This gives a reference to the required light intensity and light mixture.

## 2.2 Electronics

The following section covers the electronic components used in the device. The most important components that determine the final performance of the device are the LEDs and the buck converter powering the LEDs. The theory behind these devices will be covered to better understand how to best utilize these devices.

### 2.2.1 Pulse Width Modulation

Pulse width modulation (PWM) is a control method that changes the pulse width to regulate power. The duty cycle is the relative amount of time the signal is on compared to the total period time [23]. A higher duty cycle percentage gives a longer on duration, and a lower duty cycle means that the signal is off for a longer duration. The average current is given by evaluating the integral of current over a period and dividing it by the period time [24],

$$I_{\mathrm{d}} = \frac{1}{T_{\mathrm{s}}} \int_0^{T_{\mathrm{s}}} i_{\mathrm{d}}(t)\, dt. \tag{2.1}$$

Here, $I_{\mathrm{d}}$ is the average diode current over one period, $T_{\mathrm{s}}$ is the time period of the switching cycle and $i_{\mathrm{d}}(t)$ is the time variant current.

For a PWM signal, the duty cycle ($D$) can be computed as a ratio according to

$$D = \frac{\tau}{T_{\mathrm{s}}}, \tag{2.2}$$

where $\tau$ is the on-time period and $T_s$ is the period time. The duty cycle is a number between zero and one. Equation (2.1) can be simplified when the current is a PWM signal. The average current ($I_d$) can then be computed with the peak current ($\hat{\imath}_d$) and the previously computed duty cycle according to

$$I_d = \hat{\imath}_d \cdot D. \tag{2.3}$$

### 2.2.2 Light Emitting Diodes

LEDs are semiconductor devices based on diodes that produce light when conducting. They can produce different wavelengths depending on the band gap in the semiconductor junction [25]. During the last decades, developments in LEDs has enabled the mass manufacturing of LEDs with different wavelengths and power levels. The most significant development in LEDs has been the invention of the B LED which received the Nobel Prize in physics in 2014 [26].

LEDs have been one of the most significant developments in lighting since the first usage of incandescent bulbs in the 1800s [25]. LEDs can be manufactured to produce different spectral distributions. The light emission can be further adjusted with the usage of lenses, placed on top of the semiconductor junction, to filter or convert the light [27]. For example, with the aid of a phosphor lens a single LED can produce a wide spectrum, but this comes at the cost of efficiency. To produce white light from a single B LED the decrease in efficiency is 10–30% due to losses in the light conversion process. Depending on the composition of the substance used for conversion, the spectral output can be adjusted to better fit specific applications. The usage of phosphor lenses in combination with B LEDs allow for fulfilling the need for a wide spectral distribution of plants while reducing the required amount of different LEDs [28]. The usage of lenses is especially useful for farming purposes where covering the R and FR regions simultaneously is crucial for optimal plant development. A phosphor lens allows a single type of LED to fulfill the R and FR requirements simultaneously.

White LEDs are commonly used in farming application because of the lower costs [10]. The losses due to the conversion of the wavelength are not negligible, reducing the achievable efficiency compared to using LEDs without any conversion lens [29]. Using LEDs without any conversion lenses for grow lights requires multiple LEDs to be able to cover the necessary regions used for photosynthesis [1]. Another flaw with using white LEDs for plant growth is the substantial emission of green light which is not effectively used for photosynthesis [10].

The output intensity of a LED can be adjusted with dimming [23]. There are two ways to dim LEDs, current (analog) and PWM dimming. The preferred way to dim LEDs while minimizing spectral shift is to use PWM dimming. By rapidly turning on or off the LED, the average power of the LED can be adjusted, while the current through the LEDs is the same when the LEDs are turned on. PWM also allows for a larger dimming range. Dimming using current limits the power to a range

between 10–100% and has lower efficiency than using PWM dimming. Dimming multiple LEDs channel at once increases the complexity because the different LEDs do not behave identically. Their electrical and spectral properties change differently to changes in current and temperature.

Dimming LEDs with PWM requires a high frequency PWM signal to avoid perceivable flickering. There are claims that flickering can cause ailments such as headaches and migraines for humans, but to also trigger photosensitive epilepsy [30]. It is recommended to use a frequency above 90 Hz [31]. If a LED artificial lighting system is deployed in areas that are co-inhabited by humans, special consideration needs to be paid to the spectral output distribution as some color mixes can be perceived as uncomfortable [4].

LEDs will shift its spectral distribution as a consequence of changes in the junction temperature. Dimming the LEDs using PWM will result in smaller temperature changes compared to analog dimming [23]. The intensity also changes to a varying degree depending on the LED when the junction temperature changes. R LEDs are most susceptible to spectral shifts and also decrease in intensity faster relative to B and G when the junction temperature changes.

Changes in the intensity when dimming can be compensated for easily by increasing the duty cycle of the PWM signal [32]. A solution to manage the spectral peak shift caused by dimming is to improve the cooling of the LEDs. Another effect that is important to consider when configuring the cooling system is minimizing the thermal coupling of the LEDs. If the temperatures of the LEDs affect each other it makes developing a control system harder.

### 2.2.3 DC-DC Converters

DC-DC converters are a type of electronic circuit that changes the output DC voltage given an input DC voltage, either by increasing or decreasing it from one level to another [33]. A typical distinction of DC converters is between buck and boost converters. Buck converters are sometimes called step-down converters because the output voltage is always stepped down from the input voltage. Boost converters work in the opposite way by always increasing the voltage at the output side. Some converters can work in both ways, allowing the output voltage to be either higher or lower than the input voltage.

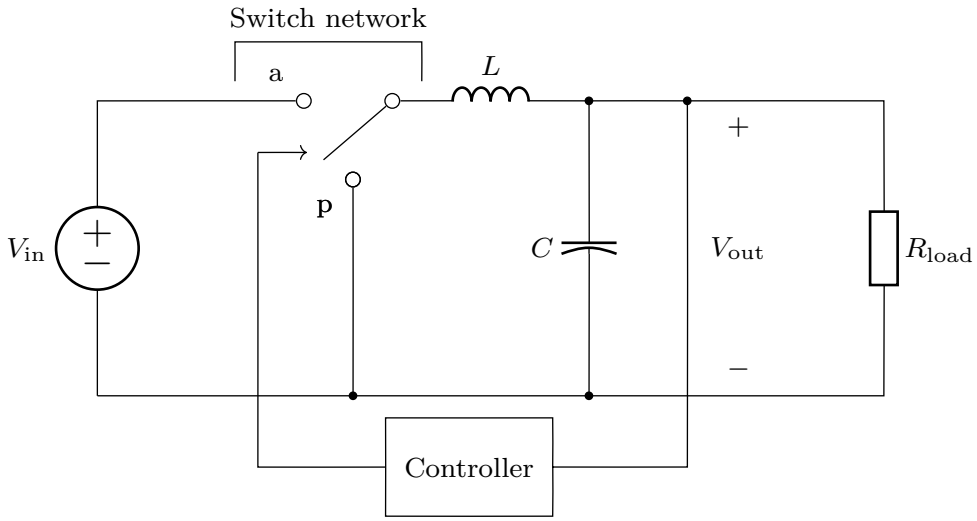


**Figure 2.3.** A simple buck converter that has input voltage $V_{\text{in}}$ and output voltage $V_{\text{out}}$. The load is represented as a resistor with the resistance $R_{\text{load}}$. The converter has a switching network consisting of a single-pole double-throw switch. The inductor and capacitor create an LC low-pass filter. A controller controls the switch.

A simple implementation of a buck converter works by charging and discharging an inductor and capacitance, and using a switch network to toggle the voltage over the inductor at a specific frequency, as can be seen in Figure 2.3. The switch network is often a semiconductor device, such as a MOSFET, that can break the circuit depending on a control signal created by a controller. To alter the output characteristics, like increasing the output current or output voltage, the timings of the switching can be adjusted by the controller. A control signal commonly used is a PWM signal. The duty cycle and frequency of the PWM are important parameters that control the output of the DC converter. In the implementation shown in Figure 2.3, the inductor and capacitor smooth out the voltage across the load. This simple DC converter has no energy loss when ideal components are used. The LC filter does not consume any power; the reactive power is continuously transferred between the capacitor and inductor.

If the DC converter is regulated, the converter has a control system to maintain constant output voltage. The implementation shown in Figure 2.3 has a closed loop feedback control circuit. The controller can sense the input voltage or current and is able to adjust the duty cycle to maintain a constant output voltage.

In actual deployments, the design of DC converters need to take different effects into account, such as the input voltage, load current changing over time, or the presence of ripple from the input source [33]. These effect can cause a closed loop control system to become unstable if not configure properly. It is therefore important to be able to analyse the DC converters and create models to describe their behavior to make sure that the control systems are stable.

The output capacitor of the DC converter acts as a low-pass filter. The low-pass filter has a cutoff frequency significantly lower than the fundamental frequency of the PWM switching signal so that only the DC component remains at the output. The higher frequency harmonic components are blocked by the low-pass filter. The output voltage $V_{\text{out}}$ can therefore, for an ideal buck converter, be simplified as a linear expression of the duty cycle and the input voltage $V_{\text{in}}$ according to

$$V_{\text{out}} = DV_{\text{in}}. \tag{2.4}$$

There are two different operational modes for DC converters: Continuous Conduction Mode (CCM) and Discontinuous Conduction Mode (DCM). These modes are separated by the behavior of the output current. For CCM converters, the output current is never allowed to become zero in the switching period. If the load resistance increases, the output current decreases and can become negative. Because the current cannot be negative, the resulting output current becomes zero. The current direction is enforced with a diode connected over the input and switch. This is because the energy is only allowed to flow from the input to the output. Equation (2.4) only holds true when the converter is operating in CCM mode. If the converter is in DCM, the equation for the output voltage becomes more complex.

Another typical distinction for duty cycle converters is whether they are isolated or non-isolated. Isolation refers to having electrical isolation between the input and output. This is typically done with the usage of transformers. The transformer breaks the galvanic connection and instead relies on inductive coupling between the input and output. This is typically used in application that require increased safety.

There are a variety of methods for controlling the duty cycle of DC converters. For instance, in voltage mode control, the controller uses the output voltage to adjust the duty cycle of the PWM signal [24]. In current mode control, the controller uses the output voltage as a reference and feedback from the inductor current to regulate the duty cycle [33]. There are different ways to implement current mode control. One example is Peak Current Mode control (PCM), where the peak of the inductor current is used for feedback.

## 2.3 Optical Physics and LED Metrics

As this thesis aims to use LEDs to provide light for plants, the characteristics of the emitted light needs to be understood to be able to dimension suitable LED arrays. First, the amount of light emitted by the LEDs is quantified. Second, the properties of the light propagating from the LED is considered in order to determine how much of the emitted light will reach a surface.

LEDs are considered imperfect Lambertian emitters [34], which means that the light intensity is the brightest perpendicular to the LED surface, but gets dimmer as the angle between the LED and plant increases. To determine the photon flux based

on the radiant flux of a single LED, the energy of each photon is determined using with Planck's equation [34],

$$E = \frac{hc}{\lambda}, \tag{2.5}$$

where $E$ denotes the energy of an individual photon in Joules (J). $\lambda$ represents the wavelength in meters, Planck's constant $h = 6.626 \cdot 10^{-34}$ Js, and $c$ denotes the speed of light in vacuum ($2.99 \cdot 10^8$ m/s). Assuming that the emitted light has wavelengths that are normally distributed around a dominant wavelength, the value of $E$ is the average energy of the photons emitted from a LED. The photon energy relative to the total radiant flux ($\Phi$) provided in the manufacturer's datasheet is then used to determine the Photosynthetic Photon Flux (PPF) of the LED. Thus, the radiant flux divided by the average photon energy provides the number of photon emitted by the LED per second. The PPF represents the total number of photons emitted per second within the PAR spectrum (400–700 nm), given in micromoles, and is determined by

$$\mathrm{PPF} = \frac{\Phi}{N_\mathrm{A} E}, \tag{2.6}$$

where $N_\mathrm{A}$ represents Avogadro's constant adjusted for micromolar units ($6.022 \cdot 10^{17}$ photons/µmol). By using the energy $E$ from Equation (2.6), the resulting PPF is expressed in µmol/s. This equation assumes that nearly all radiant flux pertains to light in the photosynthetic spectrum.

Light emitted from a LED is typically directional and comes in several different spatial distributions, oftentimes Gaussian or Cosine [35]. For many LEDs, the manufacturer provides an angle $\varphi$ relative to the central axis of the LED at which the light intensity has decreased by half. To simplify the distribution to aid with estimating incident PPFD this thesis assumes that all light emitted is constrained within this angle. It is also assumed that the incident light on a projected surface produced by this angle is uniformly distributed. If projected on a flat surface, the angle from the LED produces a cone. The base area of the cone is affected by the distance and the size of the viewing angle and contains all emitted light. The height can be considered as the distance ($h$) between the plant and the LED in our case. The radius ($r$) of the light cone from one LED is calculated using

$$r = h \cdot \tan\left(\frac{\varphi}{2}\right). \tag{2.7}$$

The equation for the cone radius is then used to calculate the area that is covered by that cone.

$$A_c = \pi \cdot r^2. \tag{2.8}$$

This simplified light distribution model is shown in Figure 2.4.

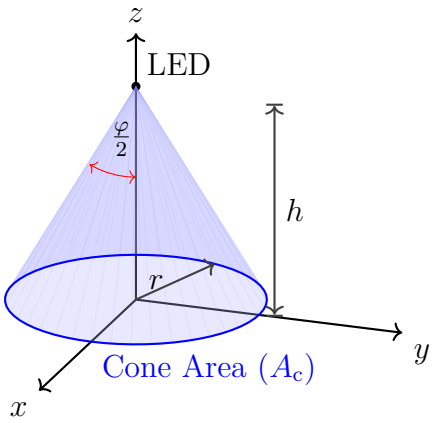


**Figure 2.4.** Visual representation of the area covered by the cone of the LED.

Figure 2.4 shows a model of the simplified distribution, where the LED projects an area on a target surface based on the angle ($\varphi$) at which the irradiance has decreased by half of the centroid intensity. The incident PPFD on the projected surface can be calculated with the PPF and the area of the cone using

$$\mathrm{PPFD}_{\mathrm{LED}} = \frac{\mathrm{PPF}}{A_{\mathrm{c}}}, \tag{2.9}$$

which can in turn be used to determine how many LEDs will be required for a certain PPFD on the target surface for a specific height. This also assumes that the LEDs are placed close enough and the target surface is far away enough that the cone surfaces overlap for the most part.

In reality, the PPFD on the cone area is likely different, as not all of the light emitted by the LED reaches the target area. These equations also do not take into account the effects of reflections. A LED with a radiation angle of 120°, for example, signifies that the radiant intensity is reduced by approximately 50% at ±60° from the optical axis, and is highest at 0°. Therefore, the incident light intensity on the target area is not uniform. Rather, it is concentrated in the center perpendicular to the LED, relative to the real distribution pattern of the particular LED. If the light distribution is regarded as uniform as the previous calculations assume, the calculated PPFD will be lower than the real peak intensity in the center and higher at the edges. Whilst imperfect, this method allows for a general conception of the PPFD from the LEDs for dimensioning the system.

## 2.4 Control Systems

Proportional–Integral-Derivative (PID) controllers are used in control systems for feedback to make the output of a process follow a target value [36]. In a basic model, a process only has one output $y$ that is fed into a controller. The controller

creates a signal $u$ based on the target $x$, and the output from the process $y$. The controller can calculate the signal in different ways. A simple controller takes the error $e$ between the target ($x$) and the output from the process ($y$), and scales this error with a constant term. The signal from the controller is used to impact the process and minimize the error from the output and target. If something in the process fluctuates and the output changes, the controller will try to eliminate the effect of the disturbance by tweaking the signal to the process to sustain the output close to the target value.

The PID regulator has three different terms that each use the error in different ways [36]. The error signal is calculated by taking the difference between the target $x(t)$ and the process output $y(t)$,

$$e(t) = x(t) - y(t). \tag{2.10}$$

The PID regulator can be described by a function that gives the signal $u(t)$ based on the error signal $e(t)$

$$u(t) = K_{\mathrm{p}} \cdot e(t) + K_{\mathrm{i}} \int_0^t e(\tau)\, d\tau + K_{\mathrm{d}} \frac{de(t)}{dt}. \tag{2.11}$$

The three terms are in order from left to right: the proportional error $K_{\mathrm{p}} \cdot e(t)$, the integral of the error $K_{\mathrm{i}} \int_0^t e(\tau)\, d\tau$, and the derivative of the error $K_{\mathrm{d}} \frac{de(t)}{dt}$. There are three constants in the regulator that describe the regulator properties [36]. The first one, $K_{\mathrm{p}}$, is called the proportional gain and effects only the error term. The second constant, $K_{\mathrm{i}}$, determines the strength of the integral action. The integral term is used to eliminate steady-state errors. The third constant is the derivative time $K_{\mathrm{d}}$ and impacts the derivative term in the controller. The derivative term is used to predict changes in the process by looking at how the error changes with time. The different regulator terms can be combined in different ways to change controller behavior. Some commonly used combinations are the P regulator, which is just the error term and proportional gain. Proportional–Integral (PI) regulators are also common and these include both the proportional and integral terms.

The use of microcontrollers for PID regulators allows the controller to update the regulator gain constants based on external sources [36]. For example, the user can increase the $K_{\mathrm{i}}$ constant to make the integral effect stronger. Microcontrollers also allows for adaptation of the regulator. Adaptation is where the regulator's gain constants are continuously updated. The microcontroller can for example calibrate the PID parameters by sending known signals to the system and studying the output. This is useful when the system behavior is unknown.

# 3
# System Design

The following sections outline the design process for the multi-channel LED system. By taking into account the power constraints and the determined light requirements, two separate PCBs were designed. The first is the lighting armature, consisting of a metal core PCB with LEDs of four different wavelengths. The LED PCB is driven by several synchronous buck-based LED drivers, the TPS92200 by Texas Instruments [37], placed on the second PCB. The LED drivers are controlled by an Arduino Nano [38], to regulate the average current delivered to the LED channels. The Arduino is connected to a Sparkfun AS7343 spectral sensor breakout board [39]. This provides optical feedback to control the duty cycle on the dim pin of the LED driver. The power board is designed to be supplied by a 30 V DC power supply. To be able to independently drive the Arduino, an auxiliary buck converter stage is added to step down the voltage from 30 V to 12 V. While the system was not designed to connect to a grid directly, protection stages are added for greater adaptability and safety. Thus, the intention is that it could theoretically be connected to the grid if a full bridge rectifier and another voltage regulator was added. The system could also be powered by a battery, but no BMS is included in the design. Figure 3.1 shows the block diagram and the overview of all parts of the system design.

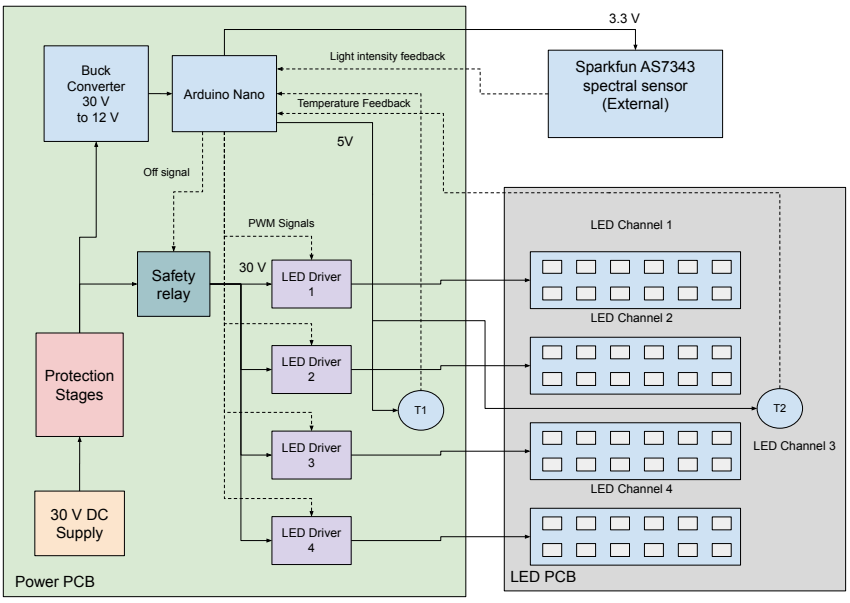


**Figure 3.1.** Overview of the entire system, represented with a block diagram.

The two PCBs in Figure 3.1 have different blocks in the diagram representing important components in the system. The system was designed by first determining the required specifications of the LED PCB, that provide the constraints to determine and select components for the LED drivers and the protection stages. The control system is implemented by considering the operational conditions of the LED drivers, and setting reference targets for each LED channel based on calibration done by calculating the duty cycle for each wavelength. KiCad is used to design the PCBs [40], and the Arduino Integrated Development Environment (IDE) is used to develop the control system for the microcontroller [41].

## 3.1 LED Selection and PCB Design

The choice of LEDs was dictated by a plant's need for specific wavelengths. The wavelengths of the LEDs are chosen to be 430, 450, 666 and 727 nm. The LED with 430 nm was chosen to match the absorption maxima for Chl *a* (Figure 2.2). The choice of LED with a 450 nm wavelength was made to match the absorption peak of Chl *b* (Figure 2.2). The LEDs with 430 and 450 nm are therefore covering these absorption maximums in the B region which is necessary for plant growth due to its interaction with photo-receptors cry and phot as discussed in section 2.1.1.2. The LED with 666 nm was chosen to match the absorption maxima for Chl *a* (Figure 2.2). The 727 nm LED is chosen instead of one corresponding to the absorption maxima of Chl *b* (~640 nm) because of the Emerson enhancement effect as well as the ability to use FR for signalling as discussed in section 2.1.1. The total required PPFD, denoted by $\mathrm{PPFD_{tot}}$ is set to 250 µmol/($\mathrm{m^2s}$) (denoted $\mathrm{PPFD_{nom}}$) at a distance of 0.2 m which was chosen according to the literature discussed in chapter 2.1.2, as well as the power budget being limited to 60 W. Multiple LEDs with different wavelengths are chosen because of the lower efficiency wide spectrum LEDs suffer from due to the light conversion process. More LED channels also allow for wider adjustability of the color spectrum.

### 3.1.1 LED Selection

High power LEDs corresponding with the wavelength set were selected with consideration made to the maximum supply voltage of 30 V while maintaining a high emission of light, or radiant flux. The LEDs chosen and their respective specifications are shown in Table I. These specifications have been gathered from the respective LEDs datasheets [42], [43], [44], [45].

**Table I.** The LEDs chosen by wavelength and typical electrical specifications.

| LED Name | Wavelength (nm) | Radiant Flux (W) | Viewing Angle (°) | Power (W) | Nominal Current (mA) | Forward Voltage (V) |
|---|---|---|---|---|---|---|
| GF CSSRML.24 | 727 | 0.465 | 120 | 0.644 | 350 | 1.84 |
| GH PUSRA1.25 | 666 | 1.113 | 130 | 1.302 | 700 | 1.86 |
| GD PUSRA2.15 | 450 | 1.474 | 125 | 1.981 | 700 | 2.83 |
| LTPL-C034UVH430 | 425 | 1 | 130 | 1.7 | 500 | 3.4 |

For each LED, their respective nominal wavelength, radiant flux, viewing angle and forward voltage are also listed in the table. These values are correct for the typical current. The power is calculated using the typical current and the corresponding forward voltage. Relevant maximum ratings, such as maximum forward voltage, current, junction temperature and thermal resistance are also considered as the design will use a current higher than typical. These are also listed in each LEDs respective datasheet and in Table II.

**Table II.** Maximum ratings for the LEDs.

| LED Name | Junction temperature (°C) | Thermal Resistance (°C/W) | Forward Current (mA) | Forward Voltage (V) |
|---|---|---|---|---|
| GF CSSRML.24 | 135 | 1.5 | 1000 | 2.20 |
| GH PUSRA1.25 | 135 | 0.41 | 1400 | 2.00 |
| GD PUSRA2.15 | 135 | 1.1 | 2000 | 2.95 |
| LTPL-C034UVH430 | 125 | 3 | 1000 | 4.4 |

The maximum forward voltage is rated for the nominal currents of the respective LEDs. The thermal resistance is between junction and solder, as well as for the first three LEDs it is within the standard deviation of $6\sigma$, the final LED has a measurement tolerance of 10%. The specifications for each LED given by Tables I and II were used to dimension the LED armature according to the desired PPFD and color mixture. This is done using the PPF, provided either in the datasheets or calculated using the radiant flux given and wavelength in Table I using Equations (2.5) and (2.6). The cone area ($A_c$) of each led is calculated using the Equations (2.7) and (2.8) in section 2.3. The number of LEDs ($n_{\text{LEDs}}$) needed is calculated using Equation (3.1).

$$n_{\text{LEDs}} = K_{\text{PPFD}} \cdot \frac{\text{PPFD}_{\text{tot}}}{\text{PPFD}_{\text{LED}}} = K_{\text{PPFD}} \cdot \frac{A_c \cdot \text{PPFD}_{\text{tot}}}{\text{PPF}_{\text{LED}}}. \tag{3.1}$$

Here, $K_{\text{PPFD}}$ refers to the relative contribution of a specific LED channel to the $\text{PPFD}_{\text{tot}}$ as a fraction from 0 to 1. The sum of each $K_{\text{PPFD}}$ corresponding to the different LED channels is equal to 1. Thus for any LED, the number of LEDs needed is based on the required PPFD of that wavelength, the cone area and PPF of the LED. Using the number of LEDs, rounded up to the nearest integer, the requirements for the LED channels were specified with regards to target voltage and current.

The value of $K_{\text{PPFD}}$ is based on the significance of each wavelength as to say the B:R:FR ratio as discussed in section 2.1.1 and 2.1.2. It was determined based on the same sections, that a light mixture of 80% R + FR and 20% B will be used as the nominal light mixture. The R:FR ratio was set to 7 which establishes R as the main energy provider and FR as a complement which aligns well with other studies and theory discussed in section 2.1.1 and 2.1.2. The number of LEDs with 425 and 450 nm are designed to contribute to the B at the ratio 1:1, meaning 10% respectively of $\text{PPFD}_{\text{tot}}$ to cover the absorption maximum for Chl *a* and Chl *b* equally. This light mix was thus denoted by $K_{\text{nom}}$ and gets the following ratio 20:70:10 (where $K_{\text{PPFD}}$

for the B is split equally between the two LED channels). This is presented in Table III which shows the necessary amount of LEDs for each wavelength.

**Table III.** The number of LEDs of each wavelength required for the desired PPFD.

| **Wavelength (nm)** | $K_{\mathrm{PPFD}}$ | $A_{\mathrm{c}}$ **(m²)** | PPF **(µmol/s)** | **Number of LEDs** |
|---|---|---|---|---|
| 727 | 0.1 | 0.45 | 2.80 | 4 |
| 666 | 0.7 | 0.58 | 5.85 | 18 |
| 450 | 0.1 | 0.38 | 5.50 | 3 |
| 425 | 0.1 | 0.58 | 3.55 | 5 |

Table III shows the number of LEDs of each wavelength, calculated using their corresponding cone area, PPF and the chosen $K_{\mathrm{PPFD}}$ value. In descending order, 18, 5, 4 and 3 LEDs were required for the desired $\mathrm{PPFD}_{\mathrm{nom}}$. This then gives the electrical specifications for the LED channel based on the nominal forward voltage and nominal currents of the LEDs in Table IV. The power loss is determined by the electrical power dissipated by the LEDs minus the radiant flux given in Table I.

**Table IV.** Electrical specifications of each LED channel.

| **Wavelength (nm)** | **Number of LEDs** | **Forward Voltage (V)** | **Current (mA)** | **Power Dissipation (W)** | **Power Loss (W)** |
|---|---|---|---|---|---|
| 727 | 4 | 7.36 | 350 | 2.576 | 0.716 |
| 666 | 18 | 33.48 | 700 | 23.436 | 3.402 |
| 450 | 3 | 8.49 | 700 | 2.576 | 0.716 |
| 425 | 5 | 17.00 | 500 | 8.500 | 3.500 |

All channels except one has a total forward voltage below 30 V according to Table IV. To lower the series forward voltage of the 666 nm channel, the $K_{\mathrm{PPFD}}$ value was adjusted to 0.6, thus requiring 3 fewer LEDs. Using the datasheet of the LED, it was also determined that at a higher forward current of 800 mA the radiant flux would increase enough to require one fewer LED. Since the $K_{\mathrm{PPFD}}$ value of the 666 nm was changed, the $K_{\mathrm{PPFD}}$ value for the 727 nm channel was increased to 0.2 to reach the sum of 1. Taking this into account, the nominal light mix $K_{\mathrm{nom}}$ is updated to 20:60:20. Finally, this resulted in the following dimensions for the LED device as shown in Table V.

**Table V.** The number of LEDs of each wavelength required for the desired PPFD.

| **Wavelength (nm)** | **Number of LEDs** | **Forward Voltage (V)** | **Current (mA)** | **Power Dissipation (W)** | **Power Loss (W)** |
|---|---|---|---|---|---|
| 727 | 7 | 12.88 | 350 | 4.508 | 1.253 |
| 666 | 14 | 26.04 | 800 | 20.832 | 3.692 |
| 450 | 3 | 8.49 | 700 | 2.576 | 0.716 |
| 425 | 5 | 17.00 | 500 | 8.500 | 3.500 |

The specifications of Table V form the basis upon which the LED driver circuit will need to be designed for. The choice was made such that the channel with the highest number of LEDs would be placed outermost, and the other channels closer

to the center descending by the number of LEDs.

### 3.1.2 PCB Design

When designing the PCB containing the LEDs, there are two main factors that are important to consider. Firstly is placing the LEDs concentrically and close enough such that the light from each wavelength will be at the desired intensity on the target surface when used in combination. Optimal placement in this way also ensures that the sensor will measure each wavelength with a relative intensity that is close to the same angle relative to every LED. The dense placement of the LEDs allows for simplifications in the equation used to calculate PPFD. The second consideration is heat management. The LEDs will emit a significant amount of energy as heat, shown in Table V. It will therefore be necessary to have effective heat dissipation in the PCB to avoid overheating the LEDs. Consequently, an aluminium metal core PCB was chosen to aid in thermal transfer. The PCB was mounted on top of a heatsink with screws and thermal paste between.

Using a metal core PCB presented important design considerations, as this PCB is limited to having traces on a single layer. This restricted the placement of the LED. The placement of the LED had to allow routing of traces without any traces crossing each other as vias could not be used. Because each LED channel negative lead is connected to a sense resistor, the bottom layer could also not be used as a ground plane. Thus, the LED channels were traced as loops, which introduces the risk of mutual- and self inductance. The magnetic field generated by the current in one loop will interfere with the magnetic field of the other loops, while also affecting the magnetic field in other segments as the trace bend [46]. Loop area was therefore minimized by having the return trace back track along the route of the LEDs, and by having the polarity of every other channel in the opposite direction in an attempt to avoid amplifying magnetic fields of the inner channels. The layout of the LEDs is shown in Figure 3.2.

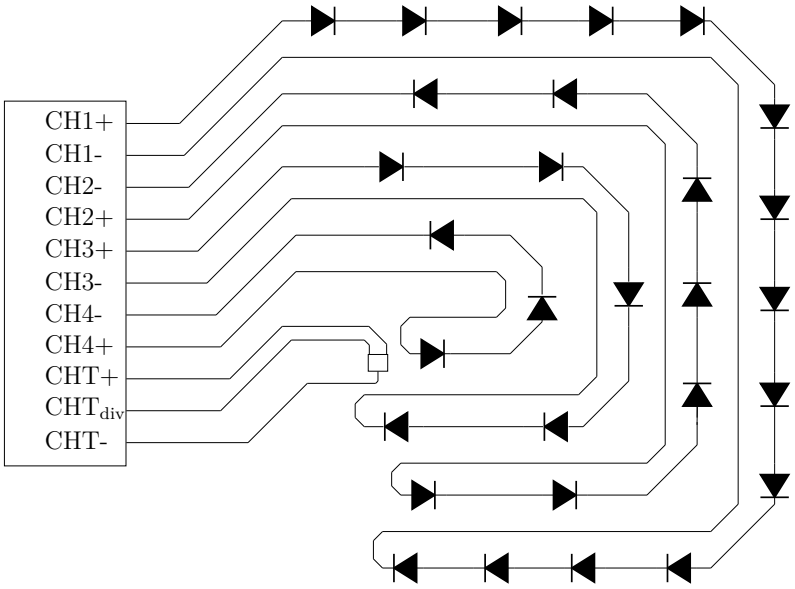


**Figure 3.2.** The schematic of the LED PCB, illustrating the measures taken to minimize interference.

### 3.1.3 Thermal Dimensioning

The ambient temperature is variable depending on the environment, but the application of a grow-light system is primarily indoors, or during colder seasons. In Gothenburg the maximum temperature recorded during the period between October to March was 21.3 °C for the years 1961-2026 [47]. A potential application of the project is inside a greenhouse which can add between 10–15 °C to the ambient temperature during periods with high sun activity. Taking this into account gives 35 °C as a worst case estimate of the ambient temperature for the purposes of the thermal calculations.

The thermal calculations assume that the LEDs will dissipate heat evenly across the PCB, due to them being spaced symmetrically and evenly. The thermal resistance of soldering and thermal paste were considered, but not taken into account for the final calculations since their contributions are much smaller than those of the LEDs and PCB. It was deemed that the omission of these thermal resistances does not impact the heatsink selection considering the safety margin also involved. Since the highest junction temperature of the LEDs are 125 °C, that was used as the maximum junction temperature for dimensioning the heat sink. Likewise, the worst case thermal resistance between junction to solder, as seen in Table II, is 3.3 °C/W, when the measuring error is taken into account. The thermal resistance of the LED PCB is estimated with [46],

$$R_{\text{th,PCB}} = \frac{t}{\lambda A}, \tag{3.2}$$

where $t$ is the thickness of the PCB, $\lambda$ is the thermal conductivity, and $A$ is the area of the board. The board has a width of 89.5 mm, height of 74.5 mm and thickness

of 1.6 mm. The board has a thermal conductivity of 1 $\mathrm{W} \cdot \mathrm{m}^{-1} \cdot \mathrm{K}^{-1}$ in the vertical path, specified by the manufacturer. Thus the thermal resistance of the LED PCB is estimated as 0.24 °C/W. Similarly, if the board would be constructed using FR-4, a common material for PCBs that has a thermal conductivity of 0.29 $\mathrm{W} \cdot \mathrm{m}^{-1} \cdot \mathrm{K}^{-1}$ [48], the thermal resistance of the PCB would be 0.83 °C/W.
Excluding the contributions from solder and thermal epoxy, the maximum required thermal resistance of the heat sink can be obtained from the worst case thermal path

$$T_{\text{junction}} = T_{\text{ambient}} + P_{\text{tot}}(R_{\text{th}} + R_{\text{th,PCB}} + R_{\text{th,heatsink}}), \tag{3.3}$$

where $P_{\text{tot}}$ is the total dissipated power and $R_{\text{th}}$ is the junction to solder thermal resistance of the LED LTPL-C034UVH430. The LEDs are thermally connected in parallel, but $P_{\text{tot}}$ is assumed to flow through the thermal path of a single LED. While not physically correct, it offers a conservative estimate of the junction temperature. Isolating the variable $R_{\text{th,heatsink}}$ gives

$$R_{\text{th,heatsink}} = \frac{T_{\text{junction}} - T_{\text{ambient}}}{P_{\text{tot}}} - R_{\text{th,LED}} - R_{\text{th,PCB}}, \tag{3.4}$$

that, using the values from Table II, Table V as well as the thermal resistance of the PCB gives the required thermal resistance of the heatsink, 6.28 °C/W. Considering the dimensions of the LED PCB that is mounted onto the heatsink, a heatsink with the dimension of 100 mm for both width and height was chosen [49]. The corresponding thermal resistance is around 2.4 °C/W when running passively, that is without fans or other external cooling. The lower thermal resistance accounts for the ignored thermal resistances of solder and thermal paste sections, it also gives a safety margin in the case of a higher ambient temperature.

## 3.2 LED Driver Configuration

For this project a LED driver IC is used as a buck converter to power the LEDs. The chosen LED driver is by Texas Instruments and the article number is TPS92200D1 [37]. The TPS92200D1 has a maximum input voltage of 30 V and maximum output current of 1.5 A, this is suitable for the project constraints and the chosen LEDs. The LED driver is configured to operate in PWM mode. In PWM dimming mode the dimming range can be between 0–100%, but is restricted by the need for whole percentages. TPS92200D1 can operate in both dimming modes depending on the voltage on the DIM pin. If analog dimming mode is desired the voltage on the DIM pin has to be set between 0.65 and 1.3 V. The LED driver is a PCM controlled synchronous buck converter [37]. TPS92200D1 has integrated low and high side MOSFETs to reduce external component use and improve power density. The TPS92200D1 has an internal clock with a frequency of 1 MHz used for PCM.

It is easier to adjust LEDs output based on current rather than voltage due to the highly exponential current voltage characteristics of LEDs [23]. This makes a PCM DC converter suitable to drive the LEDs. A feedback voltage $V_{\text{FB}}$ is used as a

reference for the PCM. The TPS92200 obtains this feedback voltage from the LED forward current by measuring the voltage over a sense resistor placed between the negative terminal of the LEDs and ground. The PCM control loop regulates the converter such that the feedback voltage equals the fixed internal reference voltage $V_{\text{ref}}$ of 99 mV. The desired maximum current through the LEDs, $I_{\text{LED}}$ is set by adjusting the value of the sense resistor accordingly:

$$R_{\text{sense}} = \frac{V_{\text{ref}}}{I_{\text{LED}}}. \tag{3.5}$$

The control loop of the PCM is composed of an error amplifier that amplifies the error between the reference voltage $V_{\text{ref}}$ and the feedback voltage $V_{\text{FB}}$. In a control system the gain of this error amplifier is desired to be as high as possible in order to minimize the steady-state error and ensure accurate regulation of the output. From this voltage comparator a control voltage $V_{\text{comp}}$ is produced. Similar to the basic PCM controller, the high side switch is turned off when the peak value of inductor current reaches the level set by $V_{\text{comp}}$ . Additionally, to prevent sub-harmonic oscillations that are common for PCM converters, the device implements slope compensating circuitry [37].

Necessary input and output components were selected based on the electrical specifications of each LED channel and constraints of the LED driver according to the datasheet. The schematic of the LED driver channels shown in Figure 3.3. The layout of the components for the LED driver on the PCB was made according to recommendations in the datasheet for the TPS92200 [37].

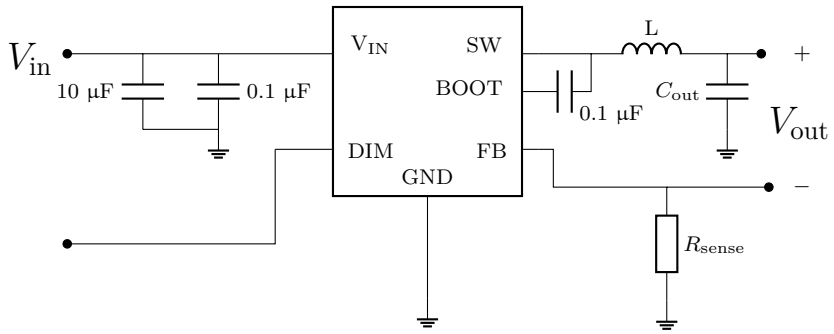


**Figure 3.3.** The schematic of a LED channel, without values for the inductor, output capacitor and sense resistor.

Figure 3.3 shows the diagram of one channel where the inductor, output capacitors and sense resistors are to be calculated. Figure 3.3 gives an overview of the connections to the LED drivers, where the DIM pin is connected to a microcontroller and the $V_{\text{in}}$ pin is supplied by the 30 V DC power supply. The bootstrap capacitor and input filter capacitors were chosen based on the recommendations provided in the datasheet [37]. A 10 µF and a 0.1 µF capacitor were thus selected for input capacitors as shown in Figure 3.3 alongside another 0.1 µF capacitor for the bootstrap capacitor. According to the datasheet, and as Equation (3.5) suggests, the sense resistor in Figure 3.3 was chosen based on the intended voltage drop of 99 mV

at max current. As shown in Table II the GD PUSRA2.15 LED has a maximum forward current of 2000 mA, which however is limited to 1400 mA [43]. This is mainly because the TPS99220 can only provide up to 1500 mA. It was also deemed unnecessary to allow the LED to increase the current that much beyond the calculated necessary amount. The maximum current from Table II and Equation (3.5) were used to calculate the chosen sense resistance values as shown in Table VI.

**Table VI.** Calculated sense resistor values.

| **Channel Wavelength (nm)** | $R_{\text{sense}}$ **(mΩ)** |
|---|---|
| 666 | 70 |
| 727 | 100 |
| 425 | 100 |
| 450 | 70 |

Table VI shows that each channel, except for 450 nm was dimensioned for maximum permissible sustained forward current as shown in Table II. This is as opposed to the typical forward current in Table I that was used to dimension the number of LEDs. This is relevant since the radiant flux of the LEDs increases as the forward current increases. As a result, the LED channels would be capable of producing higher photon flux than was strictly needed for the nominal light mix that the system was dimensioned for. This allowed for greater flexibility in light mixing and total PPFD supply. The inductors then had to be chosen, taking into account several constraints of the LED driver. The TPS92200 recommends at least 300 mA of ripple current, while also being less than 60% of the maximum LED current. Thus, the inductance was chosen first to satisfy the minimum ripple current $I_{L(\text{ripple})}$ by deriving the required inductance,

$$I_{L(\text{ripple})} = \frac{V_{\text{out}} \cdot (V_{V\text{in(max)}} - V_{\text{out}})}{V_{V\text{in(max)}} \cdot L \cdot f_{\text{SW}}}, \tag{3.6}$$

where $V_{\text{out}}$ refers to the voltage drop of the LED string and sense resistor. $V_{\text{in}}$ is the supply voltage to the LED driver, which is 30 V in this case. The value of $V_{\text{out}}$ used for each channel is given in Table V and $f_{\text{SW}}$ is the switching frequency of the driver, which is 1 MHz. Using the minimum ripple current the required inductance was determined by switching places of $L$ and $I_{L(\text{ripple})}$:

$$L \leq \frac{V_{\text{out}} \cdot (V_{V\text{in(max)}} - V_{\text{out}})}{V_{V\text{in(max)}} \cdot 0.3 \cdot f_{\text{SW}}}. \tag{3.7}$$

As the ripple current increases, the inductance value decreases, thus the inductance needs to lower than or equal to the right hand side of the inequality. Equation (3.8) was then used to verify that the value $K_{\text{ind}}$ was below 0.6. The inductance was chosen with of margin above 300 mA, while reatining the $K_{\text{ind}}$ below 0.6.

$$L = \frac{V_{\text{out}} \cdot (V_{V\text{in(max)}} - V_{\text{out}})}{V_{V\text{in(max)}} \cdot K_{\text{ind}} \cdot I_{\text{LED}} \cdot f_{\text{SW}}}. \tag{3.8}$$

The value of $I_{\text{LED}}$ was the same as the value used for determining the sense resistor, which is the maximum LED current. Once again, the value for $K_{\text{ind}}$ was determined by swapping places with the chosen value for $L$ in Equation (3.8). It was also verified that the peak current which the driver would need to drive would not breach the low-side sinking or sourcing limit of the LED driver accordingly. The peak inductor current was calculated as,

$$I_{L(\text{peak})} = I_{\text{LED}} + \frac{I_{L(\text{ripple})}}{2} \tag{3.9}$$

The inductor for each channel was finally chosen using the final value of $L$, and with ample margin for the saturation current. The required inductance, the chosen and the final value of $K_{\text{ind}}$ is presented in Table VII below.

**Table VII.** Inductance calculations and chosen inductor values for LED drivers.

| Channel | Maximum Inductance (µH) | Chosen Inductance (µH) | Resulting Ripple Current (mA) | $K$ Value | Peak Current (mA) |
|---|---|---|---|---|---|
| 1 | 10.9 | 10 | 328 | 0.5 | 1750 |
| 2 | 24.6 | 15 | 491 | 0.5 | 1250 |
| 3 | 24.5 | 15 | 489 | 0.5 | 1240 |
| 4 | 20.6 | 15 | 412 | 0.3 | 1610 |

Table VII provides the maximum inductor current, alongside the chosen inductance and result inductor ripple current. Once the inductor for each channel was chosen, the output capacitor shown in Figure 3.3 could be determined. The output capacitor serves to filter the current to provide a steady current to the LEDs, and is placed in parallel to the LED string and sense resistor. According to the datasheet, the output capacitance is calculated by first determining the dynamic resistance of the LED string, which can then be used to determine the low side impedance. Finally, the output impedance is then used to calculate the desired minimum output capacitance. The dynamic resistance refers to the proportional increase in LED resistance relative to forward voltage and current. Using voltage/current relations for each LED found in their respective datasheet [42], [43], [44], [45], the dynamic resistance was calculated using Equation (3.10) found in the datasheet for the TPS92200D1 [37].

$$R_{\text{LED}} = \frac{\Delta V_{\text{f}}}{\Delta I_{\text{f}}} \cdot n_{\text{LEDs}} = \frac{V_{\text{f(peak)}} - V_{\text{f(typ)}}}{I_{\text{f(peak)}} - I_{\text{f(typ)}}} \cdot n_{\text{LEDs}} \tag{3.10}$$

For each channel, the number of LEDs is given in Table V. The dynamic resistance of each LED string was used to calculate the output impedance with Equation (3.11) provided in the datasheet [37]:

$$Z_{C\text{out}} = \frac{(R_{\text{LED}} + R_{\text{sense}}) \cdot I_{\text{LED(ripple)}}}{I_{L(\text{ripple})} - I_{\text{LED(ripple)}}}. \tag{3.11}$$

The equation uses the sense resistance $R_{\text{sense}}$ given in Table VI and inductor ripple current $I_{L(\text{ripple})}$ from Table VII. Imperative to the output impedance is the LED ripple current $I_{\text{LED(ripple)}}$, as this is a design constraint that determines how much the current through LEDs is allowed to fluctuate. The datasheet suggests a maximum LED ripple current of 20 mA. Finally, the output capacitance was calculated with

$$C_{\text{out}} = \frac{1}{2\pi \cdot f_{\text{SW}} \cdot Z_{C_{\text{out}}}}. \tag{3.12}$$

The frequency $f_{\text{SW}}$ is the switching frequency of the LED driver selected, which is 1 MHz. Using this value, a suitable output capacitor was chosen. Note that this value is minimum capacitance. The choice of output capacitor constrains the permissible LED ripple current. This is the fluctuations of the current through the LED relative to the ripple current through the inductor. Peak current through any LED should never exceed the maximum forward current, excess ripple current can momentarily cause this, hence it has to be filtered. Table VIII shows the calculated dynamic resistance, output impedance, minimum capacitance and the capacitance chosen with significant margin.

**Table VIII.** Output impedance and capacitance values based on dynamic resistance.

| Channel | Dynamic Resistance, $R_{\text{LED}}$ (Ω) | Output Impedance, $Z_{\text{out}}$ (mΩ) | Output Capacitance, $C_{\text{out}}$ (µF) | Chosen Capacitance (µF) |
|---|---|---|---|---|
| 1 | 3.80 | 56.1 | 2.84 | 4.7 |
| 2 | 3.33 | 70.2 | 2.27 | 4.7 |
| 3 | 3.5 | 73.4 | 2.17 | 4.7 |
| 4 | 0.825 | 13.0 | 1.30 | 10 |

Table VIII provides the minimum output capacitance for each channel, and the final chosen capacitance. For all but the 450 nm channel, the output capacitor was chosen with margin for ripple current, while the 450 nm was chosen based on part availability, resulting in somewhat larger ripple current. As the datasheet suggests, the capacitor was chosen from the Murata X7R series of ceramic capacitors with sufficient voltage headroom of 50 V.

## 3.3 Control System

To control the brightness of each LED channel, the dim pin of the LED driver is connected to a PWM signal that is created by a microcontroller. In this project, an Arduino Nano was selected as the microcontroller. While the Arduino Nano was supplied with power by a computer when programming, it is meant to be able to operate solely using the 30 V power on the board [38]. As a result, an auxiliary buck converter was added to the power board design to step down the voltage to 12 V to supply the microcontroller. The LM2596S-12 was chosen as auxiliary buck converter [50]. To be able to measure and adjust the light emitted by the LEDs a control system program was developed. Using the data from the Sparkfun AS7343 spectral sensor connected to the Arduino, the references for each wavelengths were calibrated based on nominal PWM calculated to provide adequate light.

The Arduino Nano can be powered either by a 5 V regulated supply, or by a unregulated 7–15 V supply connected to the $V_{\text{in}}$ pin which is regulated by a Low-Dropout (LDO) with a maximum output current of 800 mA [38]. The LM2596S-12 voltage regulator has a maximum 40 V voltage and provides a 12 V output and can be

dimensioned for different current requirements, it was chosen as a suitable auxiliary buck converter to supply the Arduino. Similar to the main synchronous buck based LED driver, the auxiliary buck converter requires selection of output capacitor and inductor. Unlike the LED driver, the auxiliary buck is not synchronous. Thus, a catch-diode was also required to be selected. The selection of the components for the buck converter was made according to its datasheet [50]. Figure 3.4 shows the block diagram of the auxiliary buck converter, with input and output components.

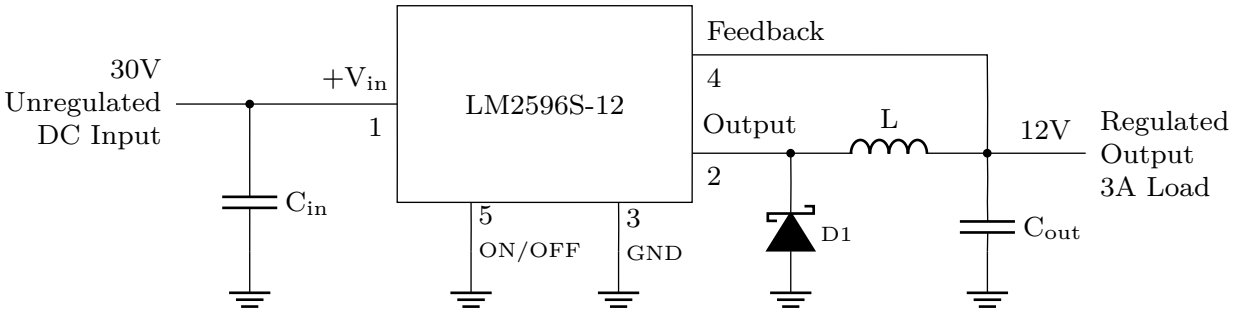


**Figure 3.4.** Block diagram of voltage regulator (LM2596S-12V) with external components.

In Figure 3.4 the inductor, catch diode and output capacitor are the components that were selected. The input capacitors were not selected, as the input voltage filtering is handled by the filter stage before the buck converter. To have some margin in the input voltage it was also dimensioned for 40 V input. Using a maximum output current of 1 A, the inductor was chosen to 220 µH and the output capacitor was chosen to 82 µF according to the datasheet [50]. A SK35 catch diode was chosen in a similar fashion.

## 3.4 Control System Design

The control system was designed in the Arduino's IDE [41], see Appendix A for the final code. All the used pins on the microcontroller were coded according to the PCB design, along with the pin datasheet for the Arduino Nano [51]. A 14 channel spectral sensor AS7343 was used to measure the spectral output of the LEDs, measure ambient light and to allow for calibration. The light sensor chosen has 14 different sensors corresponding to 14 different wavelengths [39]. As the LED PCB consists of four channels with the wavelengths (425 nm, 450 nm, 666 nm, 727 nm), the sensor's four closest wavelengths to those of the LEDs were used in the code. These channels chosen on the sensor and what wavelength they have their sensitivity peaks are as follows: F2 (425 nm), FZ (450 nm), F6 (640 nm) and F8 (745 nm). An Arduino library developed by SparkFun specifically for the AS7343 sensor was used in testing and integrated to the final code [52].

The code is initialized by calculating the PWM for each channel according to Equation (3.16). The output written to each corresponding pin using the analogWrite()

function to turn on the LEDs. The analogWrite() function's purpose is to create an approximate analog signal with the use of PWM [53]. The function can generate a signal with the duty cycle ranging from 0–100%. The function has an input which decides the duty cycle. The input has to be within the range of 0 to 255, where the highest value of 255 is 100% duty cycle. The analogWrite function on the Arduino Nano creates a PWM signal with a frequency of 490 Hz [38]. This frequency is high enough to avoid perceivable flickering.

After the LEDs are turned on there is a 5 second delay and the light sensor measures the light. The light measured by the sensor during this period will be used as the desired target/reference value. The system then activates a controller to regulate PWM signals to try to keep the process output constant and equal to the reference. The regulator is built into the `loop()` in the Arduino code and updates the PWM values continuously based on the light sensor readings. The regulator used is a PI regulator. If a faster control system is desired a PID regulator can be used. The PI regulator takes the calibrated target values and compares it to the current light measurement to give an error value. To avoid steady state error and improve the stability of the system, the proportional and integral coefficients were set by trial and error to $K_\mathrm{p} = 0.1$ and $K_\mathrm{i} = 0.09$. The PI regulator calculates the new PWM values for each channel and writes them to the corresponding channel pins.

To get useful readings from the light sensor the integration time and gain have to be set correctly. Sufficient integration time ensures that the sensor averages the light over multiple pulse widths. By setting adequate gain, crosstalk will be reduced. The crosstalk in this context is when a sensor is activated by a wavelength sensor outside its supposed wavelength sensitivity range. Too low integration time also introduces non-wanted sampling effects in the case of where the integration time is close or less than the period time of the PWM signal.

The gain setting on the AS7343 sensor set by the AGAIN variable [39]. The AGAIN can have values ranging from 0.5x to 2048x. The gain can only be set to discrete values. These values are in multiples of two and can be found in the AS7343 datasheet. The default value is set to 256x. The value of AGAIN can be set by writing to the 0xC6 register on the light sensor. If the Sparkfun AS7343 library is used AGAIN can be changed with the function if `setAgain()` [52]. The integration time can also be changed on the sensor but the process is more complex as the integration time is made up of two separate variables ASTEP and ATIME [39]. These two variables affect the total integration time of the sensor and both have to be considered when changing the integration time. The equation that describes the integration time is as such:

$$t_\mathrm{int} = (\mathrm{ATIME} + 1) \cdot (\mathrm{ASTEP} + 1) \cdot 2.78\ \mu\mathrm{s}, \tag{3.13}$$

where $t_\mathrm{int}$ is the total integration time in milliseconds. ATIME is the number of integration steps. ATIME can have an integer value between 0 and 254. The default value is zero and the value can be set by editing address 0x81. ASTEP sets the integration time per step in increments of 2.78 µs. The default value is 999. ASTEP

is set in the addresses 0xCA and 0xCA. The least significant bits [7:0] in 0xCA and most significant bits [15:8] in 0xCB. To edit the value of ASTEP manually or edit ATIME without the use of the Sparkfun AS7343 library the bits can be set with the Wire library. The Wire library is an Arduino specific library and is used to communicate with I2C devices [54]. To edit the contents of the registers a function `writeRegister()` is defined using functions find in the Wire library.

Thermistors were connected to Arduino pins A0 and A1 and were used to monitor temperatures as well as to prevent potential overheating. The values read from the pins had to be converted to a temperature according to both Arduino Nano and thermistor functions. In order to decrease the PWM, a function was used to calculate a derate factor. The derate factor function takes the measured temperature of both PCBs and compares it to maximum operating temeperature threshold values according to the different component datasheets. This allows the system to decrease its output power in order to cool down itself if a threshold margin of 10 °C is reached, and finally turns off completely if the threshold margin is exceeded. The derate factor gives a value between 0 and 1 is multiplied to the updated PWM function. On the power PCB there is also a relay that turns off the 30 V power rail connected to the input of the LED drivers. This would allow the microcontroller to turn off the LED drivers as an added safety precaution in the case that the PWM or LED drivers would be stuck in high power mode.

The code prints out relevant information in the Arduino IDE's serial monitor to overview the process.

### 3.4.1 Light Mixing and Duty Cycle Calibration

To be able to set the light mix, an algorithm to set the intended amount of output light as a value of the duty cycle was devised, as the system will use PWM to control the light. The sum of PPF emitted from one LED channel is the number of LEDs multiplied by the PPF of one LED. This is calculated using,

$$\mathrm{PPF}_{\mathrm{sum}} = \mathrm{PPF} \cdot n_{\mathrm{LEDs}}, \tag{3.14}$$

where PPF is found in Table III and the number of LEDs are found in Table V. $\mathrm{PPF}_{\mathrm{sum}}$ is therefore the incident PPF by all the LEDs in one channel. The cone area $A_{\mathrm{c}}$ from Table III is used together with the $\mathrm{PPF}_{\mathrm{sum}}$ in Equation (2.9) to calculate the $\mathrm{PPFD}_{\mathrm{sum}}$. The maximum PPFD for each LED channel, using the cone area approximation, can then be calculated using,

$$\mathrm{PPFD}_{\mathrm{max}} = \mathrm{PPFD}_{\mathrm{sum}} \cdot K_{\mathrm{PPF}} \tag{3.15}$$

$\mathrm{PPFD}_{\mathrm{max}}$ is then the PPFD at the nominal ON forward current for each LED channel. $K_{\mathrm{PPF}}$ is a factor which relates PPF at the ON forward current to the PPF at the nominal ON forward current and is opptained in the datasheetsb[42], [43], [44], [45]. This assumes all radiant flux is translated to PPF, thus only light within the PAR spectrum. The duty cycle of each channel can then be determined

as the quotient of its desired contribution to the total incident PPFD, divided by the $\text{PPFD}_{\text{max}}$ using Equation (3.16):

$$D = \frac{K_{\text{PPFD}} \cdot \text{PPFD}_{\text{tot}}}{\text{PPFD}_{\text{max}}}. \tag{3.16}$$

$\text{PPFD}_{\text{tot}}$ is the total PPFD required and $K_{\text{PPFD}}$ is the desired percentage of the $\text{PPFD}_{\text{tot}}$ radiated by a specific channel. This fraction gives the percentage of time the LEDs for a specific channel is supposed to be on, given a specified $K_{\text{PPFD}}$ as to say duty cycle in %. Multiplying this with 256 and subtracting 1 converts duty cycle to $D_{256}$ for the Arduino,

$$D_{256} = [D \cdot 256] - 1. \tag{3.17}$$

The nominal light mix (denoted by $K_{\text{nom}}$) given at the the nominal $\text{PPFD}_{\text{tot}}$ (denoted $\text{PPFD}_{\text{nom}}$) gives the nominal duty cycle $D_{\text{nom}}$. The values for the resulting maximum PPFD are listed in Table IX.

**Table IX.** Calculation of the $\text{PPFD}_{\text{max}}$ using values obtained in section 3.1.2. The number of LEDs is denoted by $n_{\text{LEDs}}$.

| **Wavelength (nm)** | $n_{\text{LEDs}}$ | $A_c$ **(m²)** | PPF **(µmol/s)** | $\text{PPFD}_{\text{sum}}$ **(µmol/m²-s)** | **Relative Factor** ($K_{\text{PPF}}$) | $\text{PPFD}_{\text{max}}$ **(µmol/m²-s)** |
|---|---|---|---|---|---|---|
| 727 | 7 | 0.45 | 2.8 | 51.58 | 2.7 | 139.26 |
| 666 | 14 | 0.58 | 5.85 | 141.21 | 1.75 | 247.11 |
| 450 | 3 | 0.38 | 5.50 | 36.67 | 1.8 | 66 |
| 425 | 5 | 0.58 | 3.55 | 30.61 | 1.75 | 53.56 |

The final $\text{PPFD}_{\text{max}}$, shown in Table IX, for each channel is used to determine duty cycle using Equation (3.16).

## 3.5 Protection and Filter Stages

Five protective measurements were taken on the input side of the circuit: A circuit breaker (fuse), a Transient-Voltage-Suppression (TVS) diode for transient suppression, a reverse polarity voltage protection, and a $\pi$-filter for Electromagnetic Interference (EMI) noise filtering, and a 30 V relay. The following sections outlines the purposes of these filters, as well as how the components and their respective values were calculated and chosen. All values are based on components worst-case scenario values.

### 3.5.1 Circuit Breaker (Fuse) and Transient Protection

The fuse rating was calculated by taking into account the power consumption of all the components of the circuit with the following equation:

$$P_{\text{tot}} = V_{\text{in}} \cdot I_{\text{tot}} \implies I_{\text{tot}} = \frac{P_{\text{tot}}}{V_{\text{in}}}, \tag{3.18}$$

where $P_{\text{tot}}$ is the sum of all power consumption in the circuit, $I_{\text{tot}}$ is the total current drawn from the power supply, and $V_{\text{in}} = 30$ V is the power supply voltage. The LED values presented in Table X below, were taken directly from their respective datasheets [42], [43], [44], [45].

**Table X.** LED maximum effect ratings.

| **LED** | **Max Effect per LED (W)** | **Number of LEDs** | **Total Max Effect per LED type (W)** |
|---|---|---|---|
| GF CSSRML.24 | 1.84 | 7 | 12.88 |
| GH PUSRA1.25 | 1.4 | 14 | 19.6 |
| GD PUSRA2.15 | 2.065 | 3 | 6.195 |
| LTPL-C034UVH430 | 2.2 | 5 | 11.0 |
| **Total** | 7.505 | 29 | **49.675** |

The total power consumption of the channels are given by summing the total max effect per LED type, as shown in Table X. Apart from the microcontroller, the power consumption of any other components, such as the sensors and LED drivers, consume less than 1 W in total. As a safety measure, the total power consumption was set to be $P_{\text{tot}} = 55$ W. This yields a max total current from the power supply of $I_{\text{tot}} = 1.83$ A, and, after adding the safety margin, a fuse rating of 2.3 A, rounding up to 3.0 A.

Transient protection is carried out by two unidirectional TVS diodes placed to recreate a bidirectional TVS diode. They are placed after the fuse to protect against big voltage spikes. The TVS diode+ and TVS diode- must have a clamping voltage which is less then the absolute maximum $V_{\text{ds}}$ rating, which is 80 V, for the P-Channel MOSFET (PMOS) in the reverse polarity protection [55]. The components in the filtering stage which has the voltage rating 50 V also need to be protected. It also needs to protect the N-Channel MOSFET (NMOS) and transistor in the 30 V relay which has max $V_{\text{ds}}$ as 55 V and max $V_{\text{CBO}}$ as 60 V respectively [56], [57]. It needs to do this in both polarities, considering that both instances yields the same case the diodes chosen are the same ones. TVS diode model SMBJ30A was chosen which is able to handle 200 W for 10 ms, has a 30 V reverse voltage, a breakdown voltage between 33.3 and 36.8 V and clamping voltage at 48.4 V [58]. The power rating is thus over three times higher then the normal power consumption. The reverse voltage is the same as the normal voltage and the breakdown voltage is slightly higher, which guarantees that a very small current will run through the diodes during normal circumstances and therefore not expose the diodes to any unnecessary wear and tear. The clamping voltage protects the most vulnerable components which is the capacitors in the filtering stage.

### 3.5.2 Reverse Voltage Protection

Reverse voltage protection is used to protect components taking damage from a backwards-connected power supply, which would lead to current flowing opposite of

the intended direction. A simple diode would be enough to block flow from happening in the opposite direction, but this would result in a higher power consumption. A typical diode has a forward voltage of $V_\mathrm{f} = 0.7$ V, resulting in a power dissipation of $P = V_\mathrm{f} \cdot I_\mathrm{tot} = 0.7 \cdot 1.83 = 1.28$ W. Using a Schottky diode leads to similar results. To minimize the heat generated, a PMOS was used. The schematic of the reverse polarity protection circuit is shown in Figure 3.5. The reason a PMOS is used are because it is on when $V_\mathrm{GS} < 0$, as to say the gate is pulled below the source, while an NMOS is turned on when $V_\mathrm{GS} > 0$, meaning the gate would need to be driven at $V_\mathrm{G} > 30$. This would technically yield an even lower power dissipation, but would require the inclusion of some kind of ideal diode controller with a charge pump, bootstrap driver, and high-side gate driver.

The PMOS has an active resistance of $R_\mathrm{ds} = 25$ mΩ [55], resulting in a voltage drop of $V_\mathrm{drop} = R_\mathrm{ds} \cdot I_\mathrm{tot} = 0.025 \cdot 1.83 = 46$ mV, and a power dissipation of $P = R_\mathrm{ds} \cdot I_\mathrm{tot}^2 = 0.025 \cdot 1.83^2 = 84$ mW. The gate to source voltage of the PMOS is rated at ±20 V, and since the power supply delivers 30 V, A Zener diode of $V_\mathrm{z} = 12$ V is used between the gate and source is used to clamp the voltage to $V_\mathrm{gs} = V_\mathrm{z} = 12$ V.

The Zener diode requires a minimum reverse current, known as the knee current ($I_\mathrm{zk}$) to stabilize the voltage at 12 V. According to the datasheet, this current is specified at 1.0 mA [59]. The gate resistor in Figure 3.5 is used to control that the knee current criteria is met. For $I_\mathrm{zk} = 1.0$ mA, a maximum resistance of $R_\mathrm{gate} = \frac{18}{0.001} = 18$ kΩ is needed, but since there is a possibility of voltage variations from the power supply, that has to be taken into account. Setting the Zener current to $I_\mathrm{zk} = 2$ mA yields $R_\mathrm{gate} = \frac{18}{0.002} = 9$ kΩ, rounding up to 10 kΩ. The MOSFET is turned on when the gate to source voltage is $V_\mathrm{gs} = -2.5$ V.

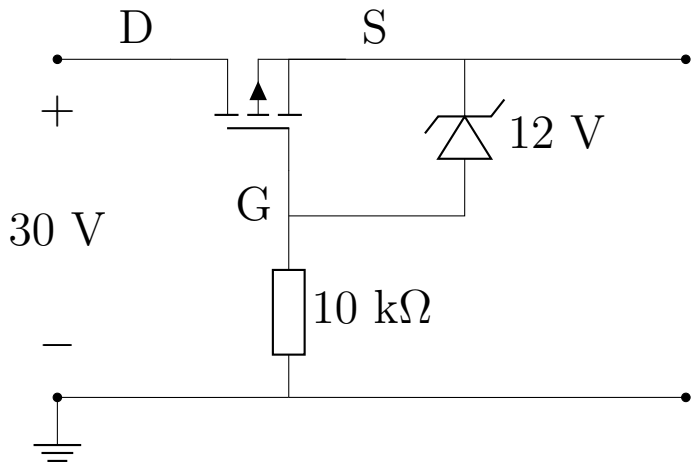


**Figure 3.5.** Reverse polarity protection schematic. Includes a PMOS, a gate Resistor, and a Zener diode.

### 3.5.3 Input Filtering and 30 V relay

The filter is used to support ripple and noise suppression from the three switching regulators. In total, six ceramic capacitors, two electrolytic capacitors, and one inductor are used. Ceramic capacitors are used to reduce the ripple voltage. These need to be physically close to the switching regulators as the wires introduce impedance with increased distance (ESR = Equivalent Series Resistance) [60]. The first ceramic capacitor will have the larger capacitance of the two, and the other with 0.1 µF. The ceramic capacitance value of the bigger conductor was picked to be 10 µF, as suggested by the LED driver datasheet [37].

The electrolytic capacitors are used to further smoothen the voltage fluctuations. The minimum electrolytic capacitance needed is calculated using

$$C_{\mathrm{B}} \geq \frac{\frac{1}{2} \cdot I_{\mathrm{STEP}} \cdot D_{\mathrm{MAX}} \cdot T_{\mathrm{R\_PS}}}{V_{\mathrm{IN\_Tran}}} - C_{\mathrm{CE\_Total}} \cdot (1 - \mathrm{Tol.}), \tag{3.19}$$

where $I_{\mathrm{STEP}} \cdot D_{\mathrm{MAX}}$ is the total current $I_{\mathrm{tot}} = 1.83$ A. The power supply response time should be at least 10-15 times greater than the switching period, and was set to $T_{\mathrm{R\_PS}} = 41.67$ µs, and the allowed input transient undershoot or overshoot $V_{\mathrm{IN\_Tran}} = 0.5$ V [61]. $C_{\mathrm{CE\_Total}}$ is the total ceramic capacitance from the six used, and Tol. is the tolerance rating given from the respective capacitor datasheets, usually ±10–20%, or Tol. = 0.1–0.2. Considering the worst case minimum value of capacitance required, the ceramic capacitors were ignored so that the bulk capacitance is calculated as

$$C_{\mathrm{B}} \geq \frac{\frac{1}{2} \cdot I_{\mathrm{tot}} \cdot T_{\mathrm{R\_PS}}}{V_{\mathrm{IN\_Tran}}}. \tag{3.20}$$

Plugging the values above into Equation (3.20) yields $C_{\mathrm{B}} \geq 76.3$ µF, which is the total capacitance, meaning that the sum of the two capacitors will have a minimum value of 76.3 µF. For safety, a rated voltage of 50 V was used, and rounding up to the lowest available capacitors resulted in two capacitors with 47 µF each, and a total electrolytic capacitance of 94 µF.

Since a second order LC-filter ($\pi$-filter) is used, an inductor is placed between the electrolytic and the ceramic conductors to reduce ripple current generated by the switching regulators. The inductance was calculated using

$$f_{\mathrm{c}} = \frac{1}{2\pi\sqrt{LC_{\mathrm{CE}}}} \implies L = \frac{1}{(2\pi f_{\mathrm{c}})^2 \cdot C_{\mathrm{CE}}}, \tag{3.21}$$

where $f_{\mathrm{c}}$ is the cutoff frequency and $C_{\mathrm{CE}}$ is the ceramic capacitance per channel. Since the LED drivers have a clock frequency ($f_{\mathrm{SW}}$) of 1 MHz, the cutoff frequency should be much lower than the switching frequency, which is why it was picked to be 0.11 MHz. The inductance was then calculated with Equation (3.21) to be 2.1 µH, rounding up to 2.2 µH.

The design of the 30 V relay was based on the principle of grounding the 30 V rail with a MOSFET to power off the 30 V rail. This was initially intended to be

done with the Arduino Nano directly connected to the gate of the MOSFET. But because the Arduino Nano would not be able to drive the MOSFET an NPN Bipolar Junction Transistor (BJT) was used. The $V_{\text{in}}$ to the relay circuit is the output from the filtering stage and the OffSignal is connected to the A2 pin on the Arduino Nano. The Arduino Nano can output either 5 V or 0 V (ground) with the `digitalWrite()` function. The value of the resistors were chosen according to simulation results of the circuit.

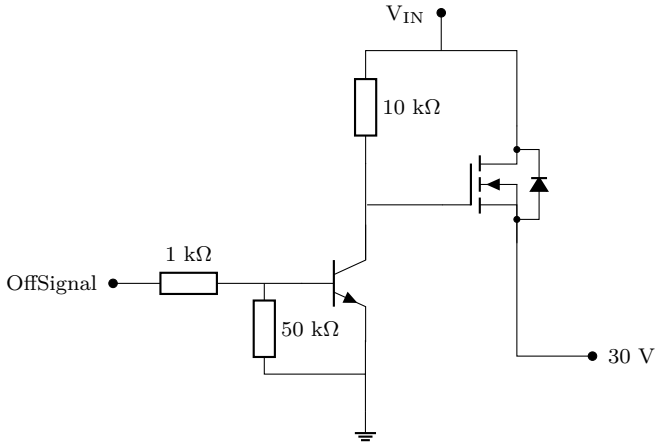


**Figure 3.6.** 30 V relay schematic. Signal OffSignal activates an NPN transistor, MOSFET serves as a relay to turn off 30 V power rail.

### 3.5.4 LED PCB Stand

For the purposes of testing and presentation, a stand used for mounting the LED PCB is constructed. The main construction was a steel central plate that was used as a base to attach the largest pipe with the height 30 cm, it was attached to the plate using welding. The pipes were steel square tubes coated with rust preventive oil. The second pipe had a height of 25 cm. The pipes were dimensioned specifically so that the smaller pipe would fit inside the larger one. Likewise on top of the smaller pipe was a horizontal arrangement made with the same steel as the other two pipes and the larger pipe was attached to the base pipe with welding. The height and length adjustments of the pipes were accomplished by the method of using a bolt that fastens the inner, smaller pipe. The bolt was fitted to a nut welded onto a drilled hole. The aluminium heatsink was attached to a stainless steel flat jumper that was constructed by cutting a sheet that was then bent in an anvil to match the width of the heatsink. The attachment of the heatsink to the jumper was done with four bolts that went through both the stainless steel jumper and the holes of the outer fin of the heatsink.

The heatsink was modified by drilling at the same locations as the through holes designed in KiCad for the LED PCB. The outermost fins of the heatsink were also modified by drilling to be able to mount it to the constructed stand. The heatsink was mounted horizontally due to the design limitations of mounting the LED PCB onto the heatsink and the LEDs pointing downwards, facing the plant.

The datasheet specifications for the heatsink does not assume a particular mounting arrangement although the arrangement does impact the efficiency of heat removal [49].

# 4
# System Testing Methodology

After designing all components of the lighting system, the PCBs and their respective parts were ordered. The PCBs were then populated with the use if a reflow oven to solder the Surface Mount Devices (SMDs) while through hole components were soldered by hand. After assembling all PCBs, they were visually inspected to check for any immediate areas of concern such as SMD drifting away from their pads or solder bridges. A multimeter was then used to measure continuity between all connected traces on the power PCB and the LED PCB. It was done to verify connections between intended components and to make sure that no traces or contacts had been bridged during soldering. The LED PCB was further tested by providing nominal forward voltage form a DC power supply to each channel while having a current restriction. This was done to verify that all LEDs were functioning and that the traces were intact. The power PCBs was then connected to a power supply, and a 30 V was applied to the terminals. The same multimeter was then used to measure the voltages on parts of the board. It was verified that 30 V was supplied at the LED drivers, and that the buck converter was supplying 12 V to the Arduino input voltage header. It was also verified that 30 V was not present at unintended places, such as to other pins on the LED drivers or any of the Arduino headers. It was also measured that the reverse polarity protection PMOS had a gate to source voltage of 12 V.

The control system is then implemented by connecting the Arduino, light sensor ,and LED PCB to their respective connectors on the the power PCB. When switched on, the current waveform measurements for each LED channel was performed. This was to study the current characteristics to use as a reference for the duty cycle calculations. Whilst calibration was done without ambient light, tests were performed to see if the control system could adjust the duty cycles of the LEDs based on ambient light or direct sunlight. Tests were also performed to measure the power draw of the system at different duty cycles. Changing position of the sensor after calibration was also done to test the control system's ability to regulate the light emitted for different distances between the LEDs and light sensor.

## 4.1 Testing equipment

The testing and measurement equipment used is listed in the following list. This excludes the Sparkfun AS7343 light sensor [39] as it is an integral part of the system.

- Multimeter: u1272A, Keysight Technologies, USA [62].
- Digital oscilloscope: RTB2002, Rohde & Schwarz GmbH & Co. KG, Germany [63].
- Laser thermometer: Fluke 62 max+, Fluke Corporation, USA [64].
- DC power supply: TENMA 72-8345A, Premier Farnell Limited, USA [65].
- Current probe: RT-ZC03, Rohde & Schwarz GmbH & Co. KG, Germany [66].
- Miscellaneous cables, clamps and probes.

Microsoft Excel [67] was used to record data and generate graphs.

## 4.2 Control System and Sensor Testing

The first tests of the control system were made to setup the sensor and PI regulator. The first initialization of the system was to create PWM signals to the dim pins on the LED drivers. These signals control the outer control loop of the LED drivers, and turns the driver off and on depending on the duty cycle supplied by the Arduino. When the PWM signal to the dim pin is high, the LED driver turns on, and regulates using its internal clock frequency of 1 Mhz to control the output current. The LED driver IC offers built-in PCM with internal compensation, which adjusts the ON current based on the output side components to achieve the desired output current. The spectral sensor was then set up and the measurements from the chosen channels were measured. Integration time and gain was set by iteration. When setting the integration time, the periodicity of the PWM has to be considered. Setting the integration time to a value that is lower or in equal terms to the period time of the PWM signal makes the sampling of the signal subject to aliasing and sampling bias, which can result in an incorrect estimation of the average value. The LED channels were turned on one by one to see how much they affected other channels' assigned sensors. The gain was set to reduce this phenomenon. The sensor was placed under sunlight and maximum LED output to set the gain to make sure the sensor did not reach saturation.

The control system was then tested with trial and error to adjust the PI regulator parameters $K_\mathrm{p}$ and $K_\mathrm{i}$. If the integral action was too slow or too weak to eliminate the steady state error the $K_\mathrm{i}$ value was increased. The goal was to find values of $K_\mathrm{p}$ and $K_\mathrm{i}$ that made the system produce a light mix that was close to the target calculated during calibration during different conditions. Disturbances such as ambient light were used to see the resilience of the control systems.

The thermistors were tested in nominal and maximum load cases. Both the thermistors' values were compared to what was deemed reasonable.

## 4.3 Electrical Power Measurements

After developing, implementing and testing the control system, the 12 V pin on the Arduino was connected to the 12 V supply from the buck converter. The 30 V input to the power board was switched on without connecting the Arduino to a computer to test if the Arduino could reliably run while being powered by the buck converter. A sweep of the the 12 V output with no load was also measured using an oscilloscope to study the voltage characteristics when switching on the 30 V power supply.

In order to figure out the actual lighting characteristics of the system when turned on, measurements were performed to compare the calculated forward voltage and forward current to what was actually present when the system was activated. This was done to verify that $K_{\mathrm{PPF}}$ taken from the LEDs datasheets were correct. The reasoning was that if the LEDs had correct, or nearly correct, ON forward current and ON forward voltage, then the chosen value for the $K_{\mathrm{PPF}}$ would be correct. If this value is correct then the calculated $\mathrm{PPFD}_{\mathrm{max}}$ should also be correct and correlate to the actual $\mathrm{PPFD}_{\mathrm{max}}$ radiated by the LEDs. The calculated PPFD at $K_{\mathrm{PPFD}}$ would then correspond to the actual PPFD. The first tests with the whole system integrated was to set a fixed PWM, a duty cycle of 50% for all channels and then measure the output characteristics of each LED. Using a digital oscilloscope the waveform of the voltage across the LED string was measured and saved. In the same way, the voltage across each sense resistor was also measured. A current clamp was then placed over one of the wires running from the LED PWM, measuring the proportional induced voltage with a ratio of 100 mV/A.

After measuring the electrical output characteristics, they were compared to the desired forward voltage and forward current as described in section 3.2. By setting the duty cycle to 50%, the RMS and peak to peak value could easily be used to study peak and average values for both current and voltage characteristics. If any significant discrepancy had been detected, particularly with regards to on forward current, the $K_{\mathrm{PPF}}$ was adjusted to follow the specifications given in the LEDs datasheets. When the $D_{\mathrm{nom}}$ had been finalized, testing of the sensor began. The aim of the testing was to evaluate if the sensor value would be cumulative and then to see if the incident light measured was directly proportional to the duty cycle. A fixed duty cycle of 10%, $D_{\mathrm{nom}}$, and 100%, was set to one LED channel at a time. The sensor values for each of the reference channels was recorded at each duty cycle. After each channel had been tested individually, the sensor measurement was recorded with all LEDs turned on at the fixed duty cycle.

To determine the power usage of the system, current and voltage supplied to the power PCB was measured using two multimeters set up in voltage true configuration. The multimeters were set up to measure true RMS voltage and current, where the resulting input power is the product of the voltage and current. The $\mathrm{PPFD}_{\mathrm{tot}}$ was increased from 50 to 350 $\mu\mathrm{mol}/(\mathrm{m}^2\mathrm{s})$ in intervals of 50, while $K_{\mathrm{nom}}$ was constant. One test was also performed to measure power at maximum duty cycle on all channels. At each step, a laser thermometer was used to measure the temperature

of the heatsink. The temperature was recorded when the temperature had stopped increasing after changing duty cycle.

## 4.4 Ambient Light Compensation Testing

One of the goals of the device was to use ambient light to supplement the LEDs with the aim of reducing the power draw. This was done by adjusting the duty cycle based on the incident light on the spectral sensor using the control system designed in section 3.4. To test the capabilities of the system with and without ambient light tests were made with both indoor ambient light and direct sunlight. To study this, the active duty cycle for each channel, sensor calibration target and actual sensor channel readings were recorded. Input RMS voltage and current measurements were also made to compare the power draw with and without supplemental light. Using $D_{\text{nom}}$ to control the LEDs, the system was enabled and calibrated with a cardboard box over the setup, which was then removed, exposing the sensor to ambient light. Then, the system was calibrating in ambient light, and placing the cardboard box on top again.

After testing with ambient light, tests were made using direct sunlight through a window. The sensor was first calibrated in direct sunlight, and then moved to shadow, to study how the control system adjusts when the incident supplemental light decreases. The second test involved calibrating the sensor in darkness, then placing the light setup in direct sunlight. The lighting setup was then rotated 90° to test for directional sensitivity of the sensor, the resulting channel measurements and active duty cycles were recorded.

## 4.5 Positional Testing

Two types of tests were performed with regards to the position of the light sensor relative to the LEDs. First was to place the sensor directly below the lights and and adjust the height of the LED PCB. This was first done with the control system active, using $\text{PWM}_{\text{nominal}}$ as input, calibrated in darkness at the height 30 cm. The height was then changed to 35 cm and 40 cm while maintaining the same initial calibration. The total current and voltage in to the system was measured using two multimeters using a voltage-correct connection. The PWM, target light intensity, and measured light intensity was measured for each channel.

Following this another test relating to height was done. The $\text{PWM}_{\text{nominal}}$ was set without the control system active when the height was 30 cm, as to say the LEDs were constant during the whole test. The heights were then changed to 35 cm, 40 cm, and 45 cm. For each height, the channels on the light sensor corresponding to the wavelengths for the LEDs were recorded.

The second position test was to alter the horizontal angle of the sensor relative to the lights at the fixed height 30 cm and at a fixed PWM, the duty cycles used in

this test are not the same as $D_{\text{nom}}$ used for other test. The angle was adjusted by hanging the sensor on a string from the LED PCB stand. The board was tilted by hand and the angle was measured with a protractor, aiming to test at 30° and 50°. For each angle, the channels on the light sensor corresponding to the LED wavelengths were recorded.

## 4.6 Protection Testing

The testing of the protection circuits was limited. The two tests that were performed was the testing of the 30 V relay and testing of the reverse polarity protection. The 30 V relay was tested by setting the appropriate pin on the Arduino to either 5 V (HIGH) or ground (LOW) with the `digitalWrite()` function. The voltage was measured at the LED driver $V_{\text{in}}$ to see if the 30 V power rail was still receiving power. To validate the reverse polarity protection, power was applied to the input terminal in a reverse bias configuration. The test aimed to confirm that the protection circuitry successfully blocked current flow to downstream components.

# 5
# Results

The design process culminated in a two final PCB designs, which were assembled and tested as described in the two previous chapters. The final Computer-Aided Design (CAD) of the power PCB and a 3D model is shown in Figure 5.1.

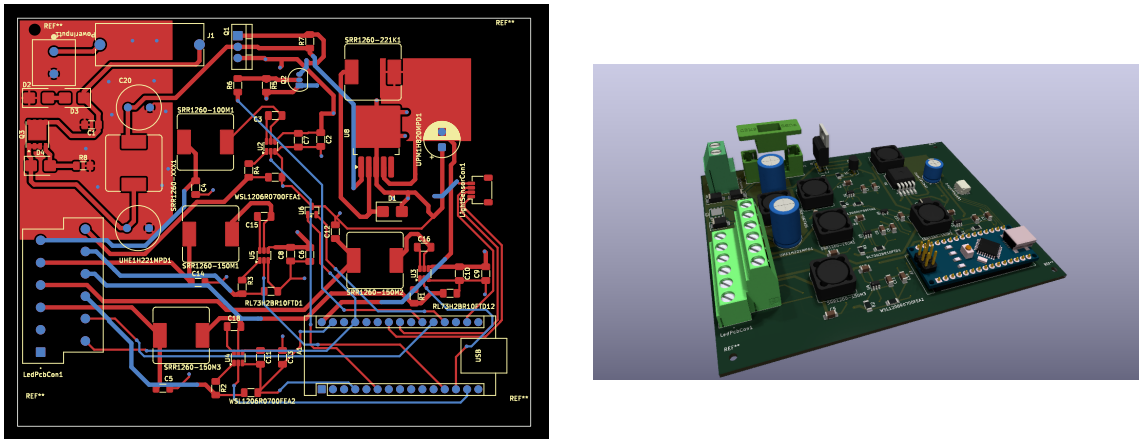

**(a)** CAD of copper layers.

**(b)** 3D view of the power PCB.

**Figure 5.1.** Front and back copper CAD view and PCB 3D model of power board.

Figure 5.1a shows the CAD view of the copper layers and the connections between all parts. This schematic shows how all different segment of the design, from power input in the top left and protections, to the buck converter, Arduino and LED drivers. Figure 5.1b shows a 3D model of what the PCB looks like. The 12 port terminal block is the connection to the LED PCB, the power terminal in the top left corner to a 30 V DC power supply. On the right hand side is a small connector to the light sensor breakout board. The 12 port block terminal on the LED PCB shown in Figure 5.2 connects to the power PCB. Here the pattern each channel of LED can be seen.

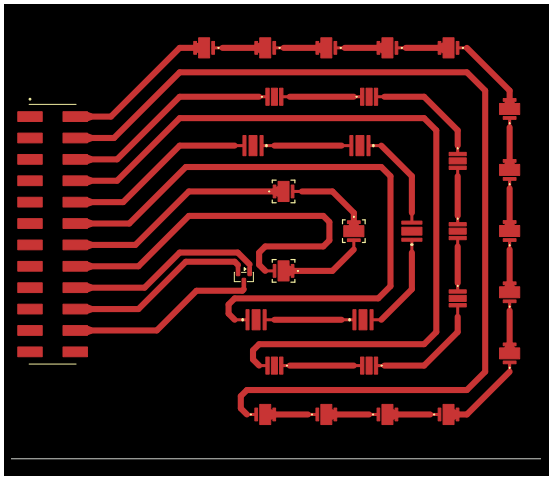

**(a)** CAD view of front copper for the LED PCB.

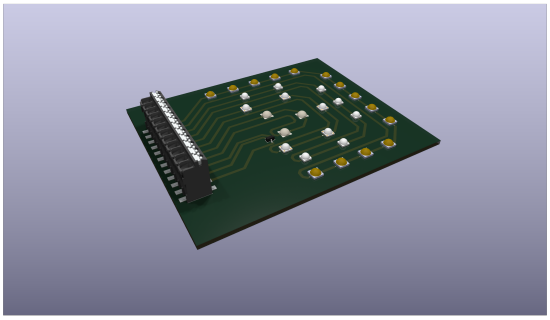

**(b)** 3D model of the LED PCB.

**Figure 5.2.** Front copper CAD view and PCB 3D model of the LED board.

The LED PCB shown in Figure 5.2 was mounted on a heatsink, placed on a height-adjustable arm, the test system with the sensor is shown in Figure 5.3. This is the main setup used for most tests, sometimes with a large cardboard box to cover the setup, in varying conditions.

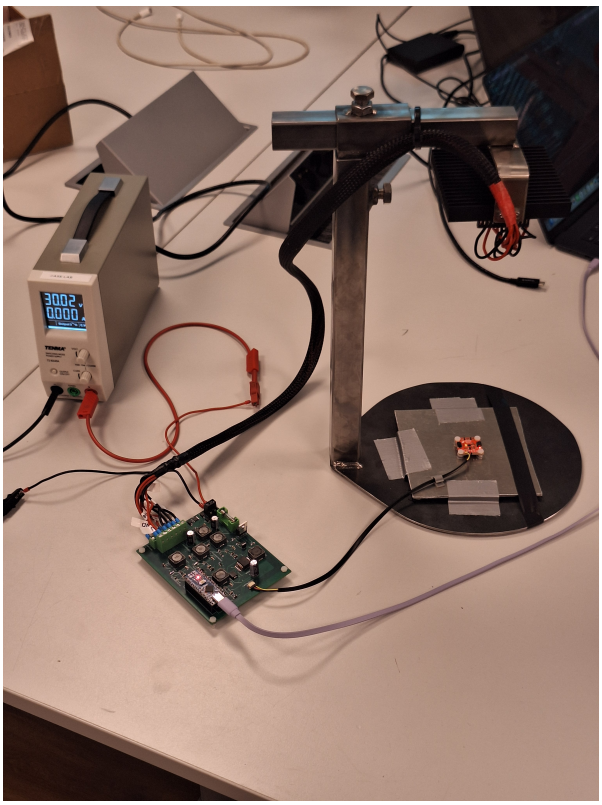

**Figure 5.3.** Image of the device mounted on its stand with no box.

Figure 5.3 shows the DC power supply on the left hand side, connected to the power PCB in the center. The power PCB is in turn connected by multiple cables, wrapped

in a sleeve, which run to the LED PCB mounted on the arm. The arm is constructed of welded pipe steel. Also connected to the power PCB is the spectral sensor and a USB cable running from a computer to the Arduino, mounted on headers on the power PCB.

Generally for all results, duty cycle and PWM refers not to the built in PCM regulation on the LED driver IC but the duty cycle of the PWM signals created by the Arduino. These PWM signals control the dim pin on the four led drivers on the power PCB. These signals are apart of the outer control loop which are adjusted by the data from the spectral sensor using the program implemented on the arduino. As opposed to the inner loop current regulation that is managed by the LED driver when the PWM signal provided to the dim pin is high.

## 5.1 Control System Testing

When the light sensor was used without configuring the gain and integration time settings, the readings from the sensor were found to be inconsistent with lots of crosstalk specifically between red and blue channels as to make the control system unusable. When the sensor readings were initially measured while driving the LED at a given duty cycle, they would fluctuate significantly. The light sensor gave measurements that differed by up to 50%, making the control systems highly unstable. The PI regulator was not provided with a enough stable input from the sensor. This made the resulting PWM signal generated by the Arduino also unstable. The PWM signals based on the unstable input caused the LEDs to flicker. By changing to a higher integration time, the sensor's measurement fluctuations were dramatically reduced to each consecutive reading being within 10% of each other. This made the inputs to PI regulator stable enough that the generated PWM did not cause flickering of the LEDs

The crosstalk and other interference between the sensor channels caused the R and FR channel LEDs to effect the B sensor channels F2 and FZ. This led to the R LEDs being able to achieve all targets set for all sensor channels simultaneously causing the B LEDs turn off. The gain and integration time of the sensor were changed by setting values for ATIME, ASTEP and AGAIN as shown in Table XI. After setting the gain and integration time the crosstalk between the B and R channels were eliminated making the R LED no longer able to effect the targers on the B channel. The chosen proportionality constant and integration constant are also shown in Table XI.

**Table XI.** AS7343 sensor and PI regulator configuration results.

| **Variable** | ATIME | ASTEP | AGAIN | $K_\mathrm{p}$ | $K_\mathrm{i}$ |
|---|---|---|---|---|---|
| **Value** | 9 | 7194 | 0.5x | 0.1 | 0.09 |

The values used to configure the AS7343 light sensor's measurement parameters

ATIME, ASTEP and AGAIN. The value chosen for the PI regulator $K_i$ and $K_p$.

The thermistor on the power PCB experienced large fluctuations in the readings between samples, jumping 100 °C every other reading. There were no fluctuations observed of the LED PCB, but a constant temperature of 2 °C higher than what the thermo gun measured was observed over all temperatures. When no LEDs were powered on, the read-ins were steady and easily readable. An increase of duty cycle to the 727 nm channel increased the sporadic measurements. This was not observed when isolating the other channels. When this LED driver was selectively turned off in proximity to the sensor while driving the other channels, the reading from the thermistor was more stable. To get better temperature data, a function code was implemented to take 40 samples of the measurement and displaying the average of the lowest 5 values in the sample. The readings stabilized but are still off by a few degrees.

An attempt to run the Arduino using board power from the buck converter was made. The Arduino switched on briefly, and then it broke. The processor broke in some way and was no longer detected by the computer. The processor also started becoming very hot. A transient of the 12 V header with no load applied was studied using the oscilloscope, the waveform of which is shown in Figure 5.4.

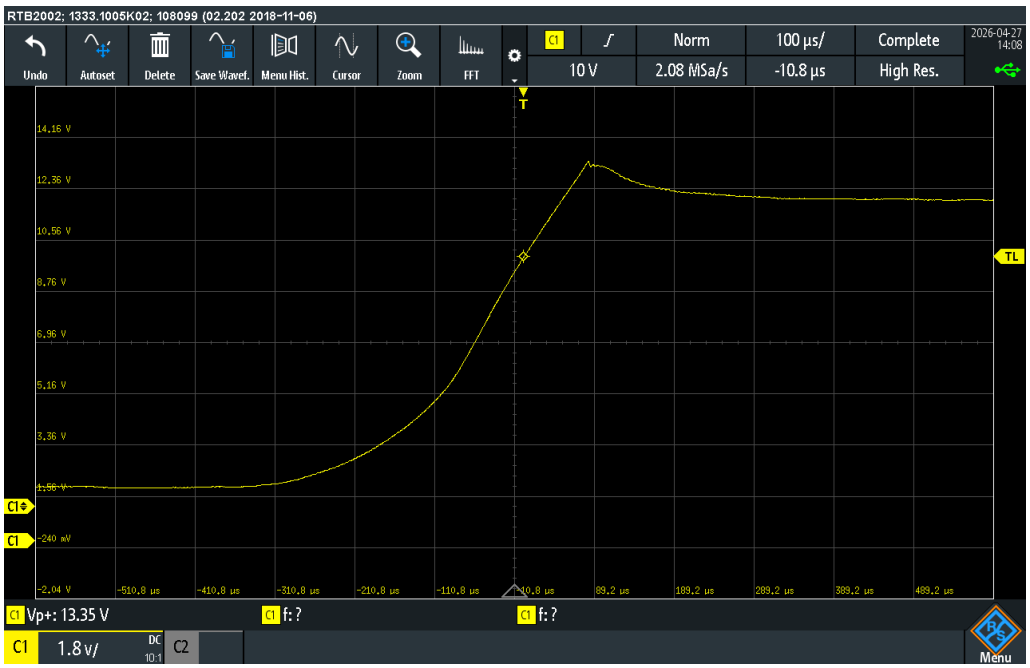


**Figure 5.4.** Startup transient from auxiliary voltage regulator. Voltage peak value of about 13.35 V.

Figure 5.4 shows how the voltage rises when the 30 V input is enabled at the auxilary voltage regulator output. No load is attached to the output. The voltage peak close to 13.35 V before stabilizing at about 12 V.

## 5.2 Electric Power and Sensor Measurements

The first electrical measurements on the LED system are recorded in Table XII which shows the measured forward voltage, current, and sense resistor voltage when dim pin PWM duty cycle is set to 50%. This measurement is based on the figures in appendix B, where for each channel the values are estimated based on the RMS, peak-to-peak and the waveform image.

**Table XII.** Forward voltage, current, and sense resistor voltage for each LED channel.

| Wavelength (nm) | ON Forward Voltage (V) | ON Forward Current (mA) | ON Sense Resistor Voltage (mV) | ON Output Power (W) |
|---|---|---|---|---|
| 727 | 16.90 | 918 | 100 | 15.51 |
| 666 | 26.70 | 728 | 50 | 19.44 |
| 450 | 9.39 | 1188 | 90 | 11.16 |
| 425 | 15.98 | 900 | 90 | 14.38 |

Table XII shows that each channel except for the 666 nm LED channel has a sense resistor voltage close to 99 mV. Similarly, the ON current was close to the expected ON current, with the exception of the 666 nm channel. The sum of the output side power for all channels put together is 60.5 W. The forward voltage of each channel is nearly nominal for some channels, whereas the 727 nm channel has a significantly higher forward voltage. The sense resistor voltage was also compared to the forward current, as the LED driver uses this voltage as reference to regulate the forward current. All but the 666 nm channel have a sense resistor voltage at, or close to 100 mV. Using the measured forward voltage in Equation (3.6), the inductor ripple current remains above 300 mA except for the 666 nm channel.

Using the current measurements in Table XII, the $K_{\mathrm{PPF}}$ was extrapolated from the datasheets of each LED [42], [43], [44], [45]. This value corrected for any difference from what was designed for in sections 3.1.2 and 3.2 as the ON current changed from what the system was designed from. These values are given in Table XIII.

**Table XIII.** The adjusted values for the $K_{\mathrm{PPF}}$, $\mathrm{PPFD}_{\mathrm{max}}$, and $D_{\mathrm{nom}}$ based on the ON forward current measured in Figure B.1, B.2, B.3 and B.4.

| Wavelength (nm) | ON Forward Current (mA) | Relative PPF Factor ($\mathrm{K_{PPF}}$) | $\mathrm{PPFD_{max}}$ (µmol/(m²s)) | $D_{\mathrm{nom}}$ (%) |
|---|---|---|---|---|
| 727 | 918 | 2.45 | 126.37 | 39.5 |
| 666 | 728 | 1 | 141.21 | 106.3 |
| 450 | 1188 | 1.6 | 58.67 | 42.6 |
| 425 | 900 | 1.7 | 52.03 | 48.1 |

Table XIII gives the $\mathrm{PPFD_{max}}$ for all channels, using the $\mathrm{K_{PPF}}$ at the ON current of each channel. $\mathrm{PPFD_{max}}$ is then used alongside $\mathrm{K_{nom}}$ for each channel and the desired $\mathrm{PPFD_{tot}}$ of 250 µmol/m$^2$s to determine the nominal duty cycle of each channel. The

calculated $D_{\text{nom}}$ for the 666 nm channel exceeds 100%, as the ON current is lower than the current which the system was dimensioned for. Thus the spectral output can not reach the desired PPFD of 250 µmol/m$^2$s. The values given in Table XIII were measured at a later date after the control system had been integrated and all other tests had been performed.

The forward ON current, and consequently the $K_{\text{PPF}}$ that was used to adjust duty cycles for many of the tests were measured earlier. These ON current measurements are based on peak-to-peak current values shown in Figure B.5, rather than reading the waveform image to discern the actual ON current. These values are shown in Table XIV.

**Table XIV.** The adjusted values for the $K_{\text{PPF}}$, $\text{PPFD}_{\text{max}}$, and $D_{\text{nom}}$ given discrepancy on the ON forward current using peak-to-peak values from Figure B.5.

| **Wavelength (nm)** | **ON Forward Current (mA)** | **Relative PPF Factor** ($\text{PPF}_{\text{rel}}$) | $\text{PPFD}_{\text{max}}$ **(µmol/(m²s))** | $D_{\text{nom}}$ **(%)** |
|---|---|---|---|---|
| 727 | 1000 | 2.7 | 139.26 | 35.9 |
| 666 | 1000 | 1.35 | 190.63 | 78.5 |
| 450 | 1400 | 1.8 | 66 | 37.9 |
| 425 | 1000 | 1.75 | 53.56 | 46.5 |

Duty cycles presented in Table XIV are not used for the later results for efficiency but for most other tests, unless written otherwise. These adjusted values given in Table XIV sets the max PPFD at the maximum duty cycle as 449.45 µmol/(m$^2$s) at the light mix 27:42:31 with the 425 nm and 450 nm LED channels contributing at the ratio 12:15 to B. Input power to the power PCB relative to the $\text{PPFD}_{\text{tot}}$ is shown in Figure 5.5.

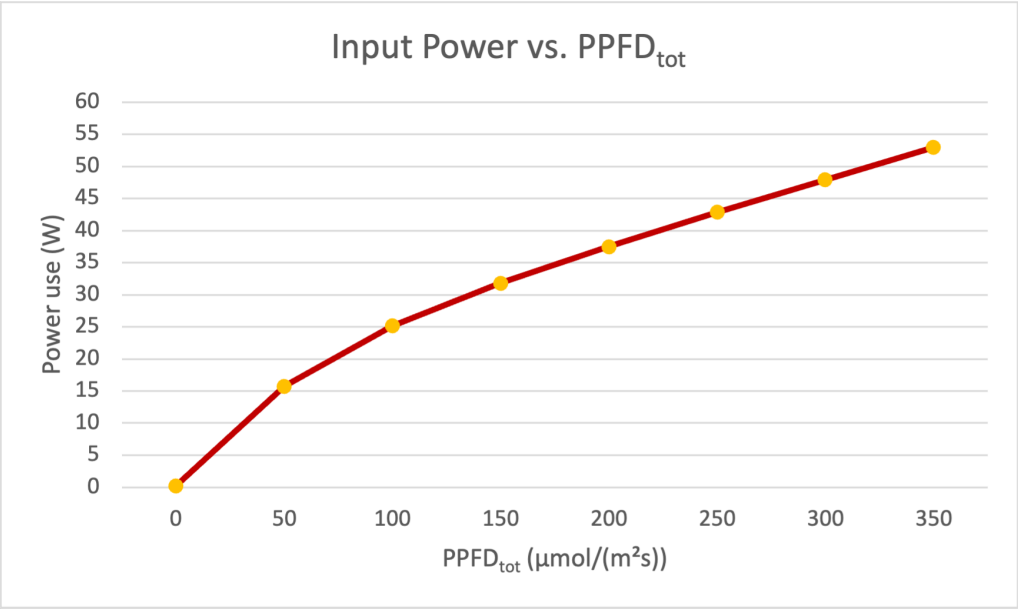


**Figure 5.5.** Input power relative to the $\text{PPFD}_{\text{tot}}$, constant $K_{\text{nom}}$.

Figure 5.5 shows the power usage at different $PPFD_{tot}$ with a constant $K_{nom}$. The power usage increases significantly at first, as the LED driver goes from being off to providing $PPFD_{tot} = 50$ µmol/($m^2$s). The power usage then increases more linearly, and reaches 53 W at $PPFD_{tot} = 350$ µmol/($m^2$s).

666 nm LED channel reaches the $PPFD_{max}$ after $PPFD_{tot}$ reaches 350 µmol/($m^2$s), it was therefore impossible to keep $K_{nom}$ constant. Due to a mathematical error this test and the one showed in Figure 5.6 used a light mix with the ratio 21.1:57.7:21.2, the $PPFD_{tot}$ is also 5% less for each measurement point in Figure 5.5 and 5.6. At maximum duty cycle for all channels as to say $PPFD_{tot}$, $K_{PPFD}$ was not equal to $K_{nom}$ for this measuring point, the power usage was 62.5 W. The sum of of output power at 100% duty cycle is 60.5 W, thus the difference is only 2 W.

At maximum duty cycle, input RMS current of 2.15 A was measured. The efficiency of each LED channel at 100% duty cycle is listed in Table XV. This table is based measured power in Table XII and theoretical radiant flux times the relative factor $K_{PPFD}$ and number of LEDs in in Tables V and XIII. The efficiency is the quotient of the useful energy by the supplied energy. The efficacy, or the photon flux per input power (PPF/W), is also calculated.

**Table XV.** Radiant flux Compared to LED input power, with resulting efficiency.

| **Wavelength (nm)** | **Radiant Flux (W)** | **Power (W)** | **Electrical Efficiency (%)** | PPF/W **(µmol/J)** |
|---|---|---|---|---|
| 727 | 7.97 | 15.51 | 51.4 | 3.10 |
| 666 | 15.58 | 19.44 | 80.2 | 4.21 |
| 450 | 7.08 | 11.16 | 63.4 | 2.37 |
| 425 | 8.5 | 14.38 | 59.1 | 2.10 |
| **Total** | 39.13 | 60.49 | 64.7 | 3.08 |

Table XV shows the LED input power for all channels at maximum duty cycle, and the corresponding efficiency for each. For all channel together, the system has an ON efficiency of 64.7%. The PPF/W ranges between 2.10 to 4.21 µmol/J for all channels. Since photons with shorter wavelengths have more energy according to Equation (2.5), the efficacy will be lower at the same efficiency for shorter wavelengths. For the whole system, the PPF/W is 3.08 µmol/J. Because the efficiency for each channel differs, the resulting efficiency will be dependent on the light mixture. With a 20.8:58.6:20.7 mix, attempting to drive 250 µmol/$m^2$s and dialing the red to max, the resulting efficiency can be seen in Table XVI. The radiant flux calculated and the output power and measured at 100% duty cycle for each channel are multiplied by their respective nominal duty cycle using $D_{nom}$ in Table XIII.

**Table XVI.** Radiant Flux, Power and Efficacy with a 21:59:20 Ratio.

| **Wavelength (nm)** | **Radiant Flux (W)** | **Power (W)** | PPF/W **(µmol/J)** |
|---|---|---|---|
| 727 | 3.16 | 6.14 | 3.10 |
| 666 | 15.58 | 19.44 | 4.21 |
| 450 | 3.02 | 4.76 | 2.37 |
| 425 | 4.08 | 6.91 | 2.10 |
| **Total** | 25.84 | 37.24 | 3.40 |

Whilst the efficiency of each LED channel in Table XVI is the same as in Table XV, which it will be if calculated, the total efficiency varies. By dividing total radiant flux by power, the resulting efficiency is 69.4%. The PPF/W increases to 3.40, which is a larger relative difference than the efficiency when compared to 100% duty cycle. This is likely caused by more of the light coming from the 666 nm channel, which has a greater efficacy than the others. Similarly, Table XVII shows the efficiency at an exact 20:60:20 light mix. The duty cycle of the 666 nm channel is maxed out, while the other channels are providing the duty cycle which corresponds to the correct light mix, resulting in $PPFD_{tot}$ of about 235 µmol/$m^2$s.

**Table XVII.** Radiant Flux, Power and Efficacy with a 20:60:20 Ratio.

| **Wavelength (nm)** | **Radiant Flux (W)** | **Power (W)** | PPF/W **(µmol/J)** |
|---|---|---|---|
| 727 | 2.97 | 5.77 | 0.44 |
| 666 | 15.58 | 19.41 | 0.30 |
| 450 | 2.83 | 4.47 | 0.79 |
| 425 | 3.84 | 6.49 | 0.42 |
| **Total** | 25.22 | 36.15 | 3.43 |

Total efficiency and PPF/W in the case of Table XVII is 69.8% and 3.43 µmol/J. Once again, the electrical efficiency increases somewhat, and the same goes for the efficacy. Furthermore, the heatsink temperature relative to the total PPFD is shown in Figure 5.6.

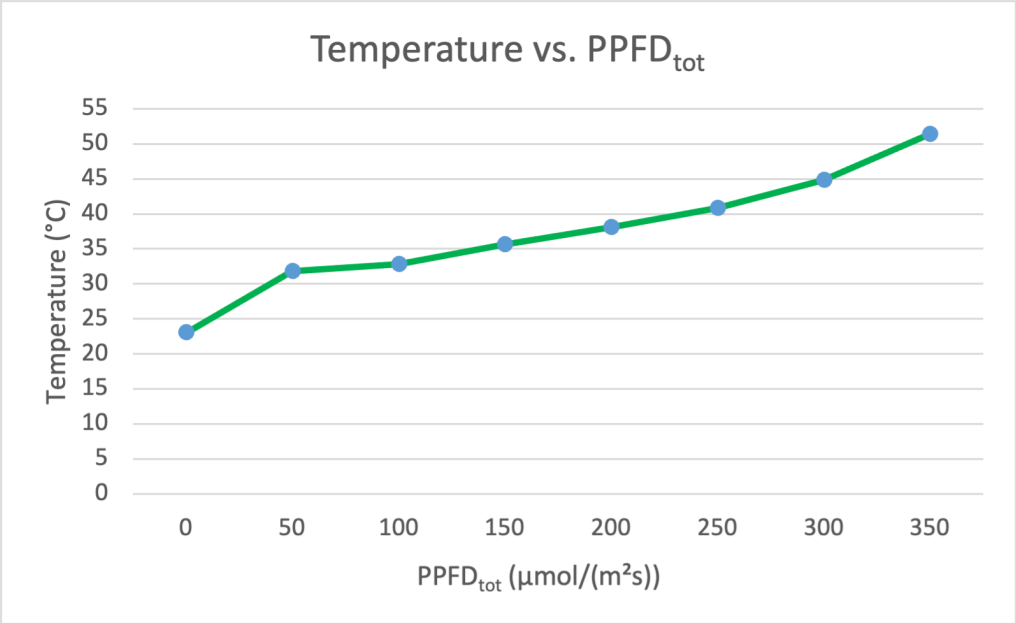


**Figure 5.6.** Temperature relative to the $\mathrm{PPFD}_{\mathrm{tot}}$, constant $K_{\mathrm{nom}}$.

The heatsink temperature increases with $\mathrm{PPFD}_{\mathrm{tot}}$ in Figure 5.6. The temperature rise does not appear linear to the $\mathrm{PPFD}_{\mathrm{tot}}$, reaching 51.4°at 350 µmol/m$^2$s. At 100% duty cycle on all channels, the measured heatsink temperature was 70.1°. Sensor measurements at constant PWM duty cycles are shown in Figure 5.7. Here the bars represent the sum of sensor readings from enabling one LED at a time at different duty cycles. The line represents the sensor readings with all LEDs enabled at the same time, at the same duty cycles.

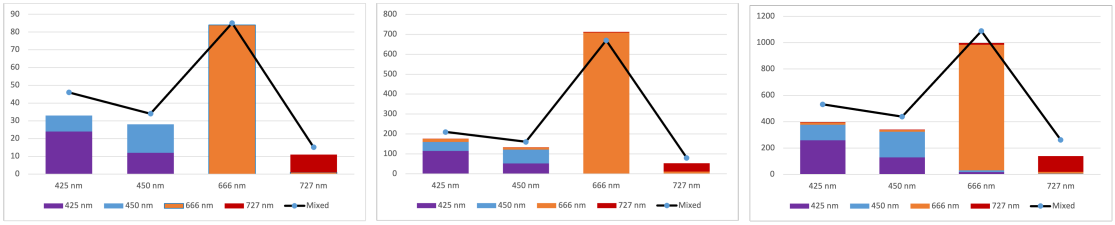


**(a)** 10% duty cycle **(b)** Nominal duty cycle **(c)** 100% duty cycle

**Figure 5.7.** Cumulative sensor reading counts compared to sensor readings with mixed light.

It can be seen in Figure 5.7 that the different LED channels give a measurement on sensor channels which does not correspond to the assigned channel for the different LED channel. There was almost always a difference between the the sum of sensor measurements compared to the measurements with all channels enabled at the same time in Figure 5.7. In all cases, except for the 666 nm channel with nominal duty cycle, the sensor reading is higher when all LEDs are enabled. Thus the sensor reading is not entirely cumulative, the sum of the sensor values is not the same as when they are measured at the same time.

## 5.3 Ambient Light Compensation measurements

Measurements comparing system performance in different external lighting conditions are shown in this section. First are calibration tests with or without a cardboard box in a room with lit ceiling lights. Tests were also performed to compare duty cycle and sensor reading in direct sunlight. These tests were made with the control system enabled to evaluate the systems ability to adjust according to the calibrated reference point for each sensor channel. Figure 5.8 shows the duty cycle of the system in stability, in the first two column groups the system is calibrated with a carboard box, the second of the groups is the duty cycle when the box has been removed. In the second two column groups in Figure 5.8, the system is first calibrated in ambient light, after which a cardboard box is place on top.

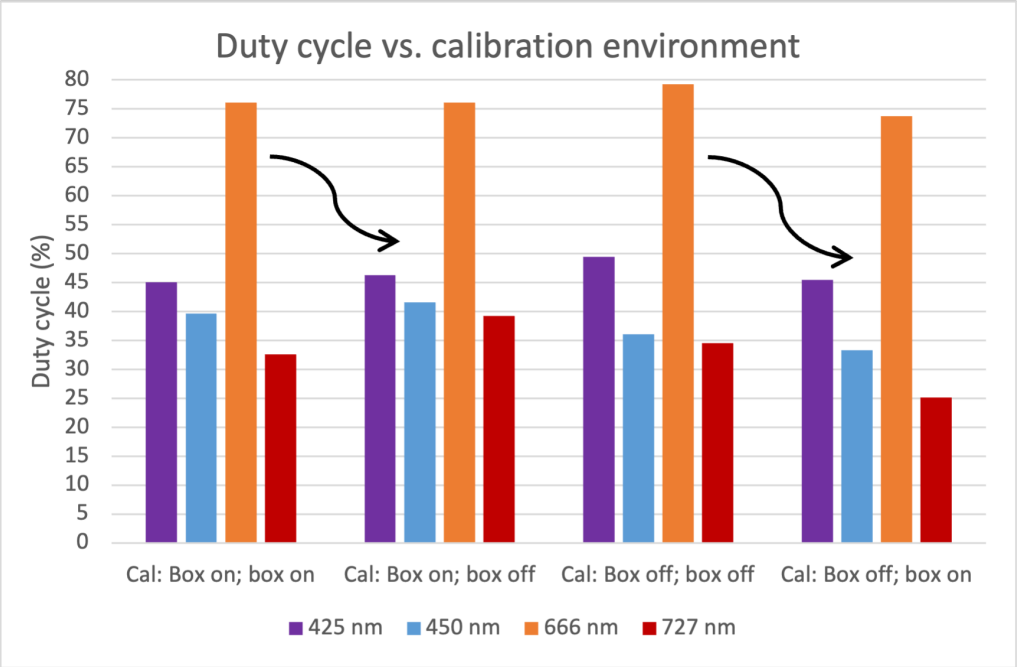


**Figure 5.8.** Channel DIM duty cycle for different calibration environments. Box on before the semicolon denotes calibration with the cardboard box on, and box off after semicolon for the measurement data.

The duty cycle increases somewhat for all but the 666 nm channel when the carboard box is removed, when calibrating with in place on top in Figure 5.8. Thus, the sensor senses measures less light overall when the cardboard box is not present. The initial duty cycle is higher for all channels except the 450 nm channel when calibrating without the cardboard box compared to with the box on. The duty cycle for all channels decrease and are lowest when the system is calibrated without the box, and it is then placed on top of the LEDs. The input power is recorded for the same cases as for Figure 5.8 in Figure 5.9.

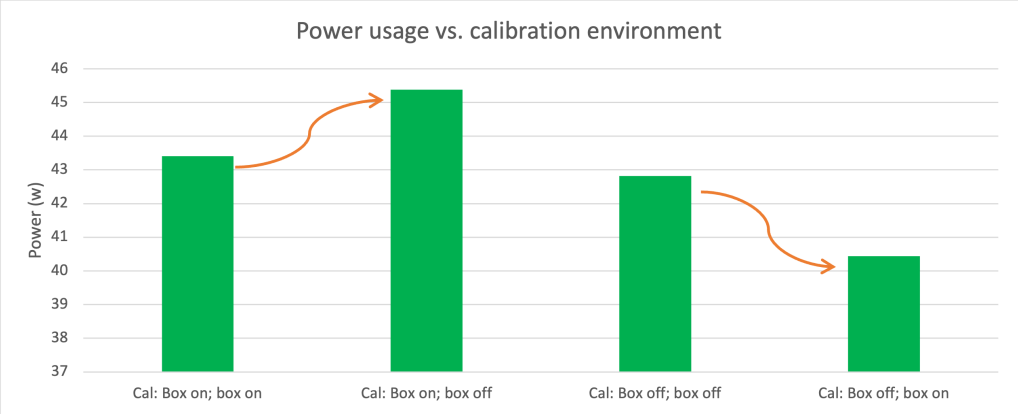


**Figure 5.9.** Power usage for different calibration environments. Box on before the semicolon denotes calibration with the cardboard box on, and box off after semicolon for the measurement data.

The measured power in Figure 5.9 follows a similar trend as the duty cycle in Figure 5.8. As the on time for each LED channel increases with duty cycle, the power should increase proportionally. Furthermore, the target sensor values in both cases are listed in Table XVIII. These targets are set in the initialization of the control system.

**Table XVIII.** Sensor targets from calibration with and without the box in ambient light.

| Calibration Method | 425 nm Channel Target | 450 nm Channel Target | 666 nm Channel Target | 727 nm Channel Target |
|---|---|---|---|---|
| Box on | 215 | 170 | 698 | 85 |
| Box off | 199 | 150 | 662 | 66 |

Table XVIII shows that the target values decrease when calibrated without the cardboard box. The decrease is present for all sensor measurements. The calibration target is determined by initially setting the nominal duty cycle on all channels. However, as Figure 5.8 shows, the duty cycle is different in each case when the control system is active. Measurements from the control system in in direct sunlight is shown in Figure 5.10. The different cases represent the position of the light system and sensor and respective calibration case. Case 1 and 2 are with calibration in direct sunlight, the system remains in sunlight in case 1 and was moved to the shadow in case 2. Case 3 and 4 are calibrated in the shadow. In case 3 and 4, the system is moved to direct sunlight after calibration, but the sensor is rotated 90 degrees in case 4. In case 5, it follows the same method as case 3 and 4 except the sensor was angled directly towards the sun by hand.

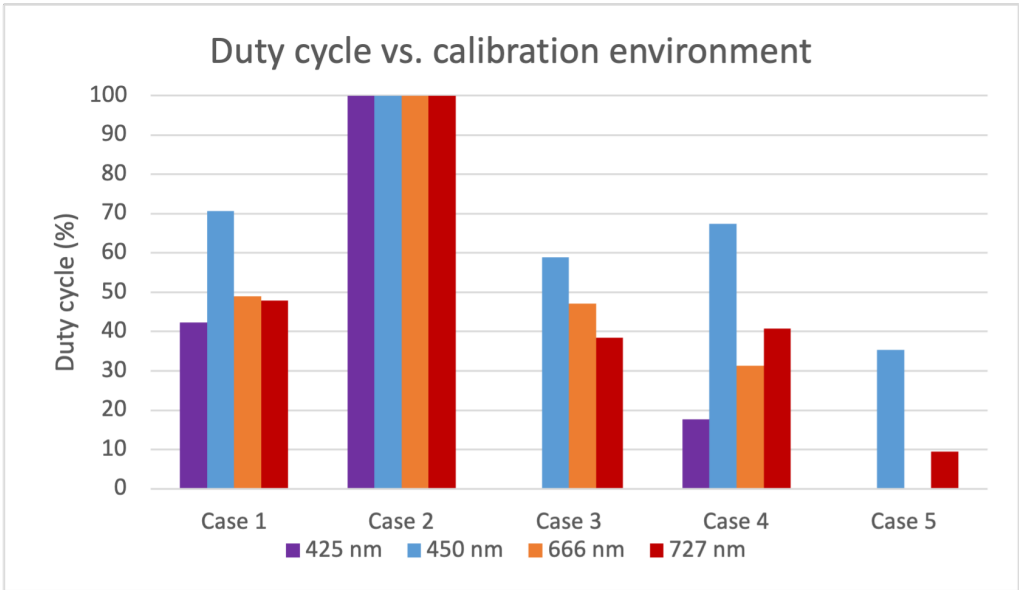


**Figure 5.10.** Channel DIM duty cycles for the different test cases in sunlight or shadow.

When calibrated in sunlight, and then moved to the shadow, the duty cycles of all channels maxed out as shown in Figure 5.10. This shows that the control system was likely unable to compensate for the loss of supplemental light solely by light from the LEDs. For case 3, 4, and 5 the duty cycle is always significantly lower for some channels than when in ambient light as in previous tests shown by Figure 5.8, although only significantly for 450 nm in case 5. The sensor channel measurements for each case are shown in 5.11.

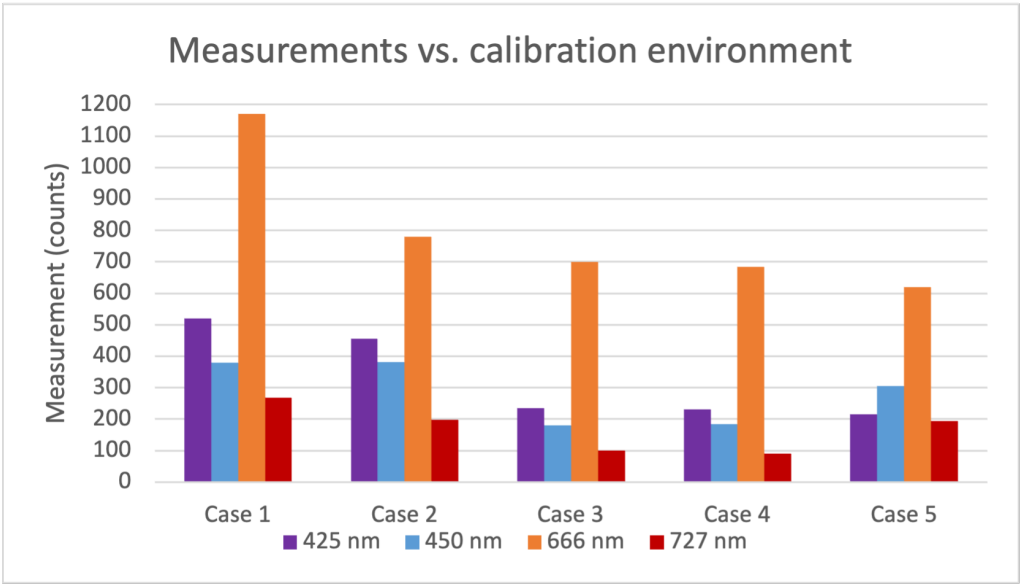


**Figure 5.11.** Control system resilience to ambient light.

When calibrated in sunlight, the sensor receives the highest channel measurements of all, when moved into the shadow, all channels decrease, except for 450 nm in

Figure 5.11. This shows that the system is not able to fully compensate the incident light to keep the measurement at the target. Compared to Figure 5.10 this makes sense since the duty cycle cannot be increased further, maximum light from the LED is already provided. When calibrated in the shadow, and then rotated, the measurements remain close to the same on all channels despite very different duty cycles. Thus the system is still able to compensate for the reference. In case 5, the measurement increases, while the duty cycles decrease or become 0. This case then is the inverse of case 2, the incident sun light provides more than enough light that the channels turn off. The measurements are however quite different between case 2 and 1.

## 5.4 Positional Testing

Positional tests are conducted to see how the lighting system performs with different placements of the sensor relative to the LEDs. These measurements were made with and without the control system enabled, at different duty cycles, heights and angles. The duty cycle and input power at different heights with the control system enabled is shown in Figure 5.12.

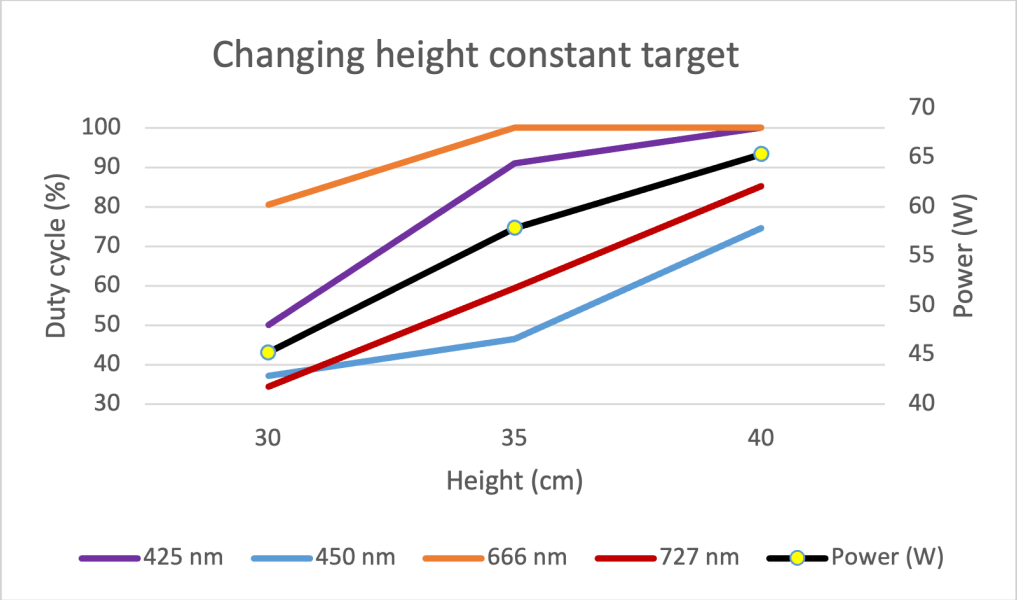


**Figure 5.12.** Changing distance between sensor and LED PCB while control system tries to keep constant measurement from sensor. The duty cycle and power increases with increasing height.

The total power consumption increases almost linearly when changing the height according to Figure 5.12. In this figure, the duty cycle of the PWM for the FR LEDs increases linearly with height. The duty cycle of the PWM for the R LEDs rises to maximum duty cycle at 40 cm. The duty cycle of the PWM for the two B LEDs do not increase linearly, when the duty cycle for the LEDs with 425 nm increase fast the one for the LEDs with 450 nm increases slower and vice versa.

Measurements when the PWM were plotted against the height with the box on in Figure 5.13a and box off in Figure 5.13b.

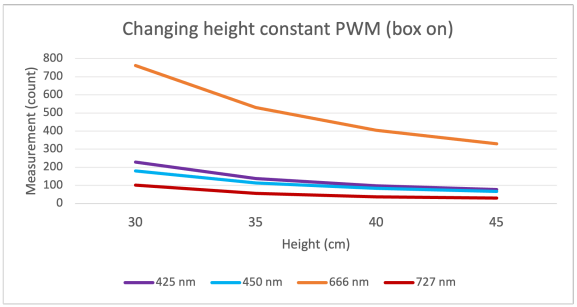


**(a)** Changing distance between sensor and LED PCB while keeping constant PWM signal. Box is on. Measurements from sensor decreases with increasing distance.

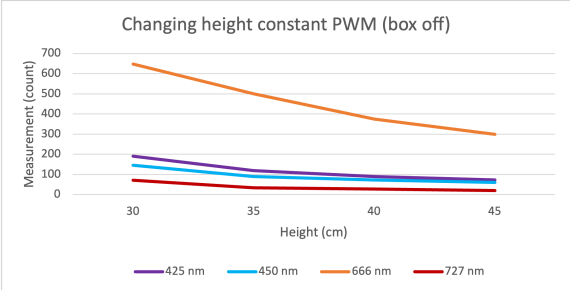


**(b)** Changing distance between sensor and LED PCB while keeping constant PWM signal, box off. Measurement from sensor decreases with increasing distance.

Taking the average of all the measuring points from one channel obtained with the box on and dividing that with the same thing for the box off gives a factor relating the the two test cases with the box on and off. Doing this for all the channels gives us that the measuring points with the box on is on average 14.9%, 21.3%, 11.3% and 48.0% higher then the measuring points with the box off. All of the channels for both Figure 5.13a and 5.13b follow roughly the same shape, they are not decreasing exponentially because the measurement does not decrease at a rate proportional do the the earlier measurement.

Figure 5.14 shows the measurements when tilting the sensor relative to the LED PCB. The LEDs are driven with a constant duty cycle. The sensor was tilted to 31°, and 55°.

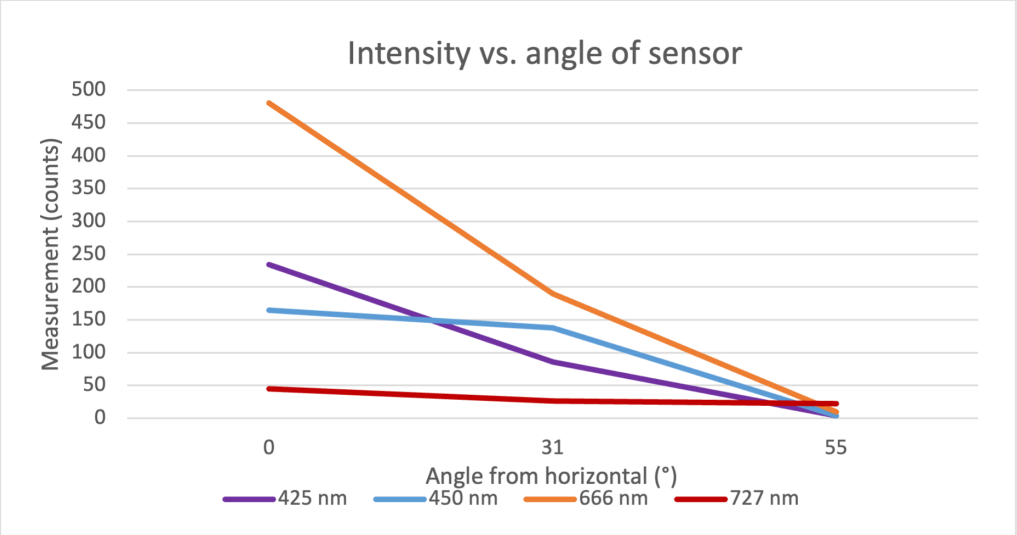


**Figure 5.14.** Measured intensity of light channels as the angle of the sensor changes relative to the horizontal positional of the LED PCB. Measurement of all channels decrease as the sensor faces less straight toward the LED PCB.

Figure 5.14 shows that for all channels, the sensor readings decrease significantly when tilting the sensor away from the LEDs. The decrease of each channel appears nearly proportional to the initial sensor reading. Note that the sensor was held steady by hand.

## 5.5 Protective Stages

The fuse rating calculated in section 3.5.1 used the test current of 700 mA and maximum forward voltage ($V_f$) values directly from the respective LED datasheets [42], [43], [44], [45]. The correct values should be based on the forward currents in Table II, and then use the datasheets plotted $I_f$-$V_f$ graphs to find the forward voltage value at those currents. The updated LED maximum effect ratings are found in Table XIX.

**Table XIX.** Correct LED maximum effect ratings.

| **LED** | $V_f$ **(V)** | **Max Effect per LED (W)** | **Number of LEDs** | **Total Max Effect per LED type (W)** |
|---|---|---|---|---|
| GF CSSRML.24 | 2.15 | 2.15 | 7 | 15.05 |
| GH PUSRA1.25 | 2.04 | 2.856 | 14 | 30.984 |
| GD PUSRA2.15 | 2.94 | 4.116 | 3 | 12.348 |
| LTPL-C034UVH430 | 3.75 | 3.75 | 5 | 18.75 |
| **Total** | | 18.872 | 29 | **77.132** |

A safety power consumption could be set to 80 W. Equation (3.18) then yields the maximum power supply current to be $I_{tot} = 2.67$ A, and a fuse rating of 3.33 A after applying the 125% rule, rounding up to 3.45 A. When 30 V was applied to the

power PCB ports, negligible voltage drop was measured over the fuse.

The reverse polarity protection worked as intended, as the voltage over any arbitrary component to ground measured 0 voltage. The 30 V relay worked as intended, but is unnecessary as the Arduino has the ability to turn off the 30 V power rail as measured at the LED driver input. A resistor associated with the circuit was found to be severely overheating with temperatures exceeding 140 °C. There was a voltage loss over the MOSFET which caused the voltage on the 30 V rail to decrease to about 29 V.

## 5.6 Thermal Dimensioning

The thermal measurements were performed with a thermal gun pointed directly at the heatsink. The maximum recorded heatsink temperature was 51.4 °C, as can be seen in Figure 5.6, and such was the case when $\mathrm{PPFD_{tot}} = 350$ µmol/(m$^2$s). The maximum measurement error of the laser thermometer is ±1 °C for temperatures ≥ 0 °C when calibrated [64], thus the considered heatsink temperature is 52.4 °C. The ambient temperature was recorded as 21 °C. At the same $\mathrm{PPFD_{tot}}$, the total power usage was 53 W, as seen in Figure 5.5. Accounting for the power converted into radiant flux at the efficiencies listed in Table XV gives the total dissipated power as 18.7 W. Using Equation (3.3) from section 3.1.3, with values from Table II, gives the worst-case estimated junction temperature as 132 °C for the ambient to junction path. Since the temperature was also measured directly on the heatsink, Equation (3.3) is simplified to ignore the $R_{\mathrm{th,heatsink}}$ term. The recorded heatsink temperature is used instead of $T_{\mathrm{ambient}}$, with the worst case value for $R_{\mathrm{th}}$ at 3.3 °C/W, and $P_{\mathrm{tot}}$ at 18.7 W, the junction temperature is estimated as 119 °C. The total dissipated power is distributed over each of the LEDs and many of them have much lower thermal resistances. A more realistic, but still conservative estimate of the junction temperature, is made by considering that the power is distributed across each LED. In the circuit model, the 29 LEDs are in parallel, so the junction temperature is instead estimated using the same method, but by dividing the thermal resistance with the amount of LEDs. This gives a junction temperature of 59 °C.

# 6
# Discussion

To evaluate the systems ability to fulfill the intended goals of the thesis, the system in its entirety has to be assessed with basis in the design and the results from the testing. The discussion is divided into the separate design elements of the system. These are the protection stages, control system, thermal dimensions and considerations for efficiency with regards to the power supply component selections. The overarching results show that the system is able to produce light at the intended wavelengths at close to the intended intensities. The system is broadly more efficient than non-LED based systems. The control system can control the intensity in a static environment, but is sensitive to positional changes or significant ambient light reduction.

## 6.1 Protection Stages

During the testing of the protection stages a current limited power supply was used. A possible restriction in the evaluation of the protection stages is that the voltage from the power supply was set according to reading given from the power supply. No calibration of the power supply was done to make sure that the applied voltage was exactly correct during this testing.

The fuse rating was mainly calculated by using the LEDs power consumptions and then adding 5 W for safety. The calculations are incorrect using the maximal forward voltages presented in the datasheets, along with the stated typical current for each LED. The correct theoretical fuse rating is 3.3 A. After testing the system it was found that, with 100% duty cycle, the maximum current was measured to be 2.15 A. This means that the system can use a smaller rated fuse without issue. Having a fuse is good practice when designing electrical devices to avoid fire risk if a short circuit were to occur. Since the voltage drop over the fuse is insignificant, this also does not affect the efficiency and therefore the efficacy of the system.

The TVS diode that was selected has one main flaw, the reverse voltage is 30 V which means it will constantly run a current through the diodes. The normal running conditions is still well below breakdown voltage which means the current would be very small but still contribute to wear and tear to the diode. During ordering of the components, due to miscommunication, SMBJ33A was ordered instead of SMBJ30A. SMBJ33A has a 33 V in reverse voltage which means no current would run through it during normal drive, but the breakdown voltage is slightly higher

and the clamping voltage is 53.3 V [58]. This means that the TVS diodes do not protect the components in the filtering stage that have a voltage rating of 50 V. This voltage rating should been more than sufficient given the voltages but because of this, the TVS diode theoretically does not fulfill its purpose. Ideally a TVS diode with a reverse voltage slightly over 30 V and a clamping voltage under 50 V should have been chosen to solve both these problems. The TVS diodes were not tested given that no access to a Electrostatic Discharge (ESD) simulator was available.

It could have been beneficial to place TVS diodes at other parts of the circuit, for instance at each LED channel on the LED PCB. While the LED drivers have internal transient protection for its output, the long cables running between the power PCB and LED PCB act as antennas for EMI and ESD. What this means is that touching the LED PCB can introduce ESDs, or that the switching of the current can create inductive spikes in the cable. Therefore placing a reverse biased TVS diode in parallel for each channel could be a good idea to protect the LEDs from transients, given that they are sensitive to over voltage. No calculations regarding these proposed TVS diodes have been made and are purely a proposal for further development.

The 30 V relay proved to be redundant and only introduced losses and possibly degraded the performance in the device. High thermal losses were observed on the resistor with thermal measurements. During the simulation of the cictuit the power losses were not considered. Different values for the resistor could have been tried to decrease losses. The relay design was initially supposed to turn off the 30 V rail for the LED drivers in case of overheating or over-current instances. Both of these cases came to be covered by other components. The over-current protection was already present in the LED driver IC and the temperature control is managed by the Arduino adjusting the duty cycle of the the PWM signal. This may have degraded the performance of the LED drivers especially channel 1 which has a maximum forward voltage close to 30 V. Thus the inclusion of this relay was ultimately unnecessary and introduced unnecessary losses, while also generating significant heat.

The reverse polarity protection system on the device is rather simple consisting of a PMOS, a Zener diode and a resistor. The test that was carried out was successful and protected the downstream components from current flow in reverse polarity. This removes the risk for accidental connections leading to component failure, overheating, or severe electrical risks thus making the product safer and more user-friendly.

The testing did not include any testing of other input filter or the input transient protection. The transient protection testing required access to some kind of pulse testing device to generate ESD, but was not available. The testing of the input filter could have been done but was not conducted due to time constraints. Because the input filter was designed with a high cutoff frequency of 0.11 MHz, while the target frequency was 1 MHz, the filter effect at the target frequency should be substantial.

## 6.2 Control System

Evaluating the control system is important to the total device performance evaluation. The control system encompasses key device functions such as color mixing and regulation of output light based on the set light mix.

The project included two thermistors on both of the PCBs. These thermistors were meant to be used to throttle the duty cycle and or turn off the 30 V relay in the case of one of the PCBs exceeded safe temperatures. During testing, it was found that the reading from these thermistors were heavily impacted by EMI from the LED driver circuits. We isolated that the power PCB thermistor's behavior was strongly linked to the closest LED driver. The values obtained from the LED PCB thermistor were found to be stable enough to be used to moderate the power like initially designed. A function that samples the values was deployed to make the values measured from the thermistors more stable, but the values form the power PCB were still not stable enough to use. Low pass filters could also have been placed at sensitive pins of the thermistor to reduce noise.

A limitation of the thermistor implementation is the lack of validation of their readings. No calibration of the thermistors was done. A comparison of the readings from the thermistor to the value of the laser thermometer could have been done. This comparison could have helped to ensure that the function that translates voltage to temperature was accurate for the device. Due to the inaccurate reading from the thermistors, this was not done and focus was instead spent on improving output signal stability with sampling.

Something discovered during testing was that the box used for testing increased the measured intensity as seen in Figure 5.8. The cardboard box could cause reflections within the box due to its proximity to the light, channeling the incident light to the sensor and increasing the measurement. A way to improve testing would be to treat the box in some kind of light absorbing material like a matte black fabric, or by using a larger box. Another way is to test in a large dark room to avoid internal reflections.

The light sensor initially gave readings that were inconsistent. The conclusion on why this happened was that the integration time of the sensor was set too low by default. The period time of the PWM is around 2 ms and the default integration time of the sensor is 2.78 ms. This meant that the integration performed by the sensor could change from reading to reading depending on how much the sampling period overlapped with the high state of the PWM signal. To remedy this, the integration time was set to a value much greater than the period time of the PWM signal. The integration time was set using the ASTEP and ATIME variables. The combination of the variables used can be found in Table XI.

The configuration of the integration time and gain did not consider the size of the Analog-to-Digital Converter (ADC) buffer of the light sensor. The ADC has the counter used to measure the amount of light [39]. The ADC has a maximum value

fullscale of 65535. The limitation comes from the maximum size of unsigned 16-bit integer used to store the measurement value at each integration cycle. The equation to calculate the $\mathrm{ADC}_{\mathrm{fullscale}}$ value can be found in the datasheet [39] and is

$$\mathrm{ADC}_{\mathrm{fullscale}} = (\mathrm{ATIME} + 1) \cdot (\mathrm{ASTEP} + 1). \tag{6.1}$$

With the choice of ATIME and ASTEP, the $\mathrm{ADC}_{\mathrm{fullscale}}$ value would be higher than 65,535. According to the sensor datasheet the value is set to the maximum by the light sensor. The light sensor could saturate when the incident light corresponds to a value beyond the full scale value. This case was deemed improbable as under direct sunlight or maximum LED setting the maximum reading observed was well below this value.

In the control system a sensor was assigned to each of the LED channels. The 425 nm and 450 nm LED channels have a corresponding sensor channel at F2 and FZ for their exact peak wavelength [39]. This made the choice of assigning sensor channels for the 425 nm and 450 nm LEDs channels trivial. The choice of which sensor channel to assign the R and FR was harder as no directly corresponding sensor channel on the light sensor exists. The light sensor has three channels close to the peak wavelength of the R and FR LED channels. These are the F6, F7 and F8 channels that have sensitivity peaks at 640 nm, 690 nm and 745 nm respectively. R was assigned to the F6 andFR to the F8 channel sensors. The reasoning was to reduce the impact of the different channels on each other's light sensor. If for example the F7 sensor channel was chosen for FR the light from the 666 nm channel would have a larger effect on the 727 nm channel's sensor. This would make it harder for control system to accurately adjust the duty cycle. The choice of light sensor channels could be further studied and methods such as taking the average of multiple adjacent channels could be implemented to improve control system performance.

The ability of the R and FR LEDs to produce B should be nearly impossible because of negligible spectral overlap between the emission spectra of the R/FR and B LEDs. Likewise, measurement sensitivity spectrum of the F2 and FZ sensor channels should not be influenced by emitted R and FR [39]. Despite adjusting gain and integration time some of R is still registered by the B sensor channels as shown in Figure 5.7. Results showed that setting the integration time to a higher value made this effect smaller but setting higher integration time made the readings from the sensor reach the peak value. To make sure the sensor would not saturate even during direct sunlight, the gain on the sensor was set conservatively to the lower value. This was done simply with the `setAgain()` function in the Sparkfun AS7343 library [52].

The light sensor channels measure incident light within a spectrum at increasing intensity relative to its dominant wavelength. It is also assumed in the dimensioning (section 3.1.2) and in the light mixing calculations (section 3.4.1) that the PPF radiated by a specific LED channel is the only one that contributes to the light radiated at that wavelength. The LEDs produces light with a given peak wavelength, but the LEDs also produces light of other wavelengths as discussed in section 2.3.

LEDs have a spectral bandwidth, and therefore also influence sensor channels other than any specific one with the same peak wavelength. This can also be seen in Figure 5.7, that the two B LED channels give large contribution to each other's sensor channels, while the contribution of the R LED channel to the B sensor channels is less notable. To balance this second phenomenon, the spectral bandwidth for each LED could be taken into account when calculating the duty cycle in section 3.4.1.

Taking this into account, and then using these duty cycles to calibrate the target, will yield the same sensor measurements as when calibrating with duty cycle values obtained without taking spectral overlap into account. The duty cycle calculated with regard to the crosstalk will however be lower than the duty cycle without taking the spectral overlap into account. Therefore, the actual $\mathrm{PPFD}_{\mathrm{tot}}$ that hits the area would be larger in the case when spectral overlap is not taken into account. This is because the calculated duty cycle, that is used for setting the target values, do not take into account the PPFD from other channels to reach the desired target values.

The measured values by the sensor with the spectral overlap taken into account would theoretically follow the predetermined ratio set by $K_{\mathrm{PPFD}}$. As the measurements from the sensor seen in Figure 5.7 appear to not be cumulative, the values would in reality not follow the desired ratio set by $K_{\mathrm{PPFD}}$. The contribution to the $\mathrm{PPFD}_{\mathrm{tot}}$ by each LED channel would in neither theory nor reality follow the ratio set by $K_{\mathrm{PPFD}}$ when spectral overlap is included in the calculations. This is because duty cycle for each channel would be influenced differently for each channel depending on the different amount of spectral overlap that affect the different channels.

This is reversed if the duty cycle is calculated without taking spectral overlap into account. The measured value by the sensor would not follow the ratio set by $K_{\mathrm{PPFD}}$. The same reason follows here, the measured overlap will depend on the spectral overlap and thus affect the measured value on the different sensor channels differently. Instead, the LED channel's contribution to $\mathrm{PPFD}_{\mathrm{tot}}$ would in this instance yield the ratio set by the $K_{\mathrm{PPFD}}$.

It is not possible to make the ratio set by $K_{\mathrm{PPFD}}$ correct for both the value measured by the sensor and the channel's contribution to $\mathrm{PPFD}_{\mathrm{tot}}$ at the same time. So it was necessary to choose between having a LED channel contribution that follows the ratio, or a sensor measurement that follows the ratio. Because the sensor appears not to be cumulative, the increase in measurement will be nonlinear. Thus, the sensor measurement would still not be correct. Keeping measured ratio correct is also less interesting compared to keeping the contribution ratio correct, this follows from the fact that it is of more interesting keeping the total bell curve of the LEDs in accordance with the ratio, rather than just the measured peak wavelength. The system will constantly undershoot $\mathrm{PPFD}_{\mathrm{tot}}$ if spectral overlap is accounted for is also important to consider, since it is generally not beneficial for plant growth, as discussed in section 2.1.1 and 2.1.2. All this together contributed to the decision to exclude the effects of the spectral overlap and thus accepting that the measured sensor values would not correspond to the actual PPFD. For the same reason as

discussed above, there is no point in integrating the spectral overlap phenomenon into the code.

The junction temperature affects the LEDs to shift both the peak wavelength and the spectral bandwidth. Because of this, multiple duty cycle and consequently multiple light mixes satisfy the targets, this will happen regardless of whether the spectral overlap is included in the initial calculation or not. The changes in temperature is not accounted for when calibrating the sensor target.

Because a PI regulator is used the possibility of this happening is reduced. The magnitude of the response will correlate to the error and the accumulated error over time. This means that the more the measured value deviates from the target, the stronger the initial response from the proportional action will be. The integral action will depend on the total error accumulated and will thus act as a steady state error and force the system into the correct equilibrium. So even though nonlinearity is introduced to the system and the system is disturbed and leaves the equilibrium, the steady state error should be able to force the system back into the right equilibrium. Regardless if the initial calibration uses duty cycle values that are calculated with, or without spectral overlap, the targets received by the PI regulator should be able to find the equilibrium.

When setting the values of $K_\mathrm{p}$ and $K_\mathrm{i}$ there was a lack of concrete testing of different values of these regulator parameters. The values $K_\mathrm{p}$ and $K_\mathrm{i}$ could have been set better if further testing was employed. The values set the regulator were judged mostly on stability and ability for the system to respond quickly. Setting the $K_\mathrm{p}$ and $K_\mathrm{i}$ in relation to the $K_\mathrm{PPFD}$ and thus the relation to the steady state error for each channel should improve the general response time. An optimal choice of regulator values was not achieved because the control system was deemed to be good enough. The exclusion of derivative action for the regulator proved a success. A PI regulator was chosen instead of a controller with derivative action since the system does not require a fast response. Changes in ambient light occur gradually throughout the day as the sunlight varies slowly, making a PI regulator sufficient for maintaining a constant light level.

The possibility of reaching the wrong equilibrium will be most notable when there are abrupt changes in ambient light that alters the steady state error a lot, therefore making it harder to return to the equilibrium point. Because of the nonlinearity of the system it might then lose track of its steady state error and thus land on an equilibrium which does not correspond to the correct light mix. One way to decrease the chance of this happening is to stop adding the error to the accumulated error when the duty cycle is zero (or one), thus it will not be pulled as far away from the steady state error by continuous exposure to ambient light that it cannot possibly calibrate for.

The light spectrum readings is restricted by the choice of the light sensor. While the sensor measurement is not an exact measurement, it can control the system using a

target based on a calibration test. The sensor would measure the incident light using the calculated duty cycle, controlling the system to according to that measurement. When calibrated the system worked quite well, generally being able to return to the target value. It was also able to compensate for sunlight when first calibrated in the shadow, as shown in Figure 5.10. If the system was calibrated in an environment where the intensity of the ambient light is greater than the LEDs can emit the system will not be able to keep this target in the case where the ambient light is removed, as demonstrated in Figure 5.10. In this case the duty cycle maxes out on all channels. The control system is similarly sensitive to positional changes as shown by Figure 5.12 and 5.14. Thus, while the system can control the light in the same setting it was calibrated in, the light output will change significantly if it is changed.

Acquiring a sensor that could accurately measure incident PPF would allow the device to regulate the system based on the desired incident light measurement rather than a calculated and calibrated reference point. The spatial distribution could be more accurately modelled to estimate the incident light at the sensor placement. Multiple sensors that only sense light of a narrow wavelength could also be used.

Using the light sensor measurement mainly as reference is no real problem in regard to plant cultivation if the measurements discussed in sections 3.1.2, 3.4.1 and 2.3 are correct. Assuming a consistent calibration environment, both $\mathrm{PPFD_{tot}}$ and $K_{\mathrm{PPFD}}$ will reach their intended values provided the operational duty cycle matches, or almost matches, the duty cycle used to set the reference. When comparing the $D_{\mathrm{nom}}$ in Table XIV and the resulting duty cycle in for example Figure 5.8, the difference is insignificant. The values in Table XIV are used to evaluate the adaptability of the system, it is observed that $D_{\mathrm{nom}}$ is below 50% for all but one of the LED channels and their total contribution to the $\mathrm{PPFD_{tot}}$ could be increased by a minimum of 100%.

The R LED channel is the only one with a $D_{\mathrm{nom}}$ that can only be increased by 27%. Even though the $D_{\mathrm{nom}}$ for this LED channel is somewhat limited the $\mathrm{PPFD_{max}}$ is still sufficient to increase $K_{\mathrm{PPF}}$ to 0.75 at $\mathrm{PPFD_{nom}}$. Looking at the theory in section 2.1.1 and 2.1.2 it is observed that the general use for R is as the main energy provider for the thylakoid reactions as well as influencing the ratio of Pr:Pfr. As for being the energy provider, the plant will require roughly the same energy throughout the whole growth stage. More developed plants which require more energy, generally also have a larger leaf area and thus a bigger light interception area, but this is subject to change depending on which plant is discussed. Changes from $\mathrm{PPFD_{nom}}$ will generally never exceed 50 $\mu\mathrm{mol}/(\mathrm{m^2 s})$, in which case the $\mathrm{PPFD_{max}}$ is enough to keep $K_{\mathrm{nom}}$.

In instances where a large deviation from $\mathrm{PPFD_{nom}}$ is requested, it would theoretically be possible to increase $K_{\mathrm{PPF}}$ of the FR LED to counteract the missing light from the R LED channel but doing so will have an influence on the Pr:Pfr ratio. This can theoretically be counteracted by increasing the B LED channels which will activate more cry which act to suppress shade avoidance as mentioned in section

2.1.1.2. The ability to do this is not discussed in this paper. As for this ratio, the fact that we can influence it with both R and FR means that despite limitation in the R LED channel, it is still possible to influence this ratio. The fact that $\mathrm{PPFD}_{\mathrm{max}}$ for the FR LED channel is high, means that R:FR ratio can actually be changed substantially while keeping the R LED channel at $D_{\mathrm{nom}}$. What this means for the adaptability of this system, is that it can provide large quantity of light which is good at driving photosynthesis (R) while keeping the Pr:Pfr ratio relatively low, thus not inhibiting shade avoidance behavior.

The 425 nm LED channels $K_{\mathrm{PPF}}$ will be kept the same as $K_{\mathrm{PPF}}$ for the 450 nm LED channel. The reason for this is that the ratio between them has no real influence and are simply their to cover the absorption maxima of Chl *a* and Chl *b* as well as the rest of the B part of the spectrum. The reason they are included are because of the their necessity in regards to cry and phot, as mentioned in section 2.1.1.2. Therefore the general rule when setting the B:R:FR ratio, apart from events such as the EOD FR, should be to never set the B to zero because the responses to above mentioned photoreceptor will stop and plant development will be influenced as discussed in section 2.1.2 and 2.1.1.2.

The code used for the Arduino Nano was based on examples provided by the [52]. Some code was also AI generated [68] because of the lack of sufficient programming knowledge in the C programming language. The code was vetted, edited and understood before integrating it into the program.

The program prints results in the serial terminal in the Arduino IDE. When the device is deployed, a computer would need to be connected to change the light mixture and read values of the output. The Arduino Nano is not configured to be reachable wirelessly therefore no changing of the configuration can be done without being onsite. This is a feature that could be implemented if a different Arduino model is used with Wi-Fi and Bluetooth connectivity. Giving the microprocessor wireless connectivity would allow setting time varying output as described in the goals section. The current implementation of the device cannot adjust the light output depending on plant growth stage or time of day by itself. Connecting the Arduino to an external time keeping source or a device that directly sends the desired color mix could allow the time varying output.

A way for the device to measure the time of day could be implemented by measuring the ambient light during the day or the use of the Arduinos internal clock. The internal clock method could be subject to drift over a longer time period and prove inconsistent if the correct time is not calibrated regularly.

A feature that could prove useful is the integration of current and voltage measurement on the LED channels. This would allow the microprocessor to estimate the PPF from the current and voltage according to the properties of each LED. This could be implemented with current and voltage measurement IC's but consideration has to be made so that the measurement devices do not affect the channel

impedances too much as to make the LED driver not able to drive the LEDs.

## 6.3 Electric Power Configuration, Efficiency and Power Metrics

The inclusion of the 0 Ω feedback resistor on the LED driver design was not necessary. These resistors are unlikely to have had an impact since they act as traces. Other devices with different LED configurations or different wiring solutions may find these feedback resistors necessary for adequate performance.

The choice to use a LED driver IC was made after much consideration. Other options, such as using a MOSFET to dim the LED, were considered. The IC has most of the components used for a buck converter integrated, such as the low and high side MOSFET and the controller. The footprint of the IC is smaller than if the components were to be external. This allows for higher power density and a reduction in the amount of components to solder. Fewer components reduce the risk of mistakes during assembly, mistakes during assembly, and reduces the risk of incorrect component selection during the designing stage. The LED driver chosen has safety features included, such as open loop and overcurrent sensing [37]. These features would have to be implemented manually if another LED driver or custom buck converter design is used.

The LED driver TPS92200D1 has the ability to run in two different LED dimming modes [37]. Analog and PWM dimming mode. For this project the PWM dimming mode is used because of the larger dimming range offered by PWM dimming compared to analog dimming. PWM dimming also typically has a smaller wavelength shift [23]. The intensity is also more consistent across different types of LEDs when PWM dimming is used. If analog dimming is desired the Arduino has to be configured to give 0.65–1.3 V with the use of an RC filter to make the PWM signal constant. Another way to adapt this device for analog dimming is switching the IC to the TPS92200D2 version. The TPS92200D2 version is restricted to analog dimming, but it can use the PWM signal provided by the Arduino directly. The decision to use the TPS92200 LED driver restricted the maximum forward voltage for each LED channel to 30 V

The cause of the 12 V buck breaking the Arduino may have been due to underdimensioning the buck converter. The component selection was made with little headroom for maximum current, possibly making the buck converter prone to voltage spikes should the Arduino require more. The buck converter provides a relatively high voltage compared to what the voltage regulator on the Arduino is designed for. The microcontroller may have been particularly sensitive since it was a cheaper, third-party product based on the Arduino Nano and not the official unit. Choosing a 7 V buck converter or dimensioning the output capacitor and inductor of the buck converter for much higher maximum current could possibly have made the

buck converter work. The 12 V startup transient had a peak of 13.35 V. But this should not have caused the Arduino Nano to break as the Arduino Nano has an LDO (LM1117IMPX-5.0) [38], which has a maximum input voltage of 15 V. Regardless, some form of transient protection could be useful to suppress transients created by the buck converter and therefore avoid breaking the Arduino. Not using the buck converter when evaluating the system means that total input power for the integrated system cannot be evaluated exactly. However, it can be assumed that the power consumption of the Arduino is at maximum 4 W. This worst case power draw comes from the LDO on the Arduino Nano having a maximum output current of 800 mA at 5 V[37].

As shown in Figure XII, most channels have some deviation from the intended output current, particularly for the 666 nm channel. The inductor ripple current decreases with forward voltage above 15 V, and more significantly as forward voltage approaches the input voltage of 30 V. The 666 nm was dimensioned with typical forward voltage rather than the forward voltage expected at the ON current value. Thus, the inductor ripple current would then decrease until the LED driver became unable to regulate the forward current any further. When ripple current decreases below 300 mA, the LED driver may not be able to distinguish the ripple current from the noise. The PCM controller is triggered by noise instead of the peak of the inductor current. Thus, the low side MOSFET is turned on for a longer part of the switching period than it should be. As a result, the average forward current cannot increase any further, even though the sense resistor voltage is below 99 mV. While it could be suspected that the forward voltage stopped increasing because the LED driver was outputting close to the input voltage, the ripple current is a more likely culprit to this result.

Should the system had been dimensioned using the forward voltage expected at the ON current, this may not have been an issue. Likewise, had the inductor been dimensioned with greater margin, taking into consideration the decreasing ripple current, the driver likely also would have been able to keep adjusting the current. The other channels were designed with significantly greater margin for ripple current, as shown in VII. Even though their calculations were based on typical forward voltage, the resulting ripple current was still high enough for the PCM to increase the current. To be consistent, all channels should have been dimensioned for the output forward voltage at the ON current, not the typical.

The cause for lower output forward current in the other channels can however not entirely be explained by inductor ripple current, as the calculated value remained over 300 mA for all channels. The waveforms for the voltage across the sense resistors shown in appendix B show that there is significant noise for most channels. Whilst the average on voltage may be close to 99 mV, if the LED driver controller senses voltage spikes above 99 mV the LED driver will not continue increasing the current during that switching period. This may be why the resulting ON current for the other channels are below their intended value. In the system overall, there are many signals that are activating at once, and since the ground planes are all

connected the LED drivers may interfere with each other and the ground on the sense resistors. It is known that there is substantial EMI problems on PCB. This was shown by thermistor on the power PCB which gives unreasonable temperature ratings when DIM duty cycle increases. A possible solution could be to place a low pass filter on the feedback pins of the led drivers. However, greater consideration for EMI in the design should have been made.

Designing the LED drivers for their maximum rated forward current, allows for significant adjustability in the light mix, at the expense of efficiency. This is because the increase in radiant flux is not proportional to the current. At double the typical current, as for the 666 nm and 450 nm channel, the relative factor is below a factor of 2, as shown in Table IX. To compensate the duty cycle has to be increased to provide the same average radiant flux, resulting in higher power as the average current increases. In this case the design was made with maximum adjustability in mind. Accidentally however, because the ON current for all channels was lower than expected, total power was probably lowered. Consequently, the ability to provide the nominal light mixture at different intensities was also quite limited. This is particularly true for the 666 nm channel. Should light mixes with less than 666 nm light be used, there is still significant adjustability. The actual $\mathrm{PPFD}_{\mathrm{max}}$ for each of the LED channels is thus lower as seen in Table XIII. The channel which is affected the most is the R LED channel which now has a $D_{\mathrm{nom}}$ equal to 106%. This is obviously not reachable, but it is still relatively close, so if the system is driven with the R duty cycle on 100%, the $\mathrm{PPFD}_{\mathrm{tot}}$ would be 9 µmol/($\mathrm{m}^2$s) lower, and the $K_{\mathrm{PPFD}}$ for the R LED channel would be slightly lower then intended. The adaptability given by the FR and B LEDs as mentioned earlier in discussion will still be the same, but we can not increase the $\mathrm{PPFD}_{\mathrm{tot}}$ while keeping $K_{\mathrm{nom}}$.

In terms of total efficiency, comparing the PPF/W of each LED channel with that of some HPS lamps, the LED system is significantly more efficient. On the driver side output, when each channel is "on" or at 100% duty cycle, the system has an efficacy of 3.08 PPF/W, as shown in Table XV. Considering maximum input power, assuming the Arduino consumes 4 W, the whole system would consume 66.5 W, which results in a efficacy of 2.8 PPF/W, which is roughly 50% more than HPS lamps. Also noteworthy is the electrical efficiency, whilst HPS lamps typically have 36% of the input energy converted into PAR light. Assuming that all radiant flux from the LEDs belongs to PAR, the efficiency was 64.7%, thus they are also nearly double the efficiency. Whilst still an improvement, taken from the input side of the system, the efficiency reached 58.8%. It is relevant to compare electrical efficiency and efficacy in terms of PPF/W, as LEDs that emit light with shorter wavelength will have lower efficacy simply because the photons have more energy. LEDs that convert most of the input energy into light may still have lower PPF/W, simply because less photon quanta will be released.

At a 20:80 light mix, the efficacy improves even further, here the output efficacy is 3.43 PPF/W, which is approaching double that of the HPS lamps. The electrical efficiency on the output side does not change as significantly, only improving about

5 percentage points. If it is assumed that the 2 W measured overhead between input power and the LED driver output side at 100% duty cycle scales with duty cycle. The theoretical electrical efficiency including maximum Arduino input power would be 61%. The smaller relative increase of the efficiency relative to the efficacy is reasonable since more of the light emitted now comes from the red LEDs, which results in more photon quanta at the same input energy compared to if it produced blue light. This can be shown using Equations (2.5) and (2.6). It is important to note that the electrical efficiency for the LEDs only counts if the radiant flux is purely within the PAR. However, since it is assumed that the light emitted by the LEDs in a narrow spectrum within PAR, the emission of light outside the PAR spectrum can be considered negligible. The power consumption while using supplemental sunlight to compensate was not measured. However, based on input power decreasing relative to duty cycle as it did in Figure 5.9, the input power should have decreased when the setup was moved into sunlight after calibration in the shadow.

## 6.4 Thermal Dimensioning

The worst case estimated junction temperature when calculating from the ambient temperature of 21 °C exceeds that of the lowest maximum rating of the LEDs, that is 125 °C. Since it is calculated solely with worst case values for the thermal resistances, for the worst thermal path and with the total dissipated power, the actual junction temperatures for the LEDs are likely much lower than this estimate. This can be further predicated on the lower estimated junction temperature when the thermal path directly from the heatsink is considered instead, 119 °C. The values from heatsink to junction are more accurate than those from ambient to junction. The difference between them is likely due to the heatsink being dimensioned for worst case estimates and that the thermal resistance of the heatsink varies depending on airflow and mounting arrangement as mentioned in the datasheet [49].

The junction temperature estimated with the thermal path of heatsink to junction is 119 °C and is close to the 125 °C limit that the heatsink was dimensioned for. Exceeding the maximum junction temperature is harmful to the electrical components on the board. The primary reason for the high estimated junction temperature is that the heatsink was dimensioned for a total power loss of 9.2 W according to Table V which is around half of the 18.7 W from Figure 5.5 when accounting for the efficiency. Another consideration is that the ambient temperature where the measurements took place was lower than the ambient temperature that was used when dimensioning the heatsink. Consequently the junction temperature might be higher in a practical implementation of the project as a result of higher ambient temperature. When running the system at a higher duty cycle or at a higher ambient temperature, forced cooling could be considered. The thermal resistance of the heatsink is considerably lower with forced cooling, 0.83 °C/W according to [49]. At this thermal resistance the ambient to junction path would give a junction temperature of 103 °C instead, even in the worst case scenario. The forced cooling solution allows the ambient temperature to rise up to 44 °C without exceeding the maximum

junction temperature of 125 °C.

Forced cooling in this application is unnecessary because the high-end estimates for the junction temperature are very conservative. The junction temperature of the LEDs does not exceed the maximum, even in the series case, where all power is dissipated over a single LED. More realistically the junction temperature is estimated as 59 °C. The decision to take worst case values and make conservative estimates is preferred because a lower junction temperature ensures that the maximum junction temperature is never exceeded. It is also better to keep the junction temperature low to increase the lifespan of the electrical components when in regular use.

# 7
# Conclusion

The light system developed in this thesis has significantly higher efficacy than non-LED lighting systems, nearly doubling the efficacy at a light mix of 20% blue and 80% red light. Similarly, the electrical efficiency of the system, increases up to 61% at this light mixture, a difference of 25 percentage points, or a relative increase of 69.4%. The system is designed with the intention of maximizing adjustability of the light mix and $\text{PPFD}_{\text{tot}}$, with the tradeoff of higher output energy use. However, due to incorrect inductor selection for the 666 nm channel, the headroom in adjustability is severely limited, even falling short in terms of reaching the its target. The LED channels have a resulting ON current lower than intended, and therefore suffer from a decrease in adjustability. This is likely caused by noise generated by the LED drivers and DIM PWM signals interfering with each other. Suggested improvements to achieve the intended on characteristics for each channel are to use low-pass filters on sensitive sections of the circuit and taking EMI into account during the design. For the 666 nm LED channel, a different inductor should have been chosen. As a result of the unintended lower adjustability, the overall system likely has a slightly increased total efficiency.

The $\text{PPFD}_{\text{max}}$ for three out of four LED channels are large enough to make significant changes to the light mix. However, the R LED channel cannot reach $\text{PPFD}_{\text{nom}}$ at $K_{\text{nom}}$. Despite failing to reach the targeted PPFD, the R LED channel is close enough, and is also the the one which needs the least amount of adjustability. Consequently, the final system enables adjustments of the B and FR LED channels to be performed at a satisfactory level.

The usage of a microprocessor allows for an adjustable and stable light output. The device is able to adjust the duty cycle of the LED channels to keep the measured spectral output constant for each of the sensor channels. The ability for the device to calibrate during setup makes sure that the device performance is not affected by sensor placement, unless the sensor is placed at an unreasonable distance, or facing in completely wrong direction. Another limitation of the device is that the calibration should be performed in an environment where ambient light is less than the maximum light that the LEDs can produce. This is to make sure that the target set during calibration is achievable even if the ambient light decreases. Because the microprocessor lacks a stable implementation of time keeping, adjusting the light mix for growth stage or time of day cannot be done.

The choice of light sensor limited the ability of the device to accurately measure the

spectral output. The light sensor can only be used for calibration, to set a reference, and cannot be used to accurately measure the incident light intensity. We can therefore not use it to confirm that the system actually produces the incident light intensity and light mix that the calculations show.

The safety and protection systems are not fully tested, apart from the reverse polarity protection and the 30 V relay, both of which worked as intended. No observation that would correlate with faults in the TVS diodes, fuse or input filter was observed. The thermistors showed inaccurate values, making them hard to use as a reliability for heat protection of the PCBs. This can be addressed by putting them further away from switching components that produce EMI.

# Bibliography


[1] S. Sena, S. Kumari, V. Kumar, and A. Husen, "Light emitting diode (LED) lights for the improvement of plant performance and production: A comprehensive review," *Current Research in Biotechnology*, vol. 7, 2024, Art. no. 100184. doi: 10.1016/j.crbiot.2024.100184.

[2] National Geographic. "The Development of Agriculture." 2025. [Online]. Available: https://education.nationalgeographic.org/resource/development-agriculture/. Accessed: Feb. 6, 2026.

[3] C. Wallace and A. J. Both, "Evaluating operating characteristics of light sources for horticultural applications," *Acta Horticulturae*, vol. 1134, pp. 435–444, May 2016. doi: 10.17660/ActaHortic.2016.1134.55.

[4] T. Wu et al., "Analyses of multi-color plant-growth light sources in achieving maximum photosynthesis efficiencies with enhanced color qualities," *Opt. Express*, vol. 26, no. 4, pp. 4135–4147, Feb. 2018. doi: 10.1364/OE.26.004135.

[5] D. Katzin, S. van Mourik, F. Kempkes, and E. J. van Henten, "GreenLight – an open source model for greenhouses with supplemental lighting: Evaluation of heat requirements under LED and HPS lamps," *Biosystems Engineering*, vol. 194, pp. 61–81, Jun. 2020. doi: 10.1016/j.biosystemseng.2020.03.010.

[6] *2-Ch RX325 SolrayX+FR LightDNA: Dynamic Lighting*, Helsinki, Finland: Valoya, 2026. [Online]. Available: https://valoya.com/wp-content/uploads/2026/03/Datasheet-2-Ch-RX325-SolrayX-FR-LightDNA.pdf. Accessed: May 11, 2026.

[7] Heliospectra. "Three Levels of Dynamic Light." [Online]. Available: https://heliospectra.com/blog/three-levels-of-dynamic-light/. Accessed: May 11, 2026.

[8] K. Benke and B. Tomkins, "Future food-production systems: Vertical farming and controlled-environment agriculture," *Sustainability: Science, Practice, and Policy*, vol. 13, no. 1, pp. 13–26, Nov. 2017. doi: 10.1080/15487733.2017.1394054.

[9] R. Shamshiri et al., "Advances in greenhouse automation and controlled environment agriculture: A transition to plant factories and urban agriculture," *International Journal of Agricultural and Biological Engineering*, vol. 11, no. 1, pp. 1–22, Jan. 2018. doi: 10.25165/j.ijabe.20181101.3210.

[10] T. Kozai, "Plant Factories with Artificial Lighting (PFALs): Benefits, Problems, and Challenges," in *Smart Plant Factory: The Next Generation Indoor Vertical Farms*, T. Kozai, Ed. Singapore: Springer, 2018, ch. 2, pp. 15–29. doi: 10.1007/978-981-13-1065-2_2.

[11] G. D. Massa, H.-H. Kim, R. M. Wheeler, and C. A. Mitchell, "Plant Productivity in Response to LED Lighting," *HortScience*, vol. 43, no. 7, pp. 1951–1956, Dec. 2008. doi: 10.21273/HORTSCI.43.7.1951.

[12] S. Zhen and M. W. van Iersel, "Far-red light is needed for efficient photochemistry and photosynthesis," *Journal of Plant Physiology*, vol. 209, pp. 115–122, Feb. 2017. doi: 10.1016/j.jplph.2016.12.004.

[13] L. Taiz, E. Zeiger, I. M. Møller, and A. Murphy, *Plant Physiology and Development*, 6th ed. Sunderland, Massachusetts, USA: Sinauer Associates, 2015.

[14] P. Aumars. "Absorption spectrum of chlorophyll a and b." [Image], Wikimedia Commons CC0 1.0. [Online]. Available: https://commons.wikimedia.org/wiki/File:Absorption_spectrum_of_chlorophyll_a_and_b.jpg. Accessed: May 6, 2026.

[15] G. Shevela and S. Dmitriy. "A simplified z-scheme representing the linear (black solid arrows) and a cyclic (black dashed arrow) electron transport in cyanobacteria." [Image], Wikimedia Commons CC BY 3.0. [Online]. Available: https://commons.wikimedia.org/wiki/File:Fpls-02-00028-g004.png. Accessed: May 6, 2026.

[16] J. Myers, "Enhancement studies in photosynthesis," *Annual Review of Plant Physiology*, vol. 22, pp. 289–312, Jun. 1971. doi: 10.1146/annurev.pp.22.060171.001445.

[17] J. Zou et al., "Morphological and physiological properties of indoor cultivated lettuce in response to additional far-red light," *Scientia Horticulturae*, vol. 257, Nov. 2019, Art. no. 108725. doi: 10.1016/j.scienta.2019.108725.

[18] D. P. Fraser, S. Hayes, and K. A. Franklin, "Photoreceptor crosstalk in shade avoidance," *Current Opinion in Plant Biology*, vol. 33, pp. 1–7, Oct. 2016. doi: 10.1016/j.pbi.2016.03.008.

[19] K. R. Cope and B. Bugbee, "Spectral Effects of Three Types of White Light-emitting Diodes on Plant Growth and Development: Absolute versus Relative Amounts of Blue Light," *HortScience*, vol. 48, no. 4, pp. 504–509, Apr. 2013. doi: 10.21273/HORTSCI.48.4.504.

[20] D. Patel et al., "Temperature-dependent shade avoidance involves the receptor-like kinase ERECTA," *The Plant Journal*, vol. 73, no. 6, pp. 980–992, Mar. 2013. doi: 10.1111/tpj.12088.

[21] G. Pennisi et al., "Optimal light intensity for sustainable water and energy use in indoor cultivation of lettuce and basil under red and blue LEDs," *Scientia Horticulturae*, vol. 272, Oct. 2020, Art. no. 109508. doi: 10.1016/j.scienta.2020.109508.

[22] J. Liu and M. W. van Iersel, "Photosynthetic Physiology of Blue, Green, and Red Light: Light Intensity Effects and Underlying Mechanisms," *Frontiers in Plant Science*, vol. 12, Mar. 2021. doi: 10.3389/fpls.2021.619987.

[23] M. Dyble, N. Narendran, A. Bierman, and T. Klein, "Impact of dimming white LEDs: chromaticity shifts due to different dimming methods," in *Fifth International Conference on Solid State Lighting*, I. T. Ferguson, J. C. Carrano, T. Taguchi, and I. E. Ashdown, Eds., International Society for Optics and Photonics, vol. 5941, SPIE, Sep. 2005, pp. 291–299. doi: 10.1117/12.625924.

[24] R. W. Erickson and D. Maksimović, "Steady-state equivalent circuit modeling, losses, and efficiency," in *Fundamentals of Power Electronics*, 3rd ed., Cham, Switzerland: Springer International Publishing, 2020, ch. 3, pp. 43–66. doi: 10.1007/978-3-030-43881-4_3.

[25] S. Pimputkar, J. S. Speck, S. P. DenBaars, and S. Nakamura, "Prospects for LED lighting," *Nature photonics*, vol. 3, no. 4, pp. 180–182, Apr. 2009. doi: 10.1038/nphoton.2009.32.

[26] The Royal Swedish Academy of Sciences. "The Nobel Prize in Physics 2014 – Press Release." [Online]. Available: https://www.nobelprize.org/prizes/physics/2014/press-release/. Accessed: Feb. 28, 2026.

[27] E. F. Schubert and J. K. Kim, "Solid-State Light Sources Getting Smart," *Science*, vol. 308, pp. 1274–1278, May 2005, Art. no. 5726. doi: 10.1126/science.1108712.

[28] S. U. Khan et al., "Phosphor converted LED technologies as a sustainable lighting strategy to enhance indoor crop growth and agricultural productivity," *Discover Sustainability*, vol. 6, Nov. 2025, Art. no. 1284. doi: 10.1007/s43621-025-02043-6.

[29] P. M. Pattison, M. Hansen, and J. Y. Tsao, "LED lighting efficacy: Status and directions," *Comptes Rendus Physique*, vol. 19, no. 3, pp. 134–145, 2018. doi: 10.1016/j.crhy.2017.10.013.

[30] A. Proykova et al., "Potential risks to human health of LEDs (Final Opinion)," Scientific Committee on Health, Environmental and Emerging Risks SCHEER, Jun. 2018. doi: 10.13140/RG.2.2.24119.62885.

[31] *IEEE Recommended Practices for Modulating Current in High-Brightness LEDs for Mitigating Health Risks to Viewers*, IEEE Std 1789–2015, Institute of Electrical and Electronics Engineers, New York, USA, 2015. doi: 10.1109/IEEESTD.2015.7118618.

[32] Q. Wang and J. Dong, "Optimizing and Controlling Nonlinear Metrics of Multichannel LED Systems With Ambient Light Interference via Reinforcement Learning," *IEEE Transactions on Power Electronics*, vol. 40, no. 11, pp. 16 265–16 280, Nov. 2025. doi: 10.1109/TPEL.2025.3591666.

[33] B. Choi, "Current Mode Control," in *Pulsewidth Modulated DC-to-DC Power Conversion: Circuits, Dynamics, Control, and DC Power Distribution Systems*, 2nd ed. Wiley-IEEE Press, Oct. 2021, ch. 8, pp. 357–463. doi: 10.1002/9781119454489.ch8.

[34] Y. H. Yao, P. Dupuis, L. Canale, B. F. Degni, T. C. Haba, and G. Zissis, "Analysis of Photosynthetic Photon Flux Distribution under LED Lighting using Genetic Algorithm for Efficient Okra Cultivation," *IEEE Transactions on Industry Applications*, pp. 1–10, Nov. 2025. doi: 10.1109/TIA.2025.3635588.

[35] I. Moreno and C.-C. Sun, "Modeling the radiation pattern of LEDs," *Opt. Express*, vol. 16, no. 3, pp. 1808–1819, Feb. 2008. doi: 10.1364/OE.16.001808.

[36] K. J. Åström and T. Hägglund, *PID Controllers: Theory, Design, and Tuning*, 2nd ed. Research Triangle Park, North Carolina, USA: ISA, 1995.

[37] *TPS92200 4-v to 30-v Input Voltage, 1.5-A Output Current, Synchronous Buck LED Driver with Flexible Dimming Options*, Dallas, Texas, USA: Texas In-

struments, 2022. [Online]. Available: https://www.ti.com/lit/ds/symlink/tps92200.pdf. Accessed: Mar. 5, 2026.

[38] *Arduino Nano*, Monza, Italy: Arduino, 2026. [Online]. Available: https://docs.arduino.cc/resources/datasheets/A000005-datasheet.pdf. Accessed: Apr. 27, 2026.

[39] *AS7343 14-Channel Multi-Spectral Sensor*, Premstätten, Austria: ams OSRAM, 2023. [Online]. Available: https://look.ams-osram.com/m/5f2d27fff9a874d2/original/AS7343-14-Channel-Multi-Spectral-Sensor.pdf. Accessed: Apr. 28, 2026.

[40] KiCad, Version 10.0.1, [Software], KiCad Developers, 2026. [Online]. Available: https://www.kicad.org/. Accessed: May 13, 2026.

[41] Arduino IDE, Version 2.3.8, [Software], Monza, Italy: Arduino, 2026. [Online]. Available: https://www.arduino.cc/en/software. Accessed: May 7, 2026.

[42] *Specific Lighting Product Data Sheet LTPL-C034UVH430*, New Taipei City, Taiwan: LITEON, 2017. [Online]. Available: https://optoelectronics.liteon.com/upload/download/DS23-2016-0024/LTPL-C034UVH430%20DataSheet.PDF. Accessed: Apr. 15, 2026.

[43] *GD PUSRA2.15-T2T4-24-1 Datasheet*, Premstätten, Austria: ams OSRAM, 2025. [Online]. Available: https://www.mouser.se/datasheet/3/5912/1/GD_PUSRA2.15_EN.pdf. Accessed: Apr. 15, 2026.

[44] *GH PUSRA1.25-SMSP-1-1-700-R33 Datasheet*, Premstätten, Austria: ams OSRAM, 2024. [Online]. Available: https://www.mouser.com/catalog/specsheets/ams_OSRAM_05-03-2024_GHPUSRA1.25_EN.pdf. Accessed: Apr. 15, 2026.

[45] *GF CSSRML.24-TNUL-1-1 Datasheet*, Premstätten, Austria: ams OSRAM, 2025. [Online]. Available: https://www.mouser.se/datasheet/3/5912/1/GF_CSSRML.24_EN.pdf. Accessed: Apr. 15, 2026.

[46] N. Mohan, T. M. Undeland, and W. P. Robbins, *Power Electronics: Converters, Applications and Design*, 3rd ed. Hoboken, New Jersey, USA: John Wiley & Sons, 2002, ch. 29, pp. 730–743.

[47] SMHI, *Historical air temperature data for Göteborg A*, 2026. [Online]. Available: https://www.smhi.se/data/temperatur-och-vind/temperatur/airtemperatureInstant/71420. Accessed: May 5, 2026.

[48] K. Azar and J. E. Graebner, "Experimental determination of thermal conductivity of printed wiring boards," in *Twelfth Annual IEEE Semiconductor Thermal Measurement and Management Symposium. Proceedings*, Mar. 1996, pp. 169–182. doi: 10.1109/STHERM.1996.545107.

[49] *RS PRO Heatsinks*, London, UK: RS PRO, n.d. [Online]. Available: https://docs.rs-online.com/d3c3/A700000009704140.pdf. Accessed: May 5, 2026.

[50] *LM2596 SIMPLE SWITCHER Power Converter 150-kHz 3-A Step-Down Voltage Regulator*, Dallas, Texas, USA: Texas Instruments, 2023. [Online]. Available: https://www.ti.com/lit/ds/symlink/lm2596.pdf. Accessed: May 4, 2026.

[51] *Arduino Nano* [Pinout Diagram], Monza, Italy: Arduino, 2021. [Online]. Available: https://docs.arduino.cc/resources/pinouts/A000005-full-pinout.pdf. Accessed: May 5, 2026.

[52] SparkFun, "AS7343 Arduino Library Setup," 2025. [Online]. Available: https://docs.sparkfun.com/SparkFun_Spectral_Sensor_Breakout_AS7343_Qwiic/arduino_setup/. Accessed: May 5, 2026.

[53] Arduino, "analogWrite()," 2026. [Online]. Available: https://docs.arduino.cc/language-reference/en/functions/analog-io/analogWrite/. Accessed: May 7, 2026.

[54] Arduino, "Wire," 2026. [Online]. Available: https://docs.arduino.cc/language-reference/en/functions/communication/wire/. Accessed: May 7, 2026.

[55] *Automotive P-Channel 80 V (D-S) 175 °C MOSFET*, San Jose, California, USA: Vishay Siliconix, 2024. [Online]. Available: https://www.vishay.com/docs/65936/sqj469ep.pdf. Accessed: Apr. 18, 2026.

[56] *IRLZ44NPbF HEXFET Power MOSFET*, Neubiberg, Germany: Infineon Technologies, 2003. [Online]. Available: https://www.mouser.se/datasheet/3/70/1/Infineon_IRLZ44N_DataSheet_v01_01_EN.pdf. Accessed: May 4, 2026.

[57] *2N3903 2N3904 SILICON NPN TRANSISTORS*, Hauppauge, New York, USA: Central Semiconductor, 2021. [Online]. Available: https://www.mouser.se/datasheet/3/312/1/2N3903.PDF. Accessed: May 4, 2026.

[58] *TVS Diodes Surface Mount—600 W > SMBJ series*, Chicago, Illinois, USA: Littelfuse, 2025. [Online]. Available: https://www.littelfuse.com/assetdocs/tvs-diodes-smbj-series-datasheet?assetguid=ba555e99-a12d-4f72-a0b6-86b06c67171e. Accessed: May 4, 2026.

[59] *SMBJ5338B THRU SMBJ5388B*, Simi Valley, California, USA: Micro Commercial Components, 2021. [Online]. Available: https://www.mccsemi.com/pdf/Products/SMBJ5338B-SMBJ5388B(SMB).pdf. Accessed: Apr. 18, 2026.

[60] J. Arrigo, "Input and Output Capacitor Selection," Texas Instruments, Application Report SLTA055, Feb. 2006. [Online]. Available: https://www.ti.com/lit/an/slta055/slta055.pdf. Accessed: Mar. 23, 2026.

[61] M. Xie, "How to select input capacitors for a buck converter," *Texas Instruments Analog Applications Journal*, no. SLYT670, pp. 8–13, 2016. [Online]. Available: https://www.ti.com/lit/an/slyt670/slyt670.pdf. Accessed: May 9, 2026.

[62] *U1270 Series Handheld Digital Multimeter*, Santa Rosa, California, USA: Keysight Technologies, 2025. [Online]. Available: https://www.keysight.com/us/en/assets/7018-02687/data-sheets/5990-6425.pdf. Accessed: May 8, 2026.

[63] *RTB2002 OSCILLOSCOPE*, Munich, Germany: Rohde & Schwarz, 2023. [Online]. Available: https://www.batronix.com/files/Rohde-&-Schwarz/Oscilloscope/RTB2000/RTB2000_dat-sw_en_3607-4270-22_v1700.pdf. Accessed: May 8, 2026.

[64] *62 MAX+ Handheld Infrared Laser Thermometer*, Everett, Washington, USA: Fluke Corpopration, 2017. [Online]. Available: https://media.fluke.com/

beb8da7f-9bd2-4f76-a431-b1060068f6c0_original%20file.pdf. Accessed: May 8, 2026.

[65] *Power Supplies Bench*, Tokyo, Japan: TENMA, 2022. [Online]. Available: https://www.farnell.com/datasheets/3767164.pdf. Accessed: May 12, 2026.

[66] *R&S RT-ZC02 R&S RT-ZC03 AC/DC Current Probe User Manual*, Munich, Germany: Rohde & Schwarz, 2020. [Online]. Available: https://scdn.rohde-schwarz.com/ur/pws/dl_downloads/dl_common_library/dl_manuals/dl_user_manual/RT-ZC02-ZC03_Manual_en_03.pdf. Accessed: May 12, 2026.

[67] Microsoft Excel, Version 16.108.3, [Software], Redmond, Washington, USA: Microsoft Corporation, 2026. [Online]. Available: https://www.microsoft.com/en-us/microsoft-365/excel. Accessed: Apr. 7, 2026.

[68] Gemini (version 3.1 Pro), Google DeepMind, 2026. [Large Language Model]. [Online]. Available: https://gemini.google.com/app. Accessed: May 12, 2026.

# A

# Appendix 1

```{c++}

#include <Wire.h>
#include <SparkFun_AS7343.h>

SfeAS7343ArdI2C mySensor;

// Thermistor pins arduino
const int tempSens_PCB = A0;     // PCB Thermistor
const int tempSens_LED = A1;     // LED PCB Thermistor

// Threshold temperatures taken from datasheets
const float thresholdTemp_PCB = 50.0;
const float thresholdTemp_LED = 70.0;

// Allowed degrees over the threshold before cutting the PWM
const float maxOvertempMargin = 10.0;

// Defining PWM pins arduino
const int PIN_PWM_666 = 3;   // Channel 1
const int PIN_PWM_727 = 9;   // Channel 2
const int PIN_PWM_425 = 10;  // Channel 3
const int PIN_PWM_450 = 11;  // Channel 4

// Change to test other light mixes
// Percentage is of the total light mix
// K_PPFD = K_PPFD_nominel for this instance
float K_PPFD425 = 0.1;
float K_PPFD450 = 0.1;
float K_PPFD666 = 0.6;
float K_PPFD727 = 0.2;

// Sets the total PPFD from all the LEDs
float PPFDtotal = 250;

// Calculated duty cycle values
int pwm425 = (K_PPFD425 * PPFDtotal/53.56) * 256-1;
int pwm450 = (K_PPFD450 * PPFDtotal/66) * 256-1;
int pwm666 = (K_PPFD666 * PPFDtotal/190.63) * 256-1;
int pwm727 = (K_PPFD727 * PPFDtotal/139.26) * 256-1;

// Creating variables for target values (Dummy values):
int TARGET_425 = 0;
int TARGET_450 = 0;
```

```
int TARGET_666 = 0;
int TARGET_727 = 0;

// Creating structure for PI regulator
struct PIController {
  float integral = 0;
  float Kp = 0.1;
  float Ki = 0.09;
  int currentPWM = 0;
};

// Creating a separate regulator for each LED channel
PIController ctrl425;
PIController ctrl450;
PIController ctrl666;
PIController ctrl727;

// Function for writing to light sensor adress manually
// If using another thermistor, change the adress value
void writeRegister(uint8_t reg, uint8_t value)
{
    Wire.beginTransmission(0x39); // AS7343 I2C address
    Wire.write(reg);
    Wire.write(value);
    Wire.endTransmission();
}

// Function that checks the thermistor values
// Breaks if the margin is exceeded
float calculateDerateFactor(float currentTemp, float thresholdTemp) {
  if (currentTemp <= thresholdTemp) {
    return 1.0;
  }
  float overTemp = currentTemp - thresholdTemp;
  if (overTemp >= maxOvertempMargin) {
    return 0.0;
  }
  return 1.0 - (overTemp / maxOvertempMargin);
}

// PI function that calculates new PWM value
int updatePWM(int target, float measured, PIController &ctrl) {
    float error = target - measured;
    ctrl.integral += error;

    // Anti-windup,
    // prevents calculation lock-up if sensor is covered
    if (ctrl.integral > 5000) ctrl.integral = 5000;
    if (ctrl.integral < -5000) ctrl.integral = -5000;

    float output = (ctrl.Kp * error) + (ctrl.Ki * ctrl.integral);
    int newPWM = (int)output;

    if (newPWM > 255) newPWM = 255;
    if (newPWM < 0) newPWM = 0;

```

```
    ctrl.currentPWM = newPWM;
    return newPWM;
}

// Thermistor values fluctuates due to component placements
// This function is used to get a stable ADC read by taking
// 40 samples and using the mean of the 5 lowest values
int readStableADC(int pin) {
  // Dummy-read
  analogRead(pin);
  delay(5);

  const int numSamples = 40;
  int samples[numSamples]; // Array to store sample values

  // Take 40 samples
  for (int i = 0; i < numSamples; i++) {
    samples[i] = analogRead(pin);
    delay(3);
  }

  // Sort the array with Bubble sort
  for (int i = 0; i < numSamples - 1; i++) {
    for (int j = 0; j < numSamples - i - 1; j++) {
      if (samples[j] > samples[j + 1]) {
        int temp = samples[j];
        samples[j] = samples[j + 1];
        samples[j + 1] = temp;
      }
    }
  }

  // Calculate mean of 5 lowest values
  long sum = 0;
  const int numLowest = 5;

  for (int i = 0; i < numLowest; i++) {
    sum += samples[i];
  }

  return sum / numLowest;
}

void setup() {
    Serial.begin(115200);   // Bits per second
    Wire.begin();
    pinMode(A2, OUTPUT);    // Relay 30V
    digitalWrite(A2, LOW);

    // Setting Channel output pins
    pinMode(PIN_PWM_666, OUTPUT);
    pinMode(PIN_PWM_727, OUTPUT);
    pinMode(PIN_PWM_425, OUTPUT);
    pinMode(PIN_PWM_450, OUTPUT);

    // Initiating light sensor
```

```
157     // Code taken from the light sensor's Arduino library
158     mySensor.begin();
159     mySensor.powerOn();
160     mySensor.setAutoSmux(AUTOSMUX_18_CHANNELS);
161     mySensor.enableSpectralMeasurement();
162     Serial.println("AutoSmux set to 18 channels.");
163
164     if (mySensor.setAgain(AGAIN_0_5) == false)
165     {
166     Serial.println("Failed to set gain.");
167     while (1);
168     }
169     if (mySensor.enableWaitTime() == false)
170     {
171         Serial.println("Failed to enable wait time.");
172         Serial.println("Halting...");
173         while (1)
174             ;
175     }
176     if (mySensor.setWaitTime(80) == false)
177     {
178         Serial.println("Failed to set wait time.");
179         Serial.println("Halting...");
180         while (1)
181             ;
182     }
183
184     // Duty cycle cannot be higher than 100%
185     // If calculation is higher, set duty cycle to 255 (100%)
186     if (K_PPFD666 * PPFDtotal > 190.63){
187       pwm666 = 255;
188       Serial.println("percentageTarget666 is too high");
189     }
190
191     if (K_PPFD727 * PPFDtotal > 139.26){
192       pwm727 = 255;
193       Serial.println("percentageTarget727 is too high");
194     }
195
196     if (K_PPFD425 * PPFDtotal > 53.56){
197       pwm425 = 255;
198       Serial.println("percentageTarget425 is too high");
199     }
200
201     if (K_PPFD450 * PPFDtotal > 66){
202       pwm450 = 255;
203       Serial.println("percentageTarget450 is too high");
204     }
205
206     mySensor.ledOff();
207
208     // Setting manual integration time for PPFD measurement,
209     // see light sensor datasheet
210     uint16_t astep = 7194; // Aprox. 20 milliseconds
211
212     // Splitting ASTEP into two 8 bit variable registers
```

```
213     // 7194 in hexadecimal is 1C1A
214     uint8_t lsb = astep & 0xFF;          // 0x1A
215     uint8_t msb = (astep >> 8) & 0xFF;   // 0x1C
216 
217     // Write to light sensor registers
218     // Registers CA and CB contains ASTEP
219     writeRegister(0x81, 9);      // ATIME
220     writeRegister(0xCA, lsb);    // ASTEP low byte
221     writeRegister(0xCB, msb);    // ASTEP high byte
222 
223     // Enable Spectral Measurement
224     if (mySensor.enableSpectralMeasurement() == false)
225     {
226         Serial.println("Failed to enable spectral measurement.");
227         Serial.println("Halting...");
228         while (1)
229             ;
230     }
231 
232     // Writing calculated PWMs to corresponding pins
233     analogWrite(PIN_PWM_425, pwm425);
234     analogWrite(PIN_PWM_450, pwm450);
235     analogWrite(PIN_PWM_666, pwm666);
236     analogWrite(PIN_PWM_727, pwm727);
237 
238     // Wait for the calibration
239     delay(5000);
240 
241     // ... inside setup() after the 5 second delay ...
242     // IMPORTANT: You must tell the sensor to take a reading first!
243     if (mySensor.readSpectraDataFromSensor()) {
244         TARGET_425 = mySensor.getChannelData(CH_DARK_BLUE_F2_425NM);
245         TARGET_450 = mySensor.getChannelData(CH_BLUE_FZ_450NM);
246         TARGET_666 = mySensor.getChannelData(CH_BROWN_F6_640NM);
247         TARGET_727 = mySensor.getChannelData(CH_DARK_RED_F8_745NM);
248 
249         Serial.println("");
250         Serial.println("--- Targets Saved Successfully ---");
251         Serial.print("425: "); Serial.println(TARGET_425);
252         Serial.print("450: "); Serial.println(TARGET_450);
253         Serial.print("666: "); Serial.println(TARGET_666);
254         Serial.print("727: "); Serial.println(TARGET_727);
255     } else {
256         Serial.println("Error: Could not read sensor to set targets!");
257     }
258     delay(5000);
259 }
260 
261 void loop() {
262     // ------------ Thermistor calculations ------------ //
263     int sensorVal_PCB = readStableADC(tempSens_PCB);
264     int sensorVal_LED = readStableADC(tempSens_LED);
265 
266     // Convert the ADC reading to voltage
267     float voltage_PCB = (sensorVal_PCB / 1024.0) * 5.0;
268     float voltage_LED = (sensorVal_LED / 1024.0) * 5.0;
```

```
269
270     // Calculate value to degrees celsius
271     // Uses thermistor datasheet to derive formula
272     float temperature_PCB = (voltage_PCB - 0.5)/0.01;
273     float temperature_LED = (voltage_LED - 0.5)/0.01;
274
275     // Calculate temperature factor for all PWM Channels
276     // Used as protective measurement if too high temp
277     // Calculate temperature factor for both sensors
278     float factor_PCB = calculateDerateFactor(temperature_PCB, thresholdTemp_PCB);
279     float factor_LED = calculateDerateFactor(temperature_LED, thresholdTemp_LED);
280
281     // Choose the lowest factor to protect the hottest component
282     float activeFactor = min(factor_PCB, factor_LED);
283     // ------------------------------------------------ //
284
285     // Read all data registers
286     // if it fails, print a failure message and continue
287     if (mySensor.readSpectraDataFromSensor() == false) {
288         Serial.println("Failed to read spectral data.");
289     }
290
291     // Fetch values of the relevant wavelengths
292     int meas425 = mySensor.getChannelData(CH_DARK_BLUE_F2_425NM);
293     int meas450 = mySensor.getChannelData(CH_BLUE_FZ_450NM);
294     int meas666 = mySensor.getChannelData(CH_BROWN_F6_640NM);
295     int meas727 = mySensor.getChannelData(CH_DARK_RED_F8_745NM);
296
297     // PI regulators calculates new PWM (0-255)
298     // Includes scaling factor "activeFactor" to decrease power at high temp
299     pwm425 = updatePWM(TARGET_425 * activeFactor, meas425, ctrl425);
300     pwm450 = updatePWM(TARGET_450 * activeFactor, meas450, ctrl450);
301     pwm666 = updatePWM(TARGET_666 * activeFactor, meas666, ctrl666);
302     pwm727 = updatePWM(TARGET_727 * activeFactor, meas727, ctrl727);
303
304     // Send signals to LED pins
305     analogWrite(PIN_PWM_425, pwm425);
306     analogWrite(PIN_PWM_450, pwm450);
307     analogWrite(PIN_PWM_666, pwm666);
308     analogWrite(PIN_PWM_727, pwm727);
309
310     // Printing light sensor and temp values in Serial Monitor
311     Serial.print("425: ");
312     Serial.print("Target: ");       Serial.print(TARGET_425);
313     Serial.print(" | Measured: ");  Serial.print(meas425);
314     Serial.print(" | PWM: ");       Serial.println(pwm425);
315
316     Serial.print("450: ");
317     Serial.print("Target: ");       Serial.print(TARGET_450);
318     Serial.print(" | Measured: ");  Serial.print(meas450);
319     Serial.print(" | PWM: ");       Serial.println(pwm450);
320
321     Serial.print("666: ");
322     Serial.print("Target: ");       Serial.print(TARGET_666);
323     Serial.print(" | Measured: ");  Serial.print(meas666);
324     Serial.print(" | PWM: ");       Serial.println(pwm666);
```

```
325
326     Serial.print("727: ");
327     Serial.print("Target: ");        Serial.print(TARGET_727);
328     Serial.print(" | Measured: ");  Serial.print(meas727);
329     Serial.print(" | PWM: ");        Serial.println(pwm727);
330
331     Serial.println("");
332     Serial.println("Thermistor Values:");
333
334     Serial.print("PCB: ");          Serial.print(voltage_PCB);
335     Serial.print(" V, ");
336     Serial.print(temperature_PCB);  Serial.println("°C");
337
338     Serial.print("LED: ");          Serial.print(voltage_LED);
339     Serial.print(" V, ");
340     Serial.print(temperature_LED);  Serial.println("°C");
341     Serial.println("");
342     delay(500);
343 }
```

# B

# Appendix 2

Each figure includes sub figures pertaining to the measured electrical characteristics of each LED channel. The figures show the waveform measured with an oscilloscope of the voltage over each LED string, LED current, and the voltage over the sense resistor in each LED channel. The current measurement was made with a current clamp with a 100 mV/A or 10 mV/A ratio.

**(a)** Current measurement.

**(b)** Channel voltage.

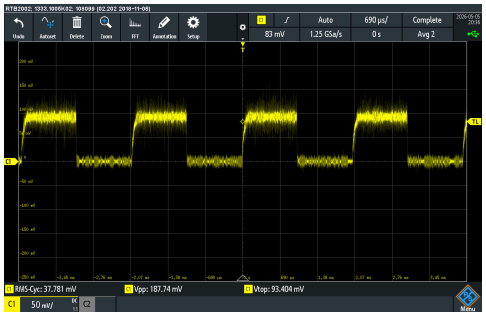

**(c)** $R_{\text{sense}}$ voltage.

**Figure B.1.** Electrical measurements 425 nm channel.

**(a)** Current measurement.

**(b)** Channel voltage.

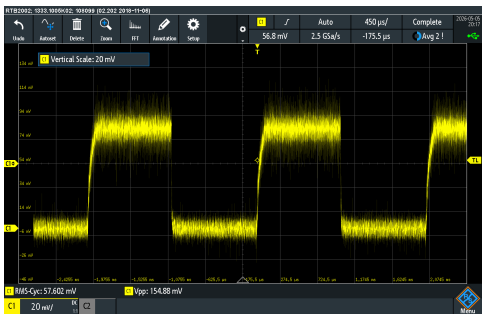

**(c)** $R_{\text{sense}}$ voltage.

**Figure B.2.** Electrical measurements 450 nm channel

**(a)** Current measurement.

**(b)** Channel voltage.

**(c)** $R_{\text{sense}}$ voltage.

**Figure B.3.** Electrical measurements 666 nm channel.

**(a)** Current Measurement.

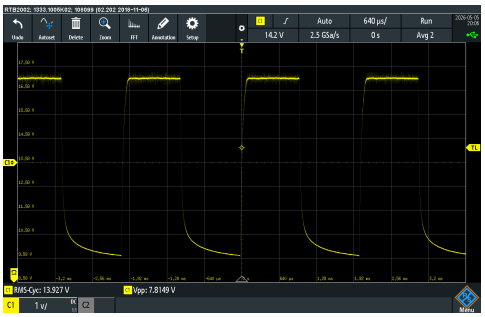

**(b)** Channel Voltage.

**(c)** $R_{\text{sense}}$ voltage.

**Figure B.4.** Electrical measurements 727 nm channel.

The Figures B.1, B.2, B.3, B.4, are interpreted in Table XIII to determine duty cycle, as well as power draw, efficiency and efficacy in Table XV. The following measurements show the initial current measurements, using a 10 mV/A resolution.

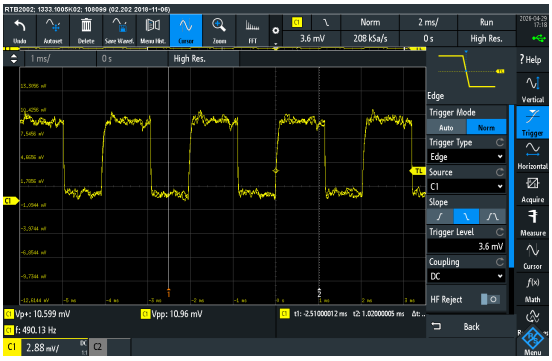

**(a)** Current measurement 425 nm channel.

**(b)** Current measurement 450 nm channel.

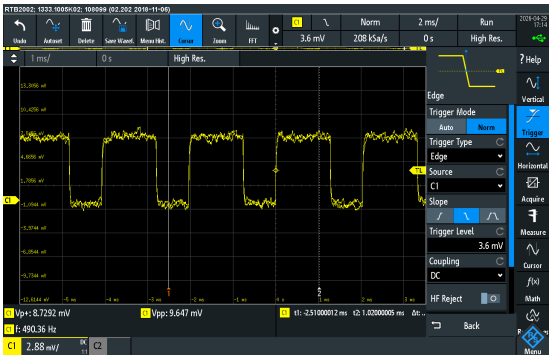

**(c)** Current measurement 666 nm channel.

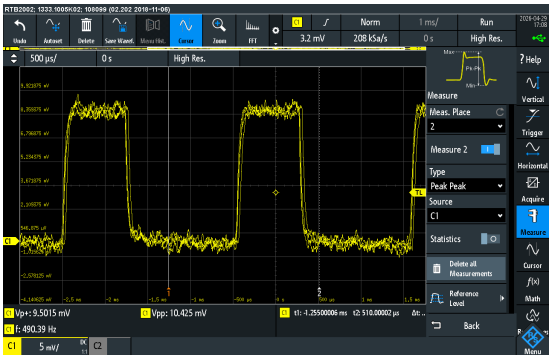

**(d)** Current measurement 727 nm channel.

**Figure B.5.** First measurement on the current for all the channels.

The peak to peak values shown in Figure B.5 were used as the resulting ON current, used in Table XIV.

# C
# Appendix 3

**Table XX.** List of all the components used for the two PCBs.

| **Component** | **Article number** | **Amount** |
|---|---|---|
| 12 V Power Converter | LM2596S-12/NOPB | 1 |
| Arduino Nano V3.0 (clone) | Unknown - A000005 | 1 |
| Bipolar transistor | 2N3904 PBFREE | 1 |
| Connector | SM04B-SRSS-TB | 1 |
| Capacitor, 47 µF | UPS1H470MED | 1 |
| Ceramic capacitor, 0.022 µF | GRM31BR7LV223KW01L | 1 |
| Ceramic capacitor, 0.1 µF | C1206C104J5JACTU | 8 |
| Ceramic capacitor, 10 µF | CC1206KKX5R9BB106 | 8 |
| Electrolytic capacitor, 82 µF | UPM1H820MPD | 1 |
| Electrolytic capacitor, 47 µF | UPM0J471MPD | 2 |
| Fuse holder | 696108003002 | 1 |
| Heatsink | 903-3087 | 1 |
| Inductor, 220 µH | SRR1260-221K | 1 |
| LED driver | TPS92200D1DDCR | 4 |
| Light sensor | 1568-SEN-23220-ND | 1 |
| NMOS | IRLZ44NPBF | 1 |
| PCB terminal block, 1.5 $mm^2$ | 1726189 | 1 |
| PCB terminal block, 2.5 $mm^2$ | 1985946 | 1 |
| PMOS | SQJ469EP-T1_GE3 | 1 |
| Power inductor, 2.2 µH | SRR1260-2R2Y | 1 |
| Power inductor, 10 µH | SRR1260-100M | 1 |
| Power inductor, 15 µH | SRR1260-150M | 3 |
| Resistor, 70 mΩ | WSL1206R0700FEA | 2 |
| Resistor, 100 mΩ | RL73H2BR10FTD | 1 |
| Resistor, 1 kΩ | RNCP1206FTD1K00 | 1 |
| Resistor, 10 kΩ | RNCP1206FTD10K0 | 1 |
| Resistor, 51.1 kΩ | RNCP1206FTD51K1 | 1 |
| Thermistor | 579-MCP9700AT-E/TT | 2 |
| TVS diode | SMBJ33A | 2 |
| Zener diode | SMBJ5349B-TP | 1 |

**DEPARTMENT OF ELECTRICAL ENGINEERING**
**CHALMERS UNIVERSITY OF TECHNOLOGY**
Gothenburg, Sweden
www.chalmers.se


CHALMERS
UNIVERSITY OF TECHNOLOGY